SIMULATION OF PRESCRIBED BOUNDARY FLOW CONDITIONS IN A MULTIPLE CONTROLLED FAN WIND TUNNEL

By

JASON THOMAS SMITH

A DISSERTATION PRESENTED TO THE GRADUATE SCHOOL
OF THE UNIVERSITY OF FLORIDA IN PARTIAL FULFILLMENT
OF THE REQUIREMENTS FOR THE DEGREE OF
DOCTOR OF PHILOSOPHY

UNIVERSITY OF FLORIDA

2011

To my wife, Katie

ACKNOWLEDGMENTS

I would like to thank my advisor, Dr. Forrest J. Masters, for providing me guidance and advice throughout my doctoral research. In addition, I want to thank my committee members, Dr. Kurtis Gurley, Dr. David Prevatt, Dr. Louis Cattafesta, and Dr. Anne Cope, for their assistance and support during various aspects of my research and graduate studies. Also, I would like to extend a thank you to Dr. Zhuzhao Liu, Dr. Tim Reinhold, Jim Austin, Scott Bolton, George Fernandez, Jimmy Jesteadt, Carlos Lopez, Dany Romero, and Abraham Alende for the help in creating and executing experimental procedures within my research. I would most of all like to thank my wife, Katie, for her continuous love and support. This research was made possible with financial support from the Institute for Business & Home Safety and the University of Florida Alumni Fellowship Program.

TABLE OF CONTENTS

page

LIST OF TABLES

LIST OF FIGURES

Abstract of Dissertation Presented to the Graduate School
of the University of Florida in Partial Fulfillment of the
Requirements for the Degree of Doctor of Philosophy

SIMULATION OF PRESCRIBED BOUNDARY LAYER FLOW CONDITIONS IN A MULTIPLE CONTROLLED FAN WIND TUNNEL

By

Jason T. Smith

December 2011

Chair: Dr. Forrest J. Masters
Major: Civil Engineering

The development of a method to simulate desired approach flow characteristics in a multiple controlled fan wind tunnel (MCFWT) is described. A MCFWT uses flow control techniques to impart the desired turbulence characteristics in a wind tunnel in lieu using a roughness grid upwind of the test section to generate a boundary layer. In contrast to other MCWFT techniques, the proposed approach (a) relies on the direct simulation of scaled wind speed and direction records collected during field experiments and (b) implements a closed-loop proportional-integral-derivative controller to modulate the wind speed and control the longitudinal turbulence characteristics. A case study is presented using a 1:10 scale model of the Institute for Business & Home Safety Research Center Full-Scale Test Facility. Simulation of marine, open and suburban approach boundary layer flow yields good agreement between the model and measured values, including mean velocity and turbulence intensity profiles, integral length scales and power spectra. Control of longitudinal and lateral fluctuations is considered herein. Good agreement between the target and measured vertical turbulence intensity profiles was also achieved after the longitudinal and lateral turbulence profiles were obtained through the proposed approach.

CHAPTER 1
INTRODUCTION

The focus of this research is the simulation of atmospheric boundary layer flow conditions in a multiple controlled fan wind tunnel (MCFWT). In contrast to boundary layer wind tunnels, MCFWTs do not use roughness element grids upwind of the test section to generate mechanical turbulence. MCFWTs implement flow control techniques (e.g, vane airfoils and controllable fan arrays) to simulate the desired boundary layer.

This dissertation presents a new technique to develop and calibrate a MCFWT to generate mean velocity and turbulence characteristics for a wide range of terrains. A closed-loop control system is implemented to simulate stationary anemometric records converted from full- to model-scale. A case study is presented using a 1:10 scale model of the Insurance Institute for Business & Home Safety (IBHS) Research Center Full-Scale Test Facility in Richburg, South Carolina. Similitude is achieved for the (a) mean velocity profile, (b) longitudinal, lateral and vertical turbulence intensity profiles, (c) the corresponding power spectra, (d) gust factors and (e) integral length scales. The main contributions of this research is an improvement to existing methods to calibrate approach flows in full-scale test facilities and a new technique to simulate a wide range of atmospheric boundary layer flow conditions in a multiple controlled fan wind tunnel (MCFWT).

The purpose of full-scale test facilities is to simulate wind loads on structures associated with extreme wind events through experiments directed at better understanding how building systems perform in extreme wind and wind-driven rain. Despite the building code changes that followed Hurricane Andrew in 1992, wind-

induced damage still remains on the rise due to failures of the building envelope. The annual economic loss due to tropical cyclones in the United States increased from $8.7 billion dollars from 1986-1995 to $19.8 billion (equivalent to 2005 dollars) from 1996-2005 (Pielke et al., 2008).

In the late 1990s, the National Research Council and the U.S. Department of Energy proposed the development of a full-scale testing facility dedicated to wind damage mitigation(NRC, 1999). The technical feasibility of the facility was experimentally validated, in part, based on the original research conducted by Kennedy (1999) at the Clemson University Wind Load Test Facility. Resulting from Kennedy's work, wind engineering researchers have created large-scale testing apparatuses capable of recreating hurricane wind loads and wind-driven rain scenarios to evaluate the performance of low rise buildings. Examples include the University of Florida's Windstorm Simulator (Masters et al., 2008) and Florida International University's Wall of Wind (Leatherman et al., 2007) (Fig 1-1). These apparatuses have relatively confined test sections due to cost and power required to simulate extreme wind loading, which consequently limits testing to singular building systems such as fenestration and roofing systems. In 2010, the Insurance Institute for Business & Home Safety commissioned a windstorm simulator capable of completely immersing a 2 story residential or commercial structure in a turbulent boundary layer. More information on these systems is presented in Chapter 2.

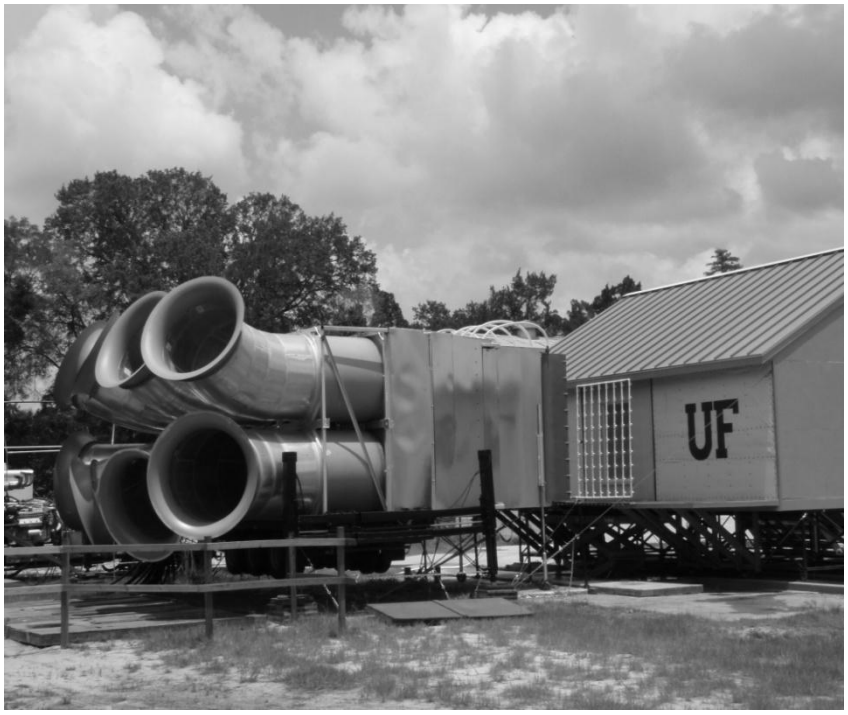

A

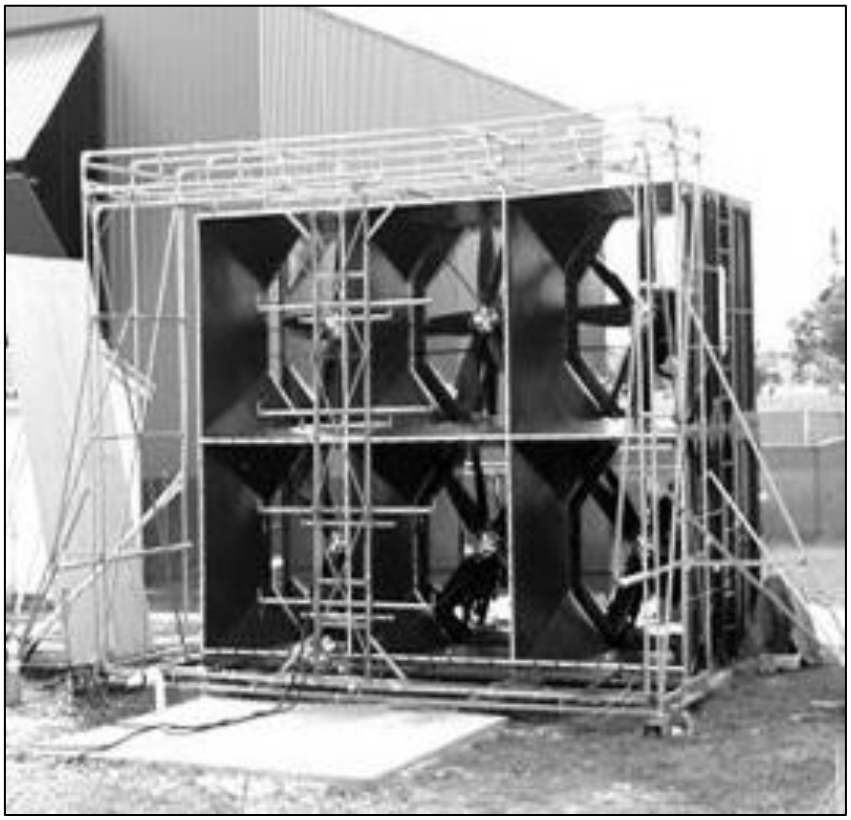

B

Figure 1-1. Full-scale testing apparatuses a) University of Florida's Windstorm Simulator b) Florida International University's Wall of Wind (http://www.eng.fiu.edu, 2011)

Research Objectives

The primary research objective was the simulation of desired scaled turbulent boundary layer wind flow characteristics using a multiple controlled fan wind tunnel (MCFWT) through the development of an active flow control system that would provide accurate and repeatable prescribed wind load scenarios. A sequence of technical questions were posed to guide the research through an experimental path, leading to the primary objective:

1. Does implementing the control system of a single fan module into an array of fan modules produce an accurate simulation of the longitudinal component of boundary layer flow?
2. Can multiple boundary layer flow conditions be accurately simulated using and active control of an airfoil system, coupled with an actively controlled fan module array?
3. Does immersing a model structure into the actively controlled boundary layer flow accurately simulate known full-scale pressure distributions?

Importance of Study

This study resulted in a new approach to recreate desired boundary layer wind profile characteristics that will effectively model similar pressure distributions on scaled test specimens that are representative of full-scale pressure distributions. With scale model pressure distributions representative of its full-scale counterpart, model testing can be conducted on different types of 1:10 model residential and commercial structures (i.e. hip, gable, and other complex geometry).

Development of an active flow control system provides a case study for the advancement of larger scaled boundary layer wind tunnels. Traditional low-rise wind tunnel testing is conducted anywhere from 1:25 to 1:500 scaled models (Tieleman et al., 1978; Surry, 1992) in test sections where fine scale turbulence could affect pressure

distributions. With 1:10 scale modeling, validation or modification of flow assumptions for larger models immersed into a turbulent boundary layer flow can be conducted (i.e. Reynolds number effects and shear layer mixing).

The experimental research will advance the knowledge base for the development of smaller and more cost effective wind tunnels. Implementation of an active flow control system into an array of fans to accurately recreate scaled atmospheric boundary layer characteristics will aid in reducing the need for large upstream fetches for which roughness elements are needed to develop desired turbulence characteristics. It will also provide simple transitions between varying terrain characteristics. A reduction in the upstream fetch will reduce the footprint and expenses related with the construction and operation of typical boundary layer wind tunnels, furthering the development and accessibility of low-speed wind tunnels. A reduced cost would make such a wind tunnel more readily attainable for facilities with limited space and budget. This will provide a viable option for the development of a functional educational tool to promote and advance the wind engineering field.

Organization of Document

Chapter 2 contains a review of previous literature describing the development of boundary layer wind tunnels to multiple controlled fan wind tunnels. Chapter 3 describes the proposed method. Chapter 4 provides a case study describing results achieved by implementing the proposed method for the experimental modeling of unobstructed atmospheric boundary layer flow. Chapter 5 is a comparative study with a 1:10 scale model immersed into prescribed flow conditions compared to an instrumented full-scale building. Finally, Chapter 6 presents conclusions about the 1:10

scaled wind tunnel and its application in wind engineering and recommendations for future research.

CHAPTER 2
LITERATURE REVIEW

Introduction

In the 20th century, determination of structural wind loads has evolved from simplified representations of static drag forces to complex modeling involving multiple aspects of aerodynamics, meteorology, structural mechanics and dynamics (Davenport, 2002). In the 1930s, civil engineers began using aeronautical wind tunnels to estimate wind loads on buildings. These aeronautical wind tunnels simulated uniform flow condition outside the boundary layer and did not accurately simulate wind loads on structures. Bailey and Vincent (1946) performed wind tunnel testing in a simplified boundary layer flow in which variations of the pressures between uniform and boundary layer flow were observed. The variations were considered to be of academic interest only because due to the large mass and stiffness of buildings at the time they were not at susceptible to fluctuating pressures. It would take the development of lighter construction materials and the introduction of taller and more flexible buildings before the effects of dynamic wind loading were taken in to consideration.

Jensen (1958) published some of the first results comparing the mean pressures on full-scale buildings with those of models in boundary layer flow wind tunnel tests. He concluded that when the ratio of building height to roughness length was equal between the full-scale and model mean, pressure distributions were similar. From this, he derived one the earliest model laws, which states:

> "The correct model test with phenomena in the wind must be carried out in a turbulent boundary layer, and the model-law requires that this boundary layer be to scale as regards the velocity profile."

Jensen's model law and better understanding of atmospheric boundary layer flow were the catalysts for a rapid development and implementation of boundary layer wind tunnels that began in the 1960s. With the continual advancement of instrumentation and mechanical system capabilities, engineers were able to transform first generation boundary layer wind tunnels to complex model and full-scale multiple controlled fan wind tunnels of today. The requirements for similitude between model- and full-scale are much more well-defined. Similarity between mean velocity and turbulence intensity profiles, power spectra, integral length scales and non-dimensional numbers (e.g., Froude, Euler, Strouhal) are of interest.

This chapter provides an overview of low-speed boundary layer wind tunnels and multiple controlled fan wind tunnels. Validation of wind tunnel modeling with full-scale experiments is discussed. The chapter concludes with an overview of an existing full-scale wind loading apparatuses and summary.

Low-Speed Boundary Layer Wind Tunnels

In the 1950s, studies of the atmospheric boundary layer led to a better understanding of its characteristics and the development of an improved set of boundary layer modeling criteria (Cochran, 2004). This led to Cermak (1958) building the first large boundary layer wind tunnel as a study to recreate turbulence within an atmospheric boundary layer flow. Cermak's initial studies established the criteria for Reynolds number independence when simulating scale boundary layer flow. Davenport (1963) determined that high winds are characterized by neutral atmosphere conditions and that simulation of a turbulent boundary layer flow over a plate provides adequate simulation of static and dynamic loads on structures. Additional studies conducted by Cermak and Davenport concluded that the objective in developing boundary layer wind

tunnels was to produce a thick, rough wall turbulent boundary layer flow in the shortest possible stream wise (development) distance (Cermak, 1971 and 1981; Davenport, 1961).

By the late 1960s, the University of Western Ontario (UWO) had established techniques for modeling natural wind in a wind tunnel. This research led to better prediction of wind-induced structural loads. Additional to recreating the mean velocity profile, Davenport established similarity requirements such as turbulence intensities, probability distributions, spectra of the individual components of turbulence and their higher order correlations (Reynolds stresses). Recreation of all turbulence characteristics proved to be difficult, which led to the development of multiple "partial model" wind tunnels that were used to obtain data on structural performance. These "partial model" wind tunnels implemented mixing devices such as rods, grid, and plates. Davenport summarized the four most common approaches at that time to simulate atmospheric boundary layer flow in wind tunnels as:

1. Curved screens (Baines, 1963) and grids of horizontal rods at a varied spacing (Owen and Zienkiewics 1957) used to model the structure of the mean wind and obtain information on time-average flow characteristics, as well as mean structural response.
2. Coarse grids used by Baines and Peterson (1950) to develop large scale turbulences that were superimposed into a uniform wind stream.
3. Grids of flat plates with added turbulence generators (Lloyd, 1967) and elliptical vortex generator (Armitt, 1967), used to model the mean and turbulence flow characteristics.
4. Large upstream working sections with varying roughness elements (Figure 2-1) used to facilitate the natural growth of the boundary layer by Jensen (1958), Cermak (1970) at Colorado State University, and Davenport (1967) at UWO (commonly referred as a turbulent boundary layer wind tunnel).

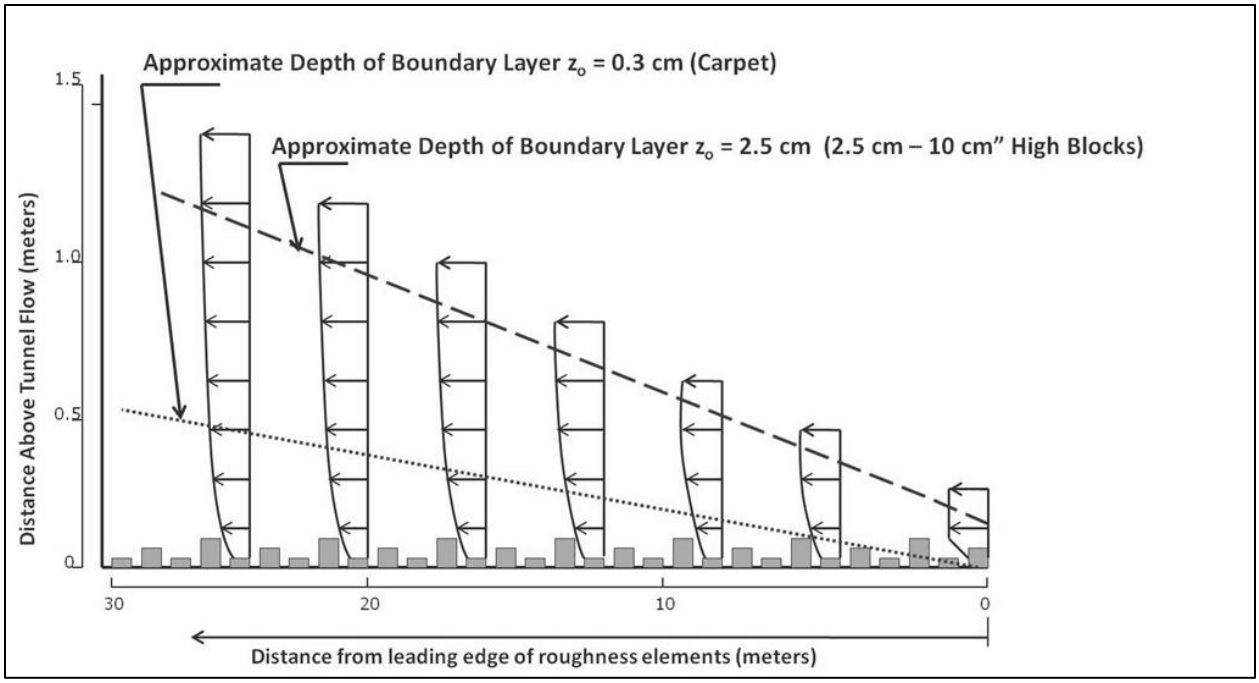

Figure 2-1. Development of boundary layer with traditional boundary layer roughness elements (after Davenport, 1963)

The most common type of low-speed wind tunnel for civil engineering applications is the turbulent boundary layer wind tunnel. Cermak (1970) adapted the closed-circuit (recirculating) wind tunnel configuration from high-speed aeronautical testing for boundary layer flow testing in civil engineering applications (Figure 2-2). The most referred open-circuit wind tunnels within North America is UWO's Boundary Layer Wind Tunnel, similar to Figure 2-3.

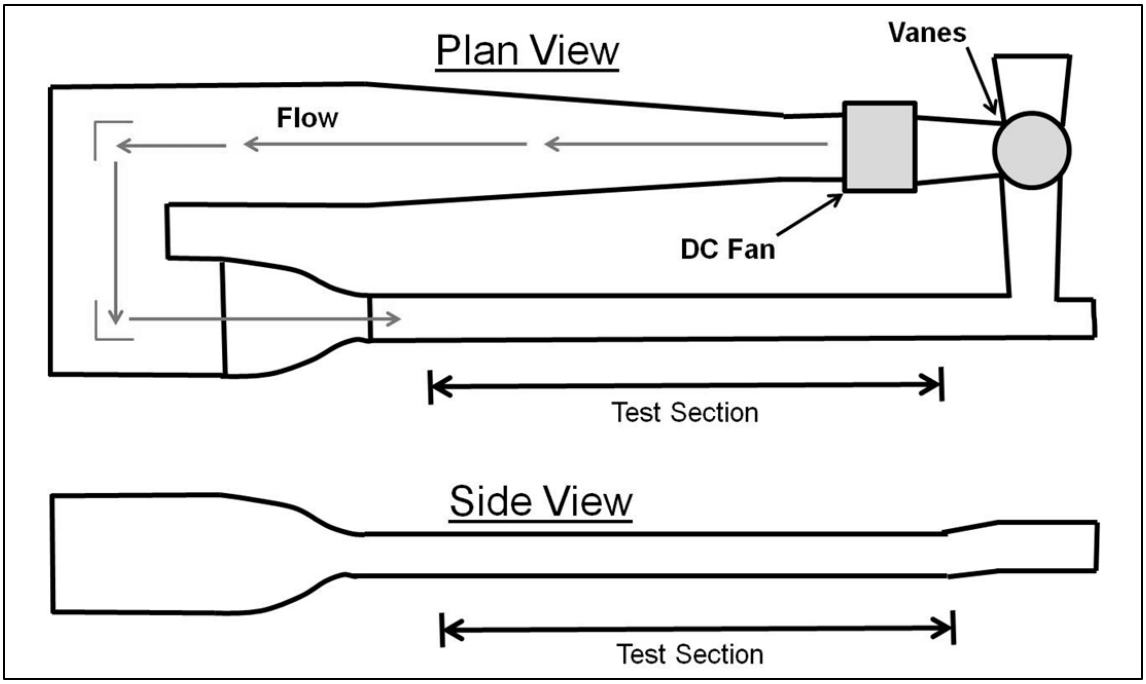

Figure 2-2. Typical closed circuit boundary layer wind tunnel

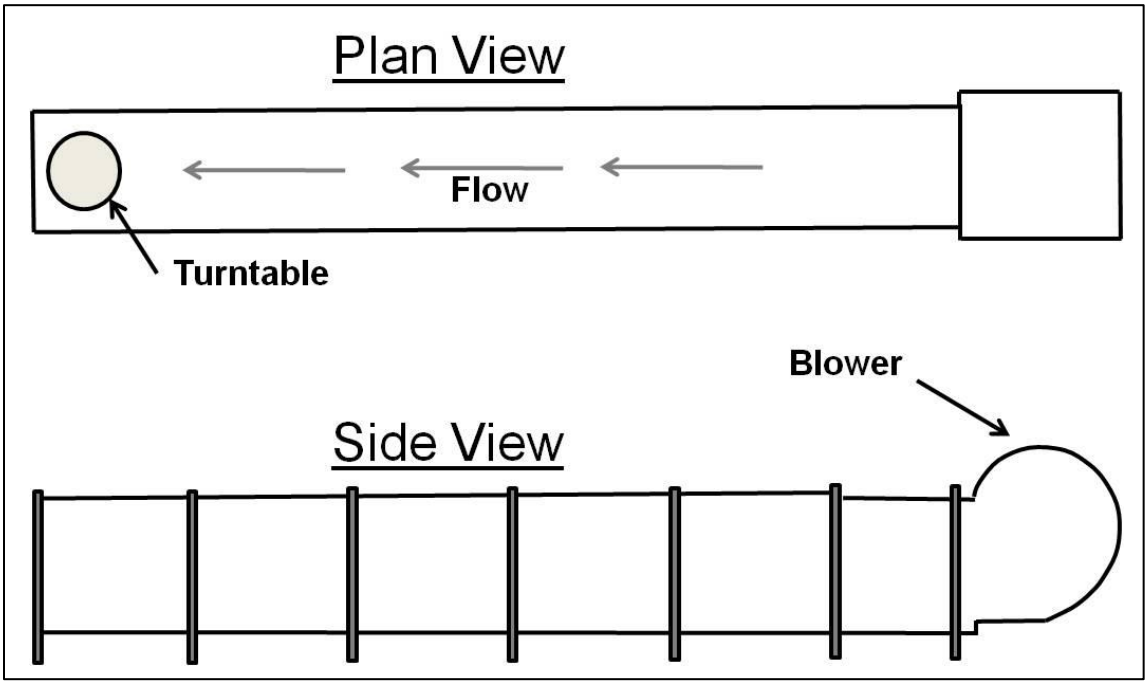

Figure 2-3. Typical open circuit boundary layer wind tunnel

The UWO Boundary Layer Wind Tunnel is an open-circuit with a working section approximately 25 m long by 2.5 m wide with a variable height roof with a mean height of 1.8 m (Davenport 1967). The long working section allowed for the development of thick turbulent boundary layers above an artificially roughened tunnel. Upon further investigation, it was observed that even with a long working section of roughness elements additional artificial thickening of the boundary layer was necessary. The initial approach for additional thickening the boundary layer was the inclusion of a 0.3 m solid wall "tripping board" at the entrance of the working section. Implementing the "tripping board" thickened the boundary layer without affecting the mean velocity profiles, but introduced additional longitudinal turbulence into the flow. This increase was later attributed the formation of separation regions in the flow (Talamelli et al., 2004). Next, a grid of horizontally oriented round bars was installed at a height of 0.3 m to produce a power law mean velocity profile with height. The grid produced a thickening of the boundary layer without increasing the turbulence. Davenport (1967) concluded that enough boundary layer flow characteristics were obtained to provide for adequate model scale (i.e. 1:100 and 1:200) structural investigations.

Open-circuit boundary layer wind tunnels have evolved since the initial commissioning of UWO's Boundary Layer Wind Tunnel (where roughness elements alone thickened the boundary layer) , and today some tunnels use active (oscillating) and passive (static) devices to better simulate atmospheric flow conditions (discussed in the following sections). The addition of passive devices, such as spires and honeycomb grids, at the beginning of working sections in combination with floor roughness elements began in the late 1960s. Passive devices are used to accomplish the dual purpose of a

mixing device and barrier in a single component, and effectively distributed the energy loss associated with the beginning of test sections (Talamelli et al., 2004).

Controllable Flow in Boundary Layer Wind Tunnels

A control system can be defined as subsystems and processes assembled for the purpose of controlling the outputs of other processes (Nise, 2004). The desire to model turbulent boundary layer flow led researchers to the development of the first generation of the boundary layer wind tunnel (BLWT), which could be classified as “passive” control system. During the 1970s, engineers began the development of using active controllers and passive devices to accelerate the growth of the boundary layer to reduce the required upstream development length. Other issues to be addressed in simulating natural wind condition are the ability to generate sharp edge gusts and produce larger turbulent length scales. With continual enhancement of computational and mechanical systems, engineers have been able to reduce the requirement of large upstream development lengths (Teunissen, 1974).

In the 1970s engineers coupled the need for smaller wind tunnel with a desire to reproduce varying velocity and turbulence profiles. Initial methods included the “counter-jet” technique (Nagib et al., 1976), in which upstream wall jets introduced flow with rapidly controlled injection velocities and angle with respect to the floor. This technique produces various boundary layer flow profiles rapidly and repeatedly. Other techniques described by Schon and Mary (1970) and Sluman et al. (1980) inject air through the wind tunnel floor in order to thicken the boundary layer. These techniques where initially perceived as a method to reduce upstream development length, but were also found to be as a cost effective upgrade to existing boundary layer wind tunnels to increase the thickness of the boundary layer. This provided for modification of existing

tunnels to produce multiple boundary layer flow conditions without the somewhat arduous task of changing the roughness element configurations of upstream development lengths.

A fundamental advancement during the 1970s related to low-speed controllable flows is the work completed by Teunissen (1974) at the Institute for Aerospace Studies located at the University of Toronto. Teunissen derived a multiple-jet boundary layer wind tunnel with independently controlled mean velocities and turbulence intensities. The method used a small open-circuit wind tunnel that was driven by an array of 64 jets whose velocities are individually controlled. By regulating the wind speed in each jet, 2-D boundary layer flows could be obtained with any desired velocity profile at any position in the test section. Use of tripping barriers and varying roughness elements produced desirable turbulence profiles independent for almost all velocity profiles. Teunissen's tunnel was one of the first that integrated active (variable jets) and passive (barriers and elements) devices to produce desirable flow conditions. One advantage of this tunnel was its ability to control the velocity profiles with the jets independently of the passive devices used to generate turbulence. At the time boundary layer tunnels were dependent on the mean velocity and roughness element configuration to created desired turbulence characteristics. Teunissen's wind tunnel provided for a simplified process in which desired boundary layer profiles where obtained. The overall improvement of the tunnel was a large reduction of its' overall length. However, a fundamental disadvantage of the multiple-jet tunnel in comparison with a typical boundary layer tunnel is the jet tunnel required approximately three times more power. Teunissen concluded that even with the drawback of large power consumption the

overall product was a simpler method for developing and adjusting desired flow conditions. (Teunissen, 1974)

Researchers continued building upon the idea of integrating active and passive devices to improve BLWT design throughout the 1980s. One issue not completely accounted for in Teunissen's work in 1974 was the difference of model turbulence length scale with those observed in atmospheric flow. Until this point, turbulence had been traditionally introduced with passive devices, such as upstream roughness elements and tripping barriers. Turbulence generated with these devices is dependent of the length of the upstream wind tunnel and mean velocity. The scale of the turbulence in these tunnels equals a fraction of the length of the test section, thus causing turbulent conditions in small wind tunnels to incorrectly modeled full-scale characteristics. Addressing this issue in the early 1980s, Bienkiewicz and Cermak (1983) created an actively controlled device to introduce turbulent energy into the flow. They constructed a pulsating grid from two grids oscillating in plane 180 degrees out of phase at low frequencies. As a result, the length scale of the turbulence was substantially increased over the test section in comparison to traditional passive devices.

With the continual development of computational and mechanical technologies, boundary layer wind tunnels have evolved into complex actively controlled systems. In the early 1990s, Kobayashi et al. (1992) built a BLWT with actively controlled velocity and turbulence devices. A gust generator consisting of a grid of plates and airfoils actively controls the longitudinal and lateral components of the desired boundary layer flow. A relationship between the angle of the airfoils and the percentage of blockage of

the plates for the wind components as a function of the input to the gust generators was realized. From this relationship an iterative approach of linearly scaling the spectral content of the controller inputs of the gust generator to the ratio of the target and measured spectral content of the wind components was conducted. This iterative approach was repeated several times until the measured spectra and phase angle converged to the targets. Implementation of actively controlled gust generators within the wind tunnel produced turbulence length scales that were an order of magnitude larger than turbulence length scales produced with traditional passive devices Generation of natural wind gust and unusual wind gusts was obtained and shown to be repeatable between tests (Kobayashi et al., 1994).

In the late 1990s, several multiple controlled fan wind tunnels (MCFWT) studies were carried out to improve boundary layer flow simulations (Nishi et al., 1999; Kikitsu et al., 1999; Cao et al., 2003). The Nishi et al. (1999) wind tunnel consisted of an array of 11 fans arranged vertically by 6 horizontal rows, for a total of 66 fans. Each fan is actively controlled through an open-loop (no feedback) inverter that is connected to a computer system. Lateral turbulence was introduced with oscillating airfoils that were actively driven by stepper motors per a prescribed input time history. Passive devices such as a honeycomb grid were also used to reduce high frequency turbulent vortices caused by the fan blades. Similar to the control system used in Kobayashi et al. (1994), Nishi used an iterative approach of scaling the spectral and phase content of the input signals of the fans in conjunction with vibrating airfoils to obtain desired boundary layer flow profiles (Nishi, 1995). Simulated mean wind velocity, turbulence intensity, turbulence scale and power spectral density profiles were observed to be in good

agreement with desired profiles. With additional testing, Nishi concluded that turbulent flow profiles could be achieved by modifying controller inputs to the fan array and airfoil system of an open-circuit MCFWT (Nishi et al, 1999). Kikitsu et al. (1999) and Cao et al. (2002) created their own MCFWTs by modifying the methodology presented by Nishi et al. (1999). Both tunnels were capable of converging to desired boundary layer turbulent flow characteristics.

Actively controlled wind tunnels have evolved from Teunissen's manually controlled multiple jet wind tunnel in 1974 to Kobayashi's actively controlled gust generators in 1992. Improvements within computational and mechanical systems have greatly reduced the need for large upstream development length for the development of atmospheric boundary layer flow. Actively controlled multiple fan wind tunnels have provided a proof of concept for the feasibility of full-scale atmospheric boundary layer testing without unrealistically large upstream development lengths. However, these actively controlled wind tunnels have focused on simulation of a singular terrain conditions and do not discuss a methodology to produce various terrain and site conditions.

Validation of Wind Tunnel Modeling with Full-Scale Experiments

Low-speed boundary layer wind tunnel testing requires full-scale validation to ensure proper modeling (Surry, 1991; Okada and Ha, 1992; Tieleman et al., 2003). Difference of pressure distributions in wind tunnel modeling and full-scale experiments is attributed to inaccurate simulation of fluid mechanics dimensionless properties (such as the Reynolds and Strouhal number). In bluff body aerodynamics, sharp corners tend to cause immediate flow separation independently of the Reynolds number of the flow, thus, bluff bodies Reynolds number simulation can be relaxed.

Aylesbury Experimental Building

One of the earlier experiments validating model and full-scale pressure distributions began in the late 1970s on the experimental full-scale house in Aylesbury, England. The Aylesbury Experimental Building was constructed by the Building Research Establishment. It had a variable pitched roof that could be reconfigured into a 5, 22.5 or 45 degree roof slope (Eaton and Mayne, 1975). A primary purpose for this research was to address and validate issues in wind tunnel modeling techniques for low rise structures. In 1979, UWO researchers addressed this by developing an identical 1:500 scaled model of the Aylesbury Experiment Building. The wind tunnel roughness elements where varied to accurately model scaled terrain conditions. Researchers concluded the mean model results agreed well with mean full-scale data when the surrounding terrain conditions are accurately modeled. As model results are sensitive to terrain details it is essential to model turbulence intensities adequately (Apperley et al., 1979).

The Wind Engineering Research Field Laboratory Test (WERFL) Building

The Wind Engineering Research Field Laboratory (WERFL) in Lubbock, Texas was constructed in 1989 on the campus of Texas Tech University. Since its commissioning (Levitan and Mehta, 1992), WERFL has produced quality data that are commonly used within wind engineering for wind tunnel validation (e.g. Tieleman, H. et al., 2003; Ho, T. et al., 2005; Surry, D., 1991; Cheung, J et al., 1997; among others). WERFL site conditions contain anemometric and pressure data collected on the full-scale test building facility (Figure 2-4). In this study, WERFL data was used for validation of a 1:10 scaled wind tunnel test to be discussed within Chapter 5.

Figure 2-4. Texas Tech University's Wind Engineering Research Field Laboratory (WERFL) test building and 48.7m meteorological tower in Lubbock, Texas (WERCS,2010)

Site wind conditions are measured from a guyed lattice 48.7 m meteorological tower instrumented at five heights: 2.4 m, 3.9 m, 10 m, 21.3 m, and 48.7 m. Instrumentation was mounted on an arm that cantilevers away from the tower to reduce wake effects from the tower on the instrumentation. Three R.M. Young Gill UVW anemometers (Model 27005) are mounted at all five heights to measure *u, v,* and *w* wind components to determine wind speed and wind direction.

The test building measures approximately 9.1 m wide by 13.7 m length by 3.9 m height. The building is attached to a rigid frame which is detached from the foundation. Wheels are attached to the steel frame at the corners of the building frame resting on a circular steel rail, in which hydraulic jacks raise the building 3 in. onto the wheels allowing the building to rotate. This system provides for 360 degrees of rotation for

control over the wind angle of attack (Levitan, 1992). Differential pressure transducers connected to a data acquisition system record differential pressures on the building surface and internal pressures inside the structure while simultaneously recording data from the meteorological tower. Data is post processed after the wind event to determine instantaneous non-dimensional pressure coefficients ($C_p(t)$), which are derived from the ratio of the differential pressure and a reference velocity pressure (Eq. 2-1):

$$\frac{\qquad}{\qquad} \tag{2-1}$$

where is the instantaneous differential pressure (between tap and reference pressure), is the density of air and, is the 3 second gust wind speed at mean roof height (3.9 m) from the instrumented meteorological tower. From the instantaneous pressure coefficients and anemometric data sampled at 30 Hz, the mean, minimum, maximum, and root mean squared (rms) pressure coefficients (Cp_{mean}, Cp_{min}, Cp_{max}, and Cp_{rms} respectively) are derived.

The quantity and location of the pressure taps have changed since the original work of Levitan and Mehta (1992), though the 5 digit pressure tap classification and angle of attack (AOA) definition have remained the same (Figure 2-5). The 5 digit pressure tap designation, *sxxyy*, aids in determining the location of the tap on the test building, where *s* dictates the surface, *xx* describes the distance in feet from a defined origin on the surface in the x-direction, and *yy* described the distance in feet from the defined origin on a surface in the y-direction. There were 204 full-scale tap locations used for this research.

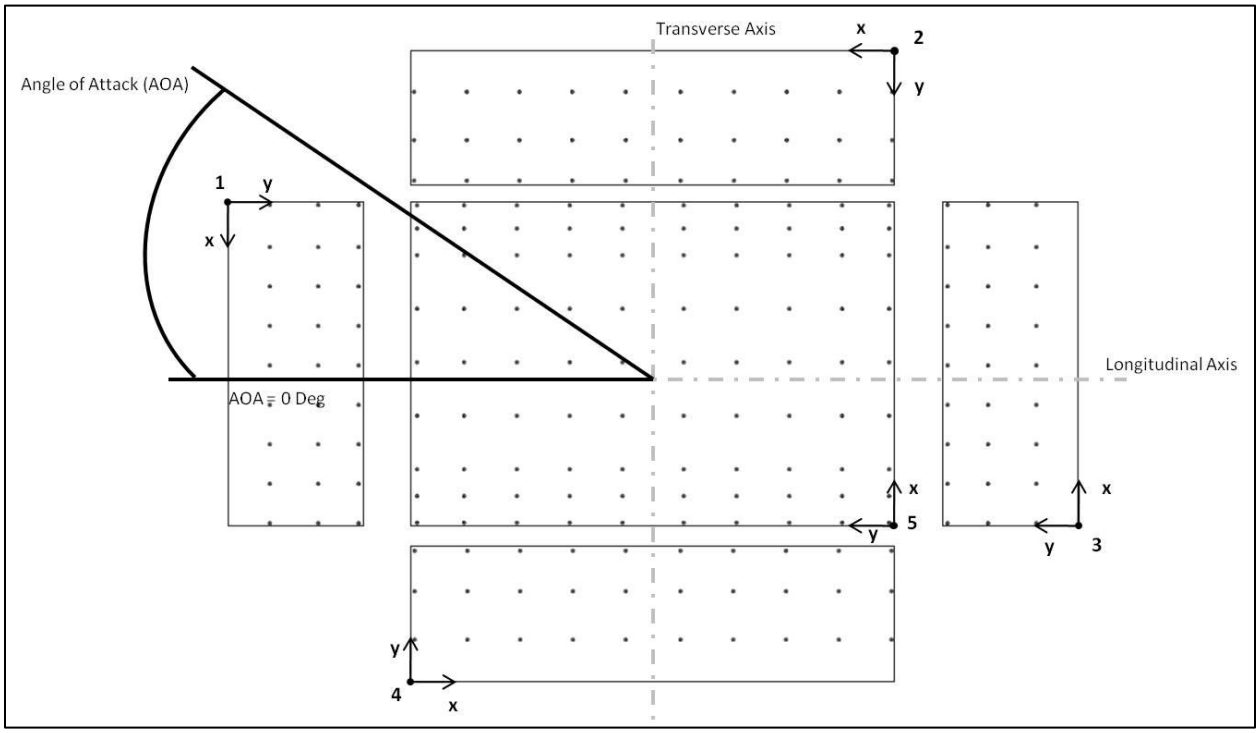

Figure 2-5. Exploded view Texas Tech University's Wind Engineering Research Field Laboratory (WERFL) test building with pressure tap location and angle of attack reference

One example of validation of wind tunnel testing with the WERFL building was the Surry (1991) study completed at the UWO's Boundary Layer Wind Tunnel Laboratory. As the wind tunnel had previously been established for flow conditions similar to those at the WERFL site, modifications to develop scaled flow condition were minimal. With accurate scaled flow conditions normal to the ridge, the model and full-scale data were in very good agreement (i.e. mean and peak pressure coefficients). It was noted that when wind flow conditions were oblique to the ridge of the building there were significant differences between peak coefficients between the model and full-scale testing. The differences were attributed to the variations within variation of gust or non-stationarity of storms (Surry, 1991).

Validation of wind tunnel modeling with full-scale experiments has been limited based upon few full-scale experimental buildings used for comparison. Complex building configurations with hip, gable and other complex geometry have a minimal about of full-scale data for model scale comparison.

Multiple Fan Full-Scale Testing Facilities

In the late 1990s, the National Research Council (NRC) and the U.S. Department of Energy proposed the development of a full-scale testing facility dedicated to wind damage mitigation (NRC, 1999). At the time there were large enough wind tunnels with test section that could immerse full scale residential structures. For example, the NASA Ames research facility is sufficiently large enough to test full-scale residential structures under design level events; however, this facility operates as closed-circuit wind tunnel created for aeronautical applications primarily. This would not suffice for destructive residential construction testing because the fans, screens, etc. would be susceptible to damage from structural debris entrained into the recirculating flow from the structure.

Resulting from Kennedy's (1999) work, wind engineering researchers created large-scale testing apparatuses ((Masters et al., 2008, Leatherman et al., 2007). capable of recreating design level wind loads and wind-driven rain scenarios to evaluate the performance of low rise buildings.

University of Florida Windstorm Simulator

The University of Florida has constructed a 2.09 MW (2800 hp) hurricane simulator (Figure 1-1A) capable of replicating turbulent wind and rain loads on a 3 m by 3 m section of a full-scale residential structure. Four 0.52 MW (700 hp) Detroit Diesel marine engines spin eight hydraulic actuated vane axial fans to produce 1676+ Pa

stagnation pressures. Research for this simulator has primarily been residential water intrusion mitigation of fenestration and soffit systems (Masters et al., 2008).

Florida International University Wall of Wind

Researchers at Florida International University constructed what is referred to as the Wall of Wind (Figure 1-1B) at the International Hurricane Research Center in Miami, FL. The Wall of Wind is capable of producing 52 m/s (125 mph) wind speed and wind driven rain scenarios on single story residential buildings. Research with this apparatus has primarily focused on mitigating water intrusion through secondary water barriers and rooftop equipment failure mechanisms (Leatherman et al., 2007).

Insurance Institute for Business & Home Safety (IBHS) Research Center Full-Scale Test Facility

The Insurance Institute for Business & Home Safety (IBHS) constructed the IBHS Research Center Full-Scale Test Facility in Richburg, South Carolina (Figure 2-6). The core facility is an open-jet wind tunnel (Figure 2-7) with a test chamber: 44.2 m (145 ft) wide by 44.2 m (145 ft) long, and a clear interior height of 18.3 m (60 ft). Wind flow is produced by 105 1.68 m (5.5 ft) diameter vane-axial fans with 350 hp medium voltage electric motors that push air through a 15 duct (tube) contraction structure. The flow through each duct is independently controlled using variable frequency drives that regulates power to the fans. At full power, the facility requires 30 MW. Fans and controls were designed to simulated flow characteristics of a variety of wind events including Category 1, 2, and 3 hurricanes, extra-tropical windstorms, and thunderstorm frontal winds. The test chamber can subject full-scale one- or two-story residential structures and commercial buildings to a variety of wind related events.

Figure 2-6. Aerial view of the Insurance Institute for Business & Home Safety (IBHS) Research Center (http://www.disastersafety.org/, 2010)

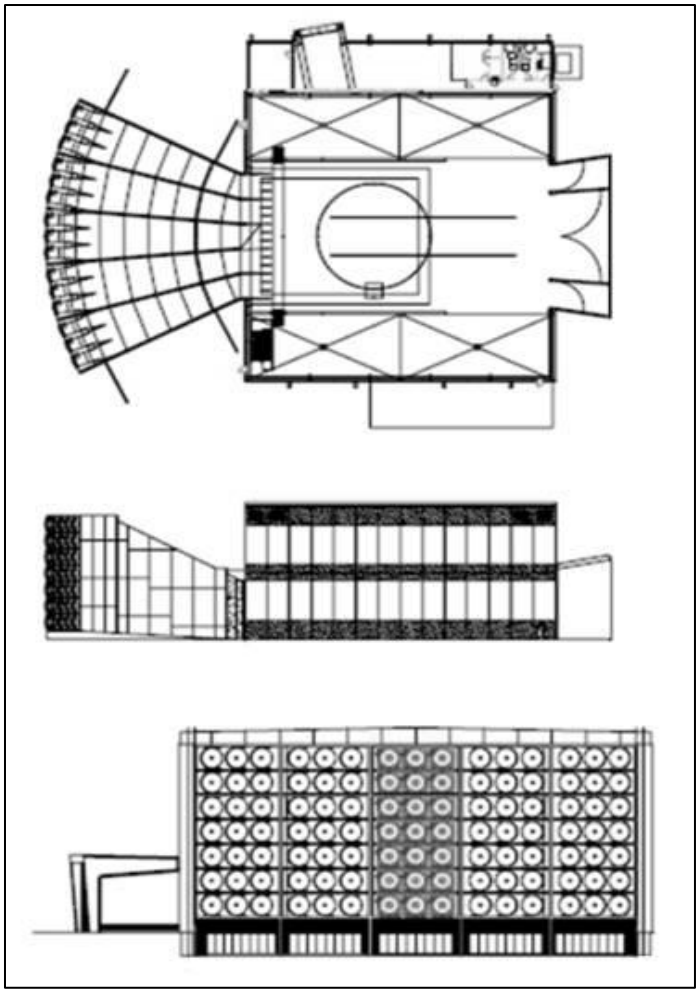

Figure 2-7. Insurance Institute for Business & Home Safety (IBHS) Research Center Full-Scale Test Facility plan and elevation views (IBHS, 2010)

IBHS's Research Center is capable of completely immersing a full-scale structure in design level flow conditions. Future testing will continue to contribute the knowledge base for better understanding of the building envelope.

Summary

The evolution of the aeronautical wind tunnels to model industrial aerodynamics and civil engineering applications has been described. Improvements of mechanical and computational systems have reduced the need for large development length with the aid of actively controlled gust generators and multiple controlled fan wind tunnels.

This chapter presented background information that contributed to the methodology and validation techniques to be discussed in Chapter 3 and 4.

CHAPTER 3
PROPOSED METHOD OF EXPERIMENTAL MODELING OF THE UNOBSTRUCTED ATMOSPHERIC BOUNDARY LAYER

Introduction

In contrast to boundary layer wind tunnels (BLWT), multiple controlled fan wind tunnels (MCFWT) do not use a roughness element grid to develop boundary layer flow conditions. Instead, flow control techniques are implemented to simulate prescribed mean velocity and turbulence profiles, spectral content and integral length scales. This study specifically focuses on the simulation of marine, open and suburban terrain flow conditions following the terrain stratification adopted by most modern wind load provisions (e.g., Exposures B, C and D in ASCE 7-10). The method matches longitudinal (*u*) and lateral (*v*) flow characteristics. Although control of the vertical (*w*) component is not addressed, the technique described herein may be adapted to include all three components. A case study using the method is presented in the next chapter.

Proposed Method

A new calibration procedure was established for a MCFWT with a 2D array of fans that drives air through an array of vertically spanning airfoils to impart directionality to the flow. A control measure for the vertical component is not presently considered, although extending this approach from a 2D calibration (*u*- and *v*-velocity components to a 3D calibration (*u*-, *v*-, *w*- velocity components) is feasible.

In contrast to spectral-based methods (e.g., Kobayashi and Hatanaka, 1992; Kobayashi et al. 1994) that reshape the desired spectra to generate command signals sent to an array of fans, the approach relies on the direct simulation of scaled wind speed and direction records collected during field experiments. Scaling is a two-step process. First, the full-scale wind speed and direction records are converted to their

model equivalent using the reduced frequency relationship. Second the ‘target’ wind speed and direction records are translated and dilated until the mean velocity and turbulence profiles are realized (i.e. mean and standard deviation of “target” records are modified until convergence)

The procedure is based upon the assumption that the desired boundary layer (BL) characteristics can be simulated by converting a single full-scale anemometric record into separate command signals for each row of fans in the MCFWT. The choice of profiles of mean velocity and longitudinal turbulence intensity determines the required scaling at each fan level. While it would be desirable to use data obtained from multiple anemometers arrayed vertically on a mast as inputs, the use of vertical airfoils that move concurrently does not allow for it. A common time scale couples the wind velocity and direction records. This condition necessarily introduces artificial correlation along the vertical extent of the jet, however the variation in the mean velocity with height acts to decorrelate the vertical structure as the wind advects away from the jet toward the test section.

In contrast to other methods that used open loop control (i.e. no feedback), a closed-loop control strategy is implemented to determine the command signals for the fan bank and the airfoil array. Controllability is essential to this approach because a given wind speed record (i.e. the ‘target’) is iteratively translated and dilated until the time histories of the target and the measured velocity above the test section closely track one another. This ensures good agreement between the spectra, length scales and probability distributions of the velocity components.

Procedure

Part 1: Determination of the wind speed and direction sequences

1. Select a reference full-scale wind speed (u_f) and direction (θ_f) records for simulation in the tunnel
2. Compute the model-scale time increment using the reduced frequency relationship

(3-1)

Where n is the sampling frequency of the time series, L is the characteristic length and U is the mean wind speed. The subscripts m and f denote model and full-scale, respectively. The model scale time increment dt_m is the inverse of n_m.

3. Let z_i denote the vertical distance between the center of the i^{th} fan and the floor of the MCFWT. Convert u_f to its model-scale equivalents,

by multiplying the full-scale record by the ratio of the model velocity desired at height z_i and the mean velocity of the full scale record selected in step 1:

(3-2)

Note that u_f is the actual wind speed measured by the anemometer (not the longitudinal component). The values are computed from the log law using,

(3-3)

Where is the friction velocity, k is von Karman's constant (0.40) and z_0 = aerodynamic roughness length. The user selects based upon the desired reference wind speed in the tunnel. The z_0 value is chosen to match the representative upwind terrain conditions at the full-scale data measurement site.

4. While keeping each constant, modify each to impart the desired longitudinal turbulence intensity profile by rescaling the amplitude of the signals appropriately for each height. This profile should be consistent with the selection of z_0 in the previous step. In the case study that follows, we used the modified form of the Harris and Deaves (1981) variance model given in Engineering Science Data Unit ESDU (1983) and described in Vickery and Skerjl (2005) to compute the standard deviation (σ_u).

(3-4)

where is the friction velocity, is the coriolis force and is the scaling parameter,

(3-5)

5. The target wind direction (θ) record at model and full-scale are identical ($\theta_m = \theta_f$). No modification is required.

Part 2: Approach flow calibration

The multiple controlled fan wind tunnel (MCFWT) is calibrated using the target model-scale wind speed and direction records from Part 1. The calibration procedure has three stages (see Figure 3-1). First, corrections are made to achieve the desired mean longitudinal velocity (U) profile. Second, the longitudinal turbulence intensity (TI_u)

profile is corrected. The algorithm then sequentially cycles through the U_m, z and TI_u corrections until both profiles match. Third, the lateral turbulence intensity (TI_v) is calibrated. The algorithm then sequentially corrects the U_m, z, TI_u, and TI_v profiles until it converges on a solution. High frequency measurements of these quantities at each fan level above the test section are required. Multiple port pressure probes (e.g. Cobra probes) are suitable for this task. If multiple instruments are not available efficiency of the method is reduced tremendously.

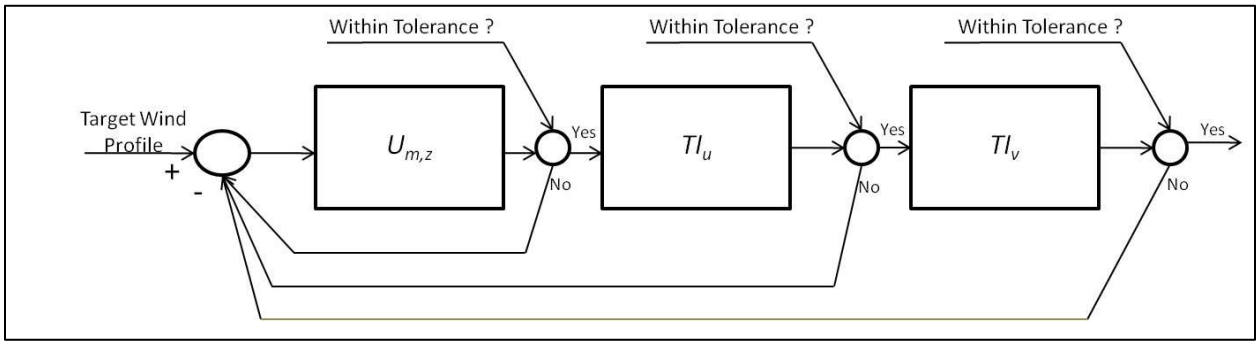

Figure 3-1. Flow diagram for convergence to desired wind profile

Continuing from Part 1,

6. Align the airfoils (for lateral turbulence injection) perpendicular to the face of the jet (i.e. $\theta = 0^o$).
7. Set the initial fan speeds to match the desired vertical profile of mean velocity (i.e.). The initial value can be determined from a single fan calibration. Do not introduce the longitudinal turbulence in this step.
8. Measure the mean velocity at each fan height. At each fan level, iteratively rescale the mean of the command signal to each fan height until the mean wind speed values converge to their targets using Eq. 3-6. We prescribe

the term to represent the mean velocity (Eq. 3-6 is reused in steps 10 and 13 to rescale the longitudinal and lateral turbulence intensities, respectively).

(3-6)

is the new input mean velocity sent to the control, is the current input mean velocity sent to the control, is the measured mean velocity, is the target mean wind velocity defined in Part 1 (i.e.), and the term is a correction parameter used to scale the magnitude of the wind speed from one iteration to the next. Based upon trial and error, = 4 appeared to be a reasonable value for the case study presented herein.

9. Once the mean velocity profile converges to within an acceptable user-defined tolerance, introduce the longitudinal turbulent component of the wind speed into the command signal, holding the average input wind speed constant.
10. Measure TI_u at each height. Iteratively apply the correction shown in Eq. 3-6 by scaling the standard deviation of the wind speed input to the fan (i.e.) holding the mean wind speed constant until the TI_u profile converges to an acceptable user-defined tolerance.
11. Repeat steps 8-10 until and TI_u converge to their target profiles.
12. Introduce the lateral turbulence component by commanding the airfoils to follow θ_f.

13. Measure TI_v at each fan height. Iteratively apply the correction shown in Eq. 3-6 by scaling the amplitude of the airfoil direction signal (i.e. $\bar{\ }$, where A = amplitude) until the TI_v profile converges to within an acceptable user-defined tolerance.
14. Repeat steps 8-13 until U, TI_u and TI_v converge to their target profiles.

Limitations

A primary goal of this research was to develop a simple approach to simulate the BL characteristics in a manner that is suitable for automation. Some limitations arose due to the experimental configuration.

First, rescaling the same velocity record to create the command signals for fan inputs imposes strong correlation along the height of the jet. This condition is valid at low frequencies, as a result of large eddies advecting through the test section. However, the spatial coherence of natural wind reduces with frequency and distance. It is not possible to directly affect this behavior with the current configuration, although dissipation and mixing between the jet and test section acts to decorrelate the signals.

Second, this approach was only evaluated using records of wind direction which did not exhibit large departures from the mean wind direction. The test configuration (discussed in the following section) had a maximum wind direction sweep of 30^o, which greatly simplified the development of the fan and airfoil controls. Larger directional variations would cause the static pressure drop across the airfoils to deviate significantly from the straight line wind case ($\theta = 0^o$), which would reduce the flow rate.

Third, the time increment (dt) computed in Step 2 is only strictly valid for the mean wind speed used in its computation. dt should vary with height since a mean velocity

profile was imposed. Slowing down or speeding up the signal is not possible because the model configuration does not allow for variation of the wind direction with height.

Summary

A new calibration procedure was established for a MCFWT with a 2D array of fans that drives air through an array of vertically spanning airfoils to impart directionality to the flow. A control measure for the vertical component is not presently considered, although extending this approach from a 2D calibration (*u*- and *v*-velocity components to a 3D calibration (*u*-, *v*-, *w*- velocity components) is feasible. Chapter 4 will implement this method into a 1:10 scaled MCFWT and discuss results.

CHAPTER 4
A CASE STUDY OF EXPERIMENTAL MODELING OF THE UNOBSTRUCTED ATMOSPHERIC BOUNDARY LAYER

Introduction

The method described in the previous chapter was applied to the simulation of marine, open, and suburban exposure BL profiles in a 1:10 scale model of the IBHS Research Center Test Facility in Richburg, SC (Figure 2-6). At the core of the facility is a large test section chamber (Figure 2-7) capable of subjecting full-scale one and two story residential or commercial buildings to Saffir-Simpson Category 3 hurricane wind induced pressure loading (Simpson 1974, Saffir 1973). Wind is generated by 105 vaneaxial fans that have a combined maximum 30 megawatt draw. The fans are grouped into cells that are individually ducted to form a jet that drives air into the test chamber. At the exit of the jet, a horizontal array of vertically spanning airfoils redirects the air in the horizontal plane to recreate the effects of wind directionality.

Model Multiple Controlled Fan Wind Tunnel

The 1:10 scale model and its dimensions are shown in Figures 4-1 and 4-2, respectively. An array of twenty one 30 cm diameter propeller fan modules arranged in 3 rows by 7 columns configuration moves air through a contraction duct that terminates at a 2.1 m W by 0.9 m H opening (jet) into a 4.9 m L by 4.6 m W and 1.8 H test chamber. An array of vertical airfoils located at the exit of the jet redirect the wind to create lateral turbulence. The airflow advects over the test section and is exhausted through a large diffuser attached to the downstream wall of the test chamber.

Figure 4-1. 1:10 scale model of the Insurance Institute for Business & Home Safety Research Center Full-Scale Test Facility

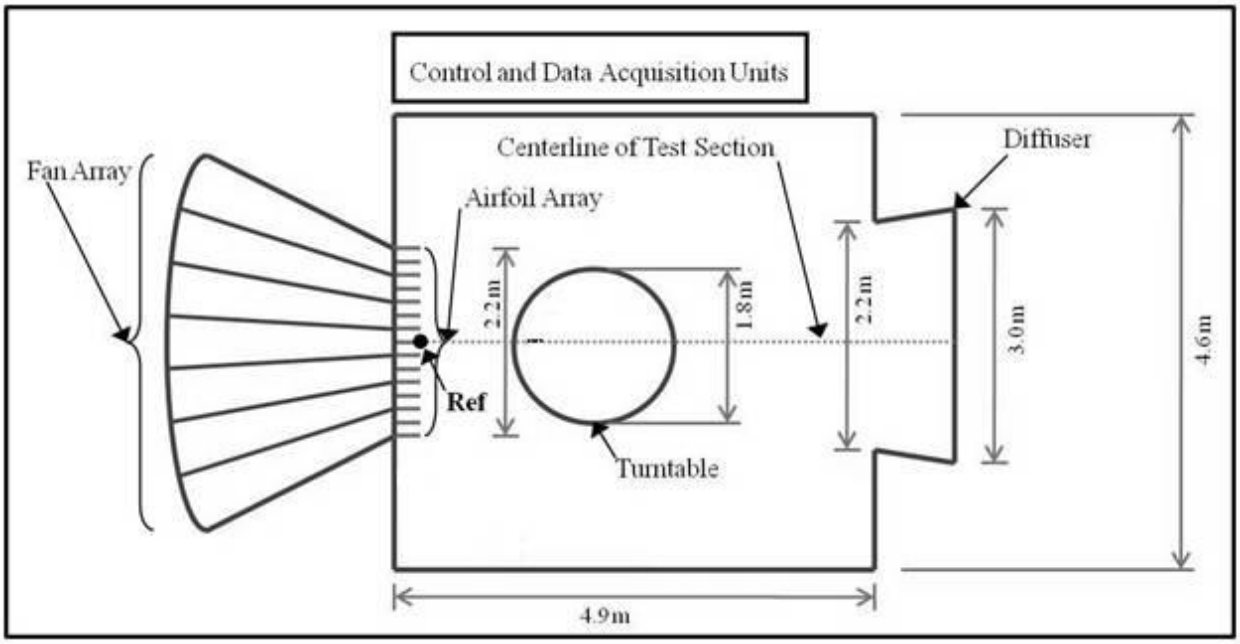

Figure 4-2. Plan view of 1:10 scale model of the Insurance Institute for Business & Home Safety Research Center Full-Scale Test Facility

Details about the hardware components follow:

1. The fan module consisted of an AstroFlight Inc. cobalt motor with a 31:19 drive reduction (Figure 4-3a), a 30 cm Master Airscrew nylon propeller, and an AstroFlight Inc. 207 D hydro-speed controller (Figure 4-3b). National Instrument PXI-6602 timing and digital I/O modules send varying pulse width modulation signals to the hydro-speed controllers to regulate power from a constant amplifier. Power was provided by two Sorenson model number DCR 16-310T power supplies

2. Custom built photoelectric laser diode tachometers measured blade passage frequency to determine the rotational speed of the propellers. Output signals were read by frequency counters on National Instruments PXI-6602 timing and digital I/O modules (Figure 4-3c).

3. Fifteen neutral shape (equal upper and lower camber), vertically oriented airfoils were distributed evenly across the exit of the jet (Figure 4-4a). Dimensions of the airfoil include a 0.9m height and a chord length of 12.7 cm. Futaba high torque 180^{o} rotation servos (Figure 4-4b) rotated the airfoil at the ¼ chord point (aerodynamic center).

Figure 4-3. Components of fan module a) AstroFlight Inc 640G cobalt motor (left) b) AstroFlight Inc 207D digital hydro-speed controller (middle) c) Custom photoelectric tachometer (right)

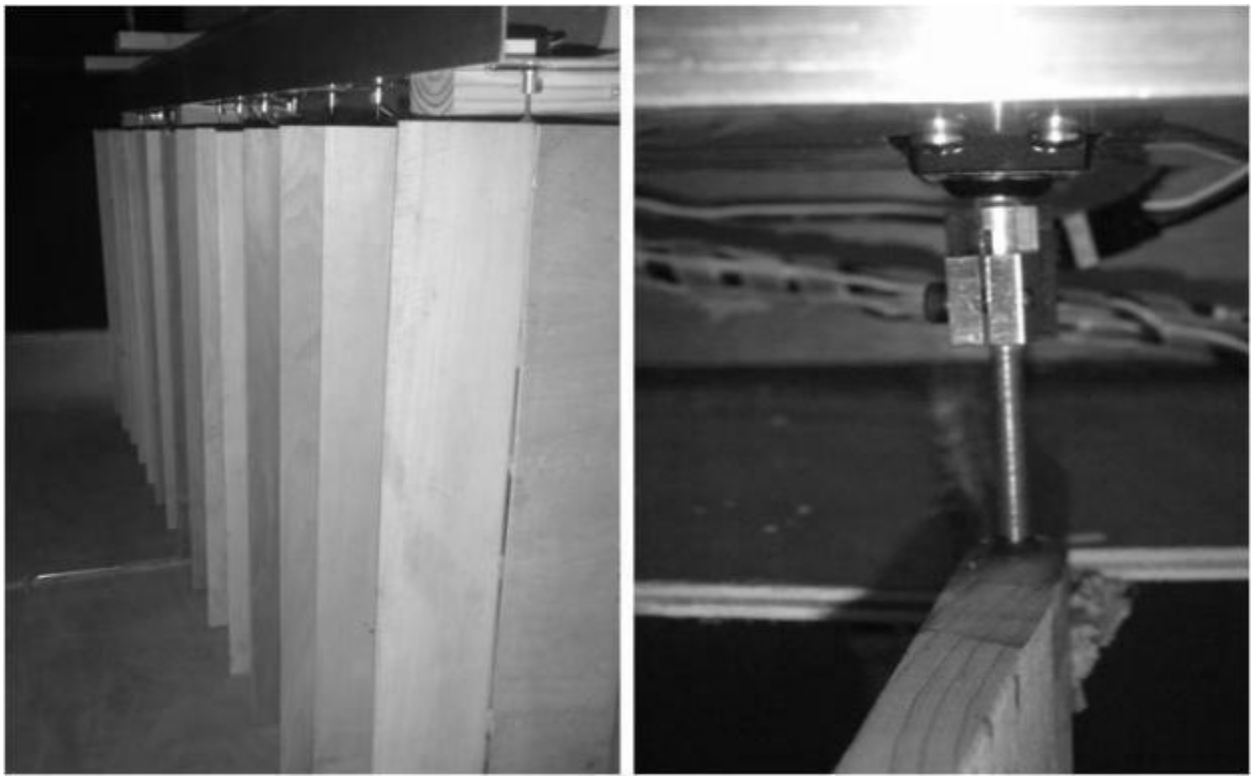

Figure 4-4. Vane airfoil system a) Array of 15 airfoils at exit of jet into test chamber (left)
b) Futaba servo high torque direct drive detail (right)

Development of Fan and Airfoil Controllers

An ANSI/ASHRAE 51-07 (American National Standards Institute/American Society of Heating, Refrigerating and Air Conditioning Engineers) test apparatus (Figure 4-5) was constructed to develop flow and control characteristics of a single fan module. The apparatus consisted of a 30.5 cm diameter by 3.1 m long PVC circular duct with a fan module on the inlet side and an adjustable servo actuated custom butterfly valve at the exit. Rotating the valve increases air resistance causing the fan to produce additional static pressure at a reduced flow rate for the development of the fan curve. The apparatus is instrumented with four Dwyer MS-321-LCD differential pressure gauges to record total and static pressure from a Dwyer SSS-1003 lightweight average flow sensor and a Dwyer 160E pitot tube. Concurrently, National Instrument multifunction

16-bit data acquisition cards recorded data and simulated pulse width modulated signals to the fan speed controller and butterfly valve servo. The angular velocity and current of the fan module was recorded at the direction of a custom-built data acquisition program to develop the flow and control characteristics of a single fan module.

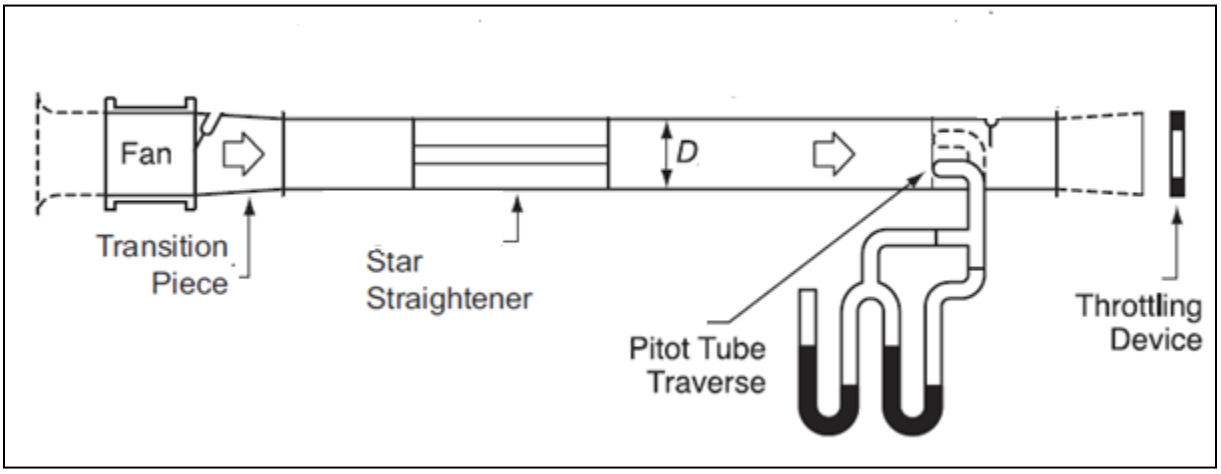

Figure 4-5. ANSI/ASHRAE 51-07 Test Apparatus

Implementation of an open-loop (non-feedback) controller was initially investigated to recreate the desired longitudinal turbulence characteristics within the test apparatus. A polynomial curve was fitted to the fan RPM versus the pulse width modulation (PWM) input to the system's speed controller. A prescribed velocity time history (previously discussed Ch. 3) was then converted to an input PWM based upon the RPM to mean wind speed relationship. After removing the delay (dead-time) in the response of the fan system, the correlation coefficient between the target and measured RPM traces were on the order of 95% or larger, which was consistent with measurements by Cao and Nishi (2002, 1999). However, the difference between the coefficients of variation of the target and measured RPM was approximately 8%. The discrepancy in the

coefficient of variation is attributed to the inertial effects of the motor and propeller, causing the fan to accelerate faster than it can decelerate.

Next, a closed loop proportional-integral-derivative (PID) controller was implemented. PID controllers are one of the more frequently used controllers within mechanical and industrial applications. The fundamental idea of the PID controller is to iteratively drive the error between target and measured values to zero by supplying the mechanical system an input derived from its performance. Eq. 4-1 and Figure 4-6 represent the PID control algorithm implemented in this research, where is the error between the target and measures values at time t, is the change in the measured value, while K_p, K_i, and K_p are constants chosen that meet the desired performance of the controller. This equation produces an output signal to the controlled system to drive its error to zero.

(4-1)

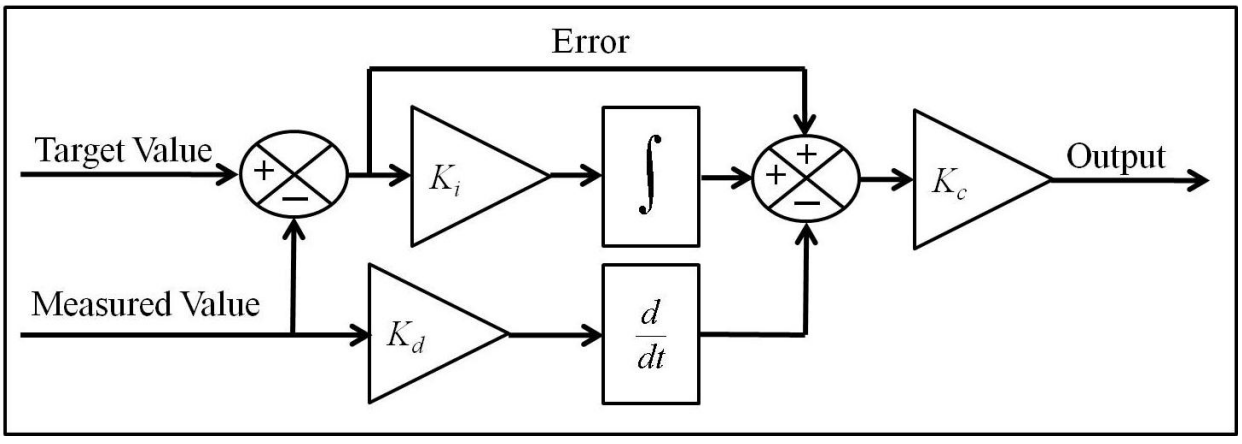

Figure 4-6. Proportional-Integral-Derivative (PID) control algorithm block diagram

A point by point PID controller for a fan system was implemented using National Instrument's LabView 8.6 Control and Design &Simulation PID subroutine at 50 Hz.

The correlation between the input RPM and measured RPM was consistently 95% or higher. However unlike the open loop controller, the closed loop PID controller produced a difference in coefficients of variation between the target and measured RPM that was consistently 1% or less. Comparisons of the controllers' performance are shown in Figure 4-7 where the vertical axis represents the fan module's RPM and the horizontal axis represents time.

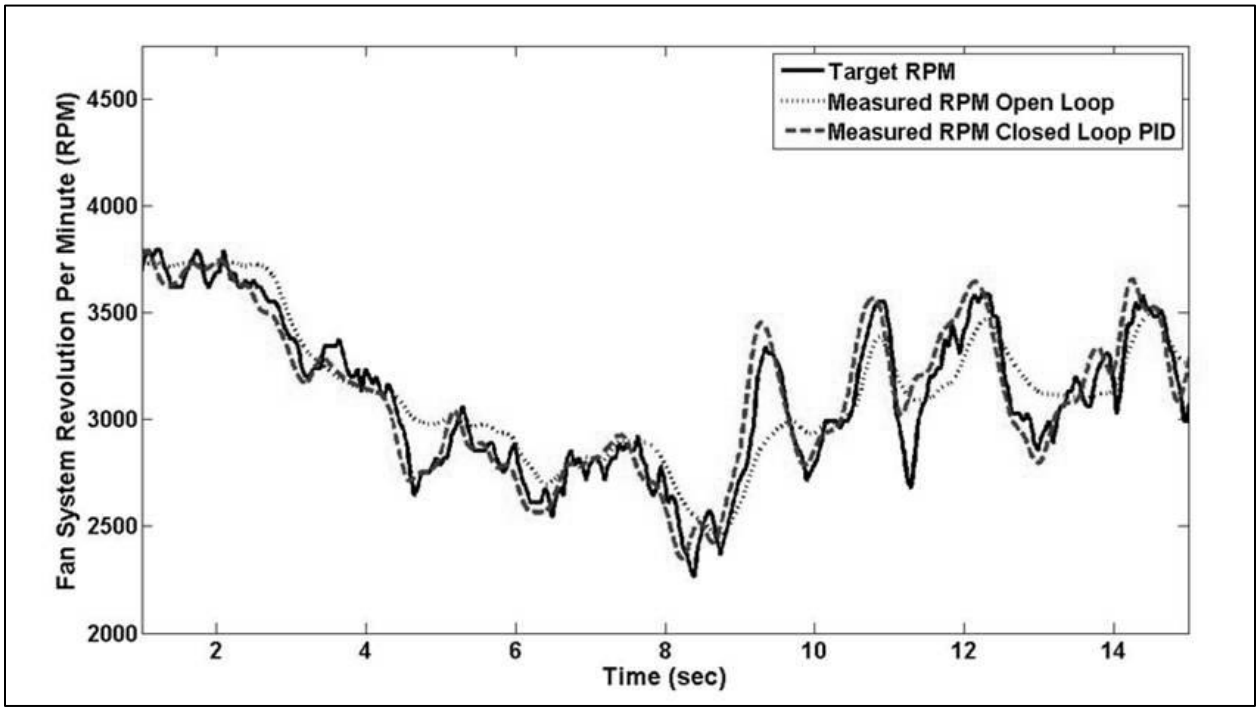

Figure 4-7. Comparison of open loop and closed loop Proportional-Integral-Derivative (PID) controllers with a target Revolution Per Minute (RPM)

The airfoil array was actuated by high torque servos with built-in closed loop PID controllers that cycled at a rate of 50 Hz to introduced later turbulence characteristics. Accuracy was determined to not be an issue, so details on this configuration are omitted here. An open loop control input without feedback was sufficient for achieving the desired movement of the airfoils.

Instrumentation and Measurement Locations

Three Turbulent Flow Instrument (TFI) Cobra Probes (Figure 4-8) collected 3d velocity data above the turntable in the test chamber. Characteristics of the probes include a maximum usable frequency of 2000 Hz (sample frequency is about 10kHz) at an accuracy of ±0.1 m/s at a flow angle ±20°. With a mean flow angle of 0° in pitch and yaw a turbulence intensity of 40-50% can be measured. The instruments were mounted at the centerline of each fan level in a column array as shown in Figure 4-9 at the seven test locations shown in Figure 4-10. Probes were mounted forward into the flow to prevent wake interference from the support arm and body of the probe.

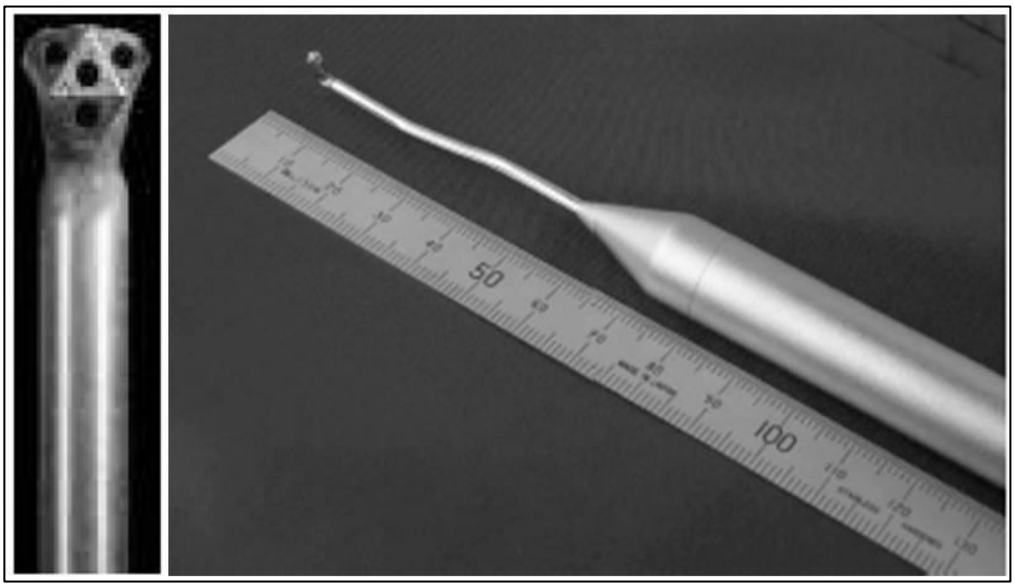

Figure 4-8. Turbulent Flow Instrument (TFI) Cobra Probe (http://www.turbulentflow.com.au, 2011)

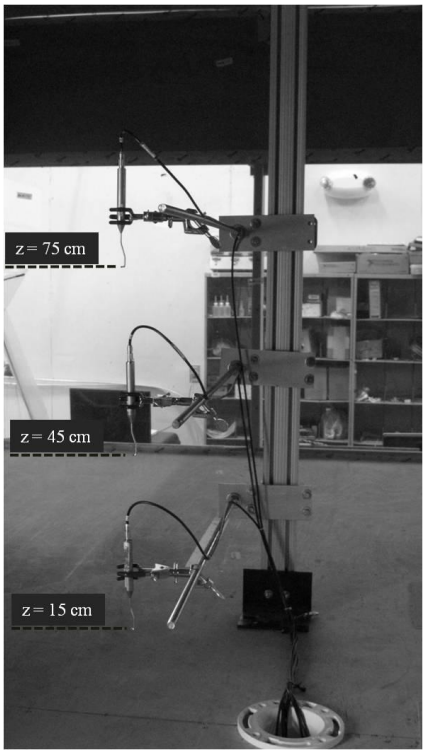

Figure 4-9. Cobra probe gantry

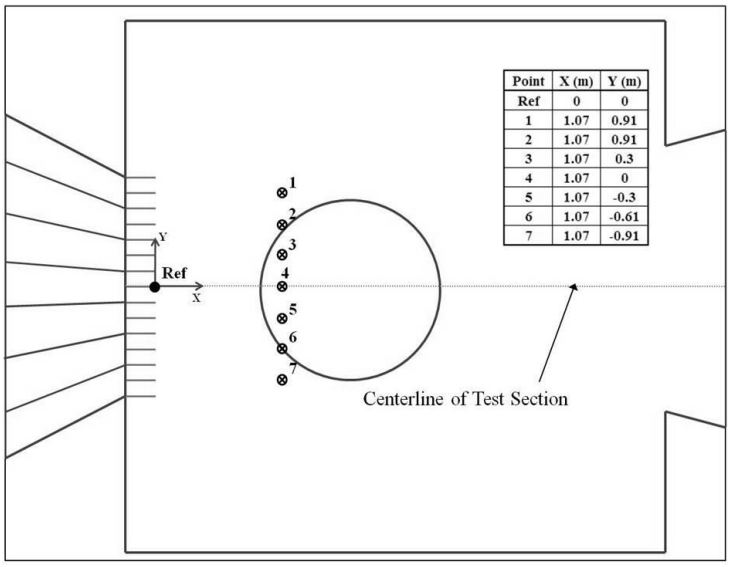

Figure 4-10. Plan View of the 1:10 Scale Insurance Institue for Businees & Home Safety Research Center Test Facility Test Locations

Selection of the Wind Speed and Direction Records

The target wind speed and direction records shown in Figure 4-11 were obtained from a 10 m wind velocity measurement collected on an instrumented tower at the

Texas Tech University Wind Engineering Research Field Laboratory (WERFL; Levitan and Mehta, 1992). Characteristics of the record include U_f = 11.25 m/s, TI_u = 0.173, TI_v = 0.125, and a 68.3 m longitudinal length scale. The up wind aerodynamic roughness length (z_0) is 0.013 m. This record was standardized and rescaled at each fan level to achieve the desired profiles for marine (z_0 = 0.005 m), open (z_0 = 0.03 m) and suburban (z_0 = 0.3 m) exposure following the procedure outlined in Chapter 3. The model scale time-increment was computed from Eq. 3-1 using the full-scale metadata (f_f = 10 Hz and U_f = 11.25 m/s), the geometric ratio of the full-scale to the model buildings (= 10) and the wind speed in the model (m/s). From Eq. 3-1, f_m= 50 Hz which is five times faster than full-scale. Therefore, three minutes at model scale is equivalent to 15 minutes at full-scale.

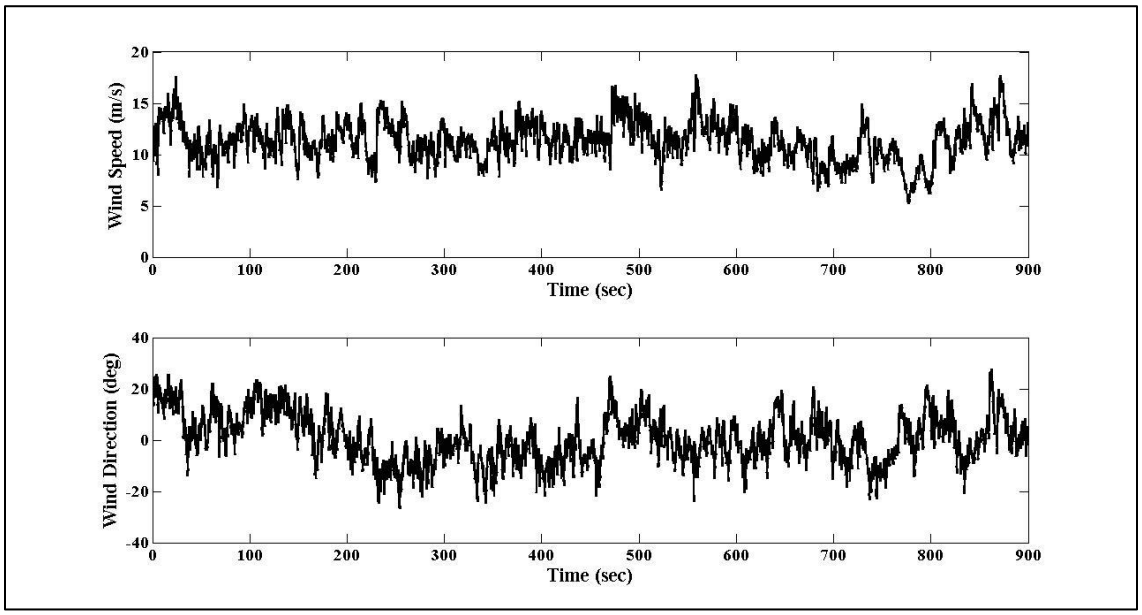

Figure 4-11. 10 m wind speed and direction records obtained from the Wind Engineering Research Field Laboratory (WERFL) Site

Results and Discussion

Once the multiple controlled fan wind tunnel (MCWFT) was calibrated following the procedure previously described, similitude of the approach flow was evaluated. Criteria include matching data to height dependent model profiles of mean velocity, longitudinal turbulence intensity, lateral turbulence intensity, and gust factors. Simulation of a constant shear stress was considered, followed by point assessments of the probability distribution, power spectra and length scales at the height of model one-story building. With few exceptions, the results demonstrate good agreement between the model and measured values. The method produced highly repeatable results, thus the analysis presented herein is limited to a single run at location 4 on the centerline of the test chamber(Figure 4-10) with the exception of the gust factors and integral length scales, which are the averages of five runs.

The procedure described is highly dependent on the ability of the control system to replicate the desired time histories. The correlation coefficient between the scaled input determined from the target wind speed (shown in Figure 4-11) and the measured wind speed above the test section at the height of a one-story model building were consistently between 0.92-0.95, which is slightly higher the values (0.80-0.90) reported by Cao and Nishi (2002). We attribute this slight improvement to the implementation of a closed loop control system to modulate the fan speeds (Figure 4-7).

Figures 4-12 through 4-14 depict measured and target mean velocity, longitudinal turbulence intensity (TI_u), lateral turbulence intensity (TI_v) and gust factor (GF) profiles for marine, open, and suburban terrain conditions (z_0 = 0.3, z_0 = 0.03, and z_0 = 0.005 respectively). The GF values were computed for full-scale conditions (T = 900 s, t = 3 s) using the zero up crossing rate described in Masters et al. (2010). The mean velocity

and TI_u profiles were calculated from Eqs. 3-3 and 3-4. TI_v was set to 72% of TI_u based on the ratio the measured values of the anemometric record. The corresponding data used to generate these plots are provided in Tables 4-1 through 4-3. The vertical axes correspond to the height above the floor of the test chamber divided by the height of the jet (nominally 1 m at model-scale or 10 m at full-scale). The horizontal axis corresponds to either the turbulence intensity, gust factor or the mean wind speed divided by the reference wind speed in the MCFWT. Discrepancies near the floor can be attributed to improper simulation of boundary conditions due to the vortices introduced by the fan propellers. Good agreement between mean velocity and turbulence intensity profiles was generally found for locations 2-6. As expected, shear-layer interaction between the sides of the jet and the stagnant air region was evident for location 1 and 7 as shown in Tables 4-4 through 4-6.

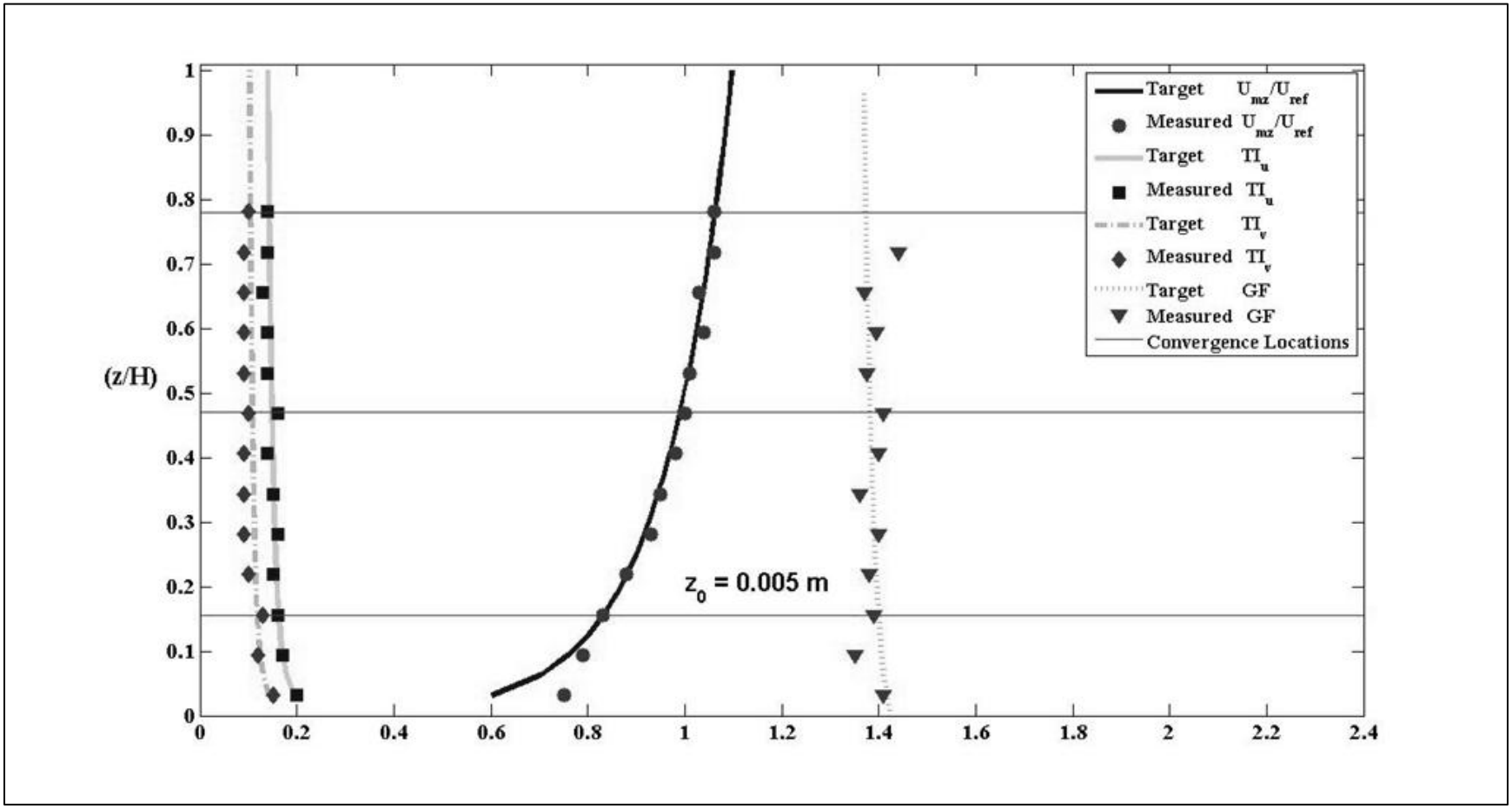

Figure 4-12. Wind profile for marine exposure (z_0 = 0.005 m)

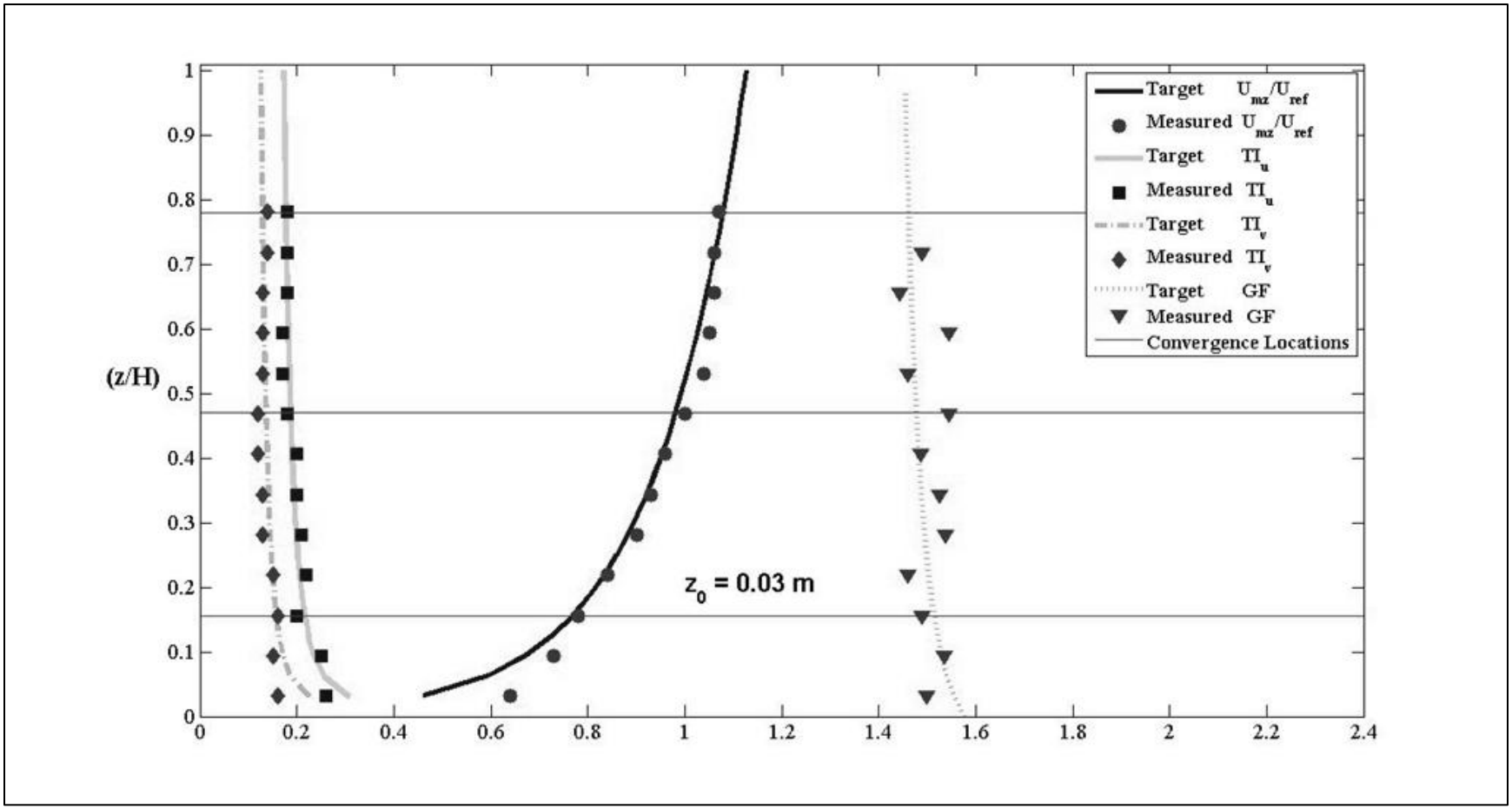

Figure 4-13. Wind profile for open exposure (z_0 = 0.03 m)

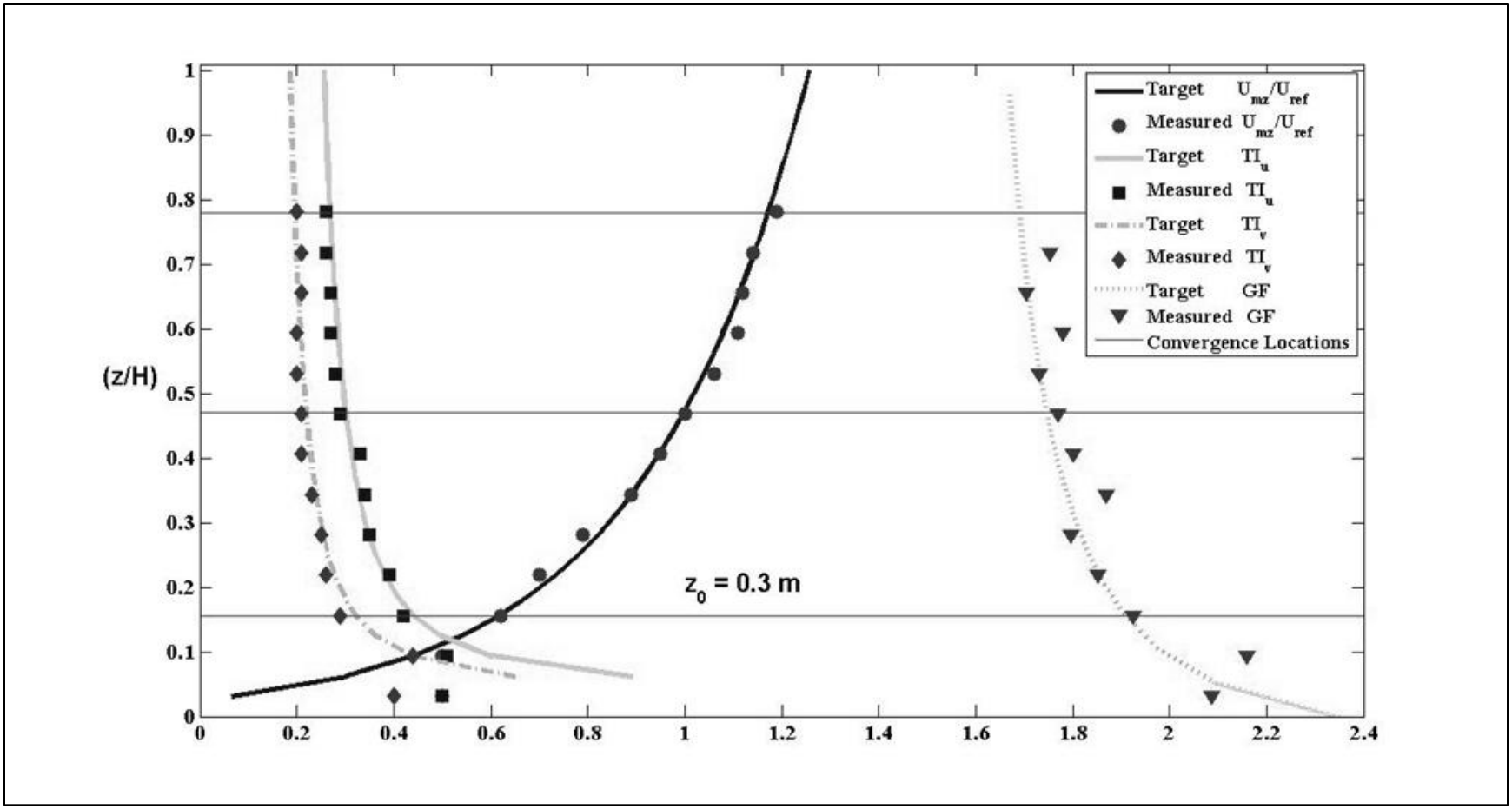

Figure 4-14. Wind profile for suburban exposure (z_0 = 0.3 m)

The data matched the desired *U* and *TI* profiles in all cases except near the floor for the open and suburban cases. These discrepancies can be attributed to improper simulation of boundary conditions due to the vortices introduced by the fan propellers.

The majority of the residuals listed in Tables 4-1 through 4-3 are less than 0.02 over the range of $0.16 \leq z/H \leq 0.78$. Below that range, the mean wind speed exhibits an overshoot and the turbulence intensities are less than the targets. Whether this is a result of configuration or the limitations of the Cobra Probes (which lose accuracy when *TI*> 30%) is not certain. Regardless, the differences are observed to occur at 1 m full scale above the ground, which will have little effect on the wind loading on the subject building. The GF profiles match the modeled values well, even in the lowest region of the suburban BL where the differences in the turbulence intensity are largest.

Table 4-1. Target and meaured wind profile characteristics for marine terrain (z_0 = 0.005 m)

Height (z/H)		0.03	0.09	0.16	0.22	0.28	0.34	0.41	0.47	0.53	0.59	0.66	0.72	0.78
U/U_{ref}	**Target**	0.60	0.76	0.84	0.89	0.93	0.95	0.98	1.00	1.02	1.03	1.05	1.06	1.07
	Measured	0.75	0.79	0.83	0.88	0.93	0.95	0.98	1.00	1.01	1.04	1.03	1.06	1.06
	Residual	0.15	0.03	0.01	0.01	0.01	0.01	0.00	0.00	0.01	0.01	0.02	0.00	0.02
TI_u	**Target**	0.20	0.17	0.16	0.16	0.16	0.15	0.15	0.15	0.15	0.15	0.15	0.14	0.14
	Measured	0.20	0.17	0.16	0.15	0.16	0.15	0.14	0.16	0.14	0.14	0.13	0.14	0.14
	Residual	0.00	0.00	0.00	0.01	0.00	0.00	0.01	0.01	0.01	0.00	0.02	0.01	0.01
TI_v	**Target**	0.14	0.12	0.11	0.11	0.11	0.11	0.11	0.10	0.10	0.10	0.10	0.10	0.10
	Measured	0.15	0.12	0.13	0.10	0.09	0.09	0.10	0.09	0.09	0.09	0.09	0.09	0.10
	Residual	0.01	0.00	0.01	0.01	0.02	0.02	0.02	0.00	0.01	0.01	0.01	0.02	0.01

Table 4-2. Target and meaured wind profile characteristics for open terrain (z_0 = 0.03 m)

Height (z/H)		0.03	0.09	0.16	0.22	0.28	0.34	0.41	0.47	0.53	0.59	0.66	0.72	0.78
U/U_{ref}	**Target**	0.46	0.68	0.78	0.85	0.90	0.94	0.97	1.00	1.02	1.05	1.07	1.09	1.10
	Measured	0.64	0.73	0.78	0.84	0.90	0.93	0.96	1.00	1.04	1.05	1.06	1.10	1.11
	Residual	0.18	0.05	0.01	0.01	0.01	0.01	0.01	0.00	0.15	0.01	0.01	0.02	0.01
TI_u	**Target**	0.31	0.24	0.22	0.21	0.20	0.19	0.19	0.19	0.19	0.18	0.18	0.18	0.18
	Measured	0.26	0.25	0.20	0.22	0.21	0.20	0.20	0.18	0.17	0.17	0.18	0.18	0.18
	Residual	0.05	0.01	0.01	0.01	0.01	0.01	0.01	0.00	0.02	0.01	0.00	0.00	0.00
TI_v	**Target**	0.22	0.17	0.15	0.14	0.14	0.14	0.13	0.13	0.13	0.13	0.13	0.13	0.12
	Measured	0.16	0.15	0.16	0.15	0.13	0.13	0.12	0.12	0.13	0.13	0.13	0.14	0.14
	Residual	0.06	0.02	0.01	0.00	0.01	0.01	0.01	0.01	0.00	0.01	0.00	0.01	0.02

Table 4-3. Target and meaured wind profile characteristics for suburban terrain (z_0 = 0.3 m)

Height (z/H)		0.03	0.09	0.16	0.22	0.28	0.34	0.41	0.47	0.53	0.59	0.66	0.72	0.78
U/U_{ref}	**Target**	0.14	0.41	0.60	0.72	0.81	0.89	0.95	1.00	1.05	1.09	1.12	1.16	1.19
	Measured	0.58	0.59	0.62	0.70	0.79	0.89	0.95	1.00	1.06	1.11	1.12	1.14	1.19
	Residual	0.44	0.18	0.03	0.02	0.02	0.00	0.00	0.00	0.11	0.02	0.00	0.02	0.00
TI_u	**Target**	0.74	0.60	0.44	0.38	0.35	0.33	0.31	0.30	0.29	0.29	0.28	0.27	0.27
	Measured	0.36	0.41	0.42	0.39	0.35	0.34	0.33	0.29	0.28	0.27	0.27	0.26	0.26
	Residual	0.38	0.19	0.03	0.01	0.00	0.01	0.01	0.01	0.02	0.02	0.01	0.01	0.01
TI_v	**Target**	0.52	0.42	0.31	0.27	0.24	0.23	0.22	0.21	0.20	0.20	0.20	0.19	0.19
	Measured	0.38	0.35	0.29	0.26	0.25	0.23	0.21	0.21	0.20	0.20	0.21	0.21	0.20
	Residual	0.14	0.07	0.02	0.01	0.01	0.00	0.01	0.00	0.00	0.00	0.01	0.01	0.01

Table 4-4. Target and meaured wind profile characteristics for marine terrain (z_0 = 0.005 m) at varying locations across the centerline

	Height (z/H)	Location							Target
		1	**2**	**3**	**4**	**5**	**6**	**7**	
U/U_{ref}	**0.16**	0.75	0.79	0.82	0.83	0.84	0.83	0.79	**0.84**
	0.47	1.00	1.00	1.00	1.00	1.00	1.00	1.00	**1.00**
	0.78	0.99	1.50	1.20	1.19	1.80	1.40	1.10	**1.07**
TI_u	**0.16**	0.09	0.13	0.15	0.16	0.16	0.14	0.10	**0.16**
	0.47	0.10	0.14	0.16	0.16	0.15	0.13	0.09	**0.15**
	0.78	0.09	0.10	0.12	0.13	0.14	0.11	0.07	**0.14**
TI_v	**0.16**	0.10	0.11	0.14	0.13	0.13	0.10	0.11	**0.11**
	0.47	0.09	0.11	0.11	0.10	0.10	0.09	0.08	**0.10**
	0.78	0.08	0.10	0.11	0.10	0.10	0.10	0.08	**0.10**

Table 4-5. Target and meaured wind profile characteristics for open terrain (z_0 = 0.03 m) at varying locations across the centerline

	Height (z/H)	Location							Target
		1	**2**	**3**	**4**	**5**	**6**	**7**	
U/U_{ref}	**0.16**	0.73	0.74	0.79	0.77	0.80	0.77	0.73	**0.78**
	0.47	1.00	1.00	1.00	1.00	1.00	1.00	1.00	**1.00**
	0.78	1.04	1.10	1.12	1.12	1.13	1.09	1.06	**1.10**
TI_u	**0.16**	0.14	0.16	0.19	0.20	0.21	0.18	0.13	**0.22**
	0.47	0.12	0.14	0.18	0.18	0.19	0.17	0.12	**0.19**
	0.78	0.10	0.15	0.17	0.18	0.19	0.16	0.11	**0.18**
TI_v	**0.16**	0.10	0.11	0.14	0.16	0.16	0.15	0.10	**0.15**
	0.47	0.09	0.10	0.13	0.12	0.11	0.12	0.10	**0.13**
	0.78	0.08	0.11	0.12	0.14	0.11	0.11	0.09	**0.12**

Table 4-6. Target and meaured wind profile characteristics for suburban terrain (z_0 = 0.3 m) at varying locations across the centerline

Height (z/H)		Location							Target
		1	**2**	**3**	**4**	**5**	**6**	**7**	
U/U_{ref}	**0.16**	0.58	0.60	0.63	0.62	0.62	0.61	0.60	**0.60**
	0.47	1.00	1.00	1.00	1.00	1.00	1.00	1.00	**1.00**
	0.78	1.14	1.16	1.20	1.19	1.18	1.17	1.15	**1.19**
TI_u	**0.16**	0.15	0.33	0.40	0.42	0.41	0.32	0.18	**0.44**
	0.47	0.12	0.19	0.24	0.29	0.27	0.20	0.14	**0.30**
	0.78	0.11	0.18	0.25	0.26	0.24	0.22	0.12	**0.27**
TI_v	**0.16**	0.11	0.17	0.20	0.28	0.24	0.17	0.10	**0.31**
	0.47	0.10	0.16	0.19	0.21	0.20	0.18	0.11	**0.21**
	0.78	0.11	0.16	0.19	0.20	0.18	0.16	0.12	**0.19**

By definition should be constant in the region where the logarithmic law (Eq. 3-3) is valid, which requires that the following expression be satisfied:

(4-2)

where the shear velocity is computed from the square root of the eddy covariance between the longitudinal and lateral fluctuating components (Weber, 1999):

(4-3)

In Figure 4-15, the left- and right-hand sides of Eq. 4-2 are plotted in coordinate pairs for the three terrain conditions at the measurement heights shown in Figures 4-12 through 4-14, and the solid line depicts a condition of parity (1:1 slope). Fitting the 1:1 slope line to the data using a linear regression yields a coefficient of determination ( ) value of 0.90, which indicates that a constant shear stress profile is achieved.

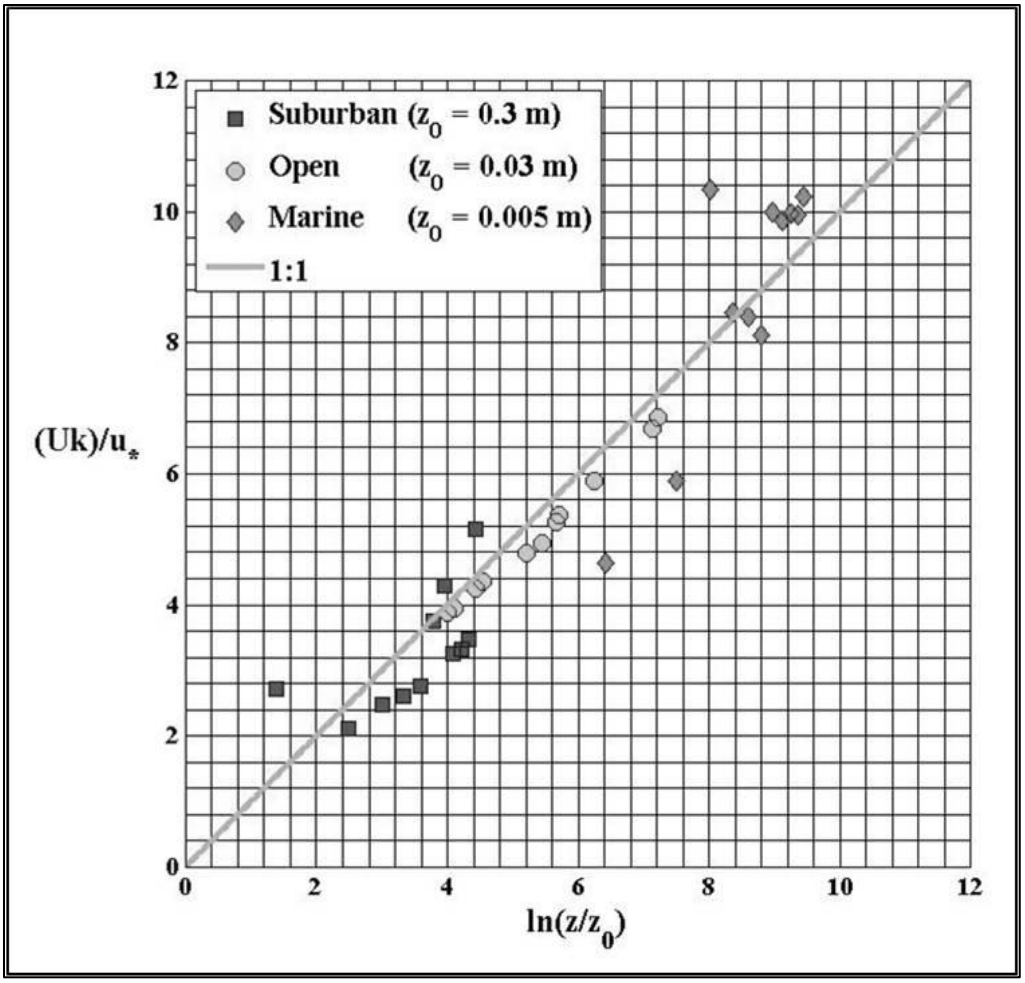

Figure 4-15. Uniformity of the shear velocity along the marine, open and suburban vertical profiles. (shear velocity values were computed from the eddy covariance).

The probability density functions of the standardized instantaneous u-, v- and w-velocities are shown for one location (*z/H* ~= 0.5) in Figure 4-16. The observation level corresponds to the height of the one-story test building at the WERFL site. The solid black line depicts the corresponding normal distribution (using and TI_u to compute the parameters). The power spectra densities (PSD) for the instantaneous *u*-, *v*- and *w*-velocities at this same location are shown in Figure 4-17. Following the approach outlined in Bendat and Piersol (2000), segments were divided into m contiguous blocks and *m*-1 overlapping blocks sharing the immediate 75% data common to the

neighboring contiguous blocks. Each block was tapered with a Hanning window to suppress side-lobe leakage and passed through a Fast Fourier Transform. The 2*m*-1 Fourier amplitudes were converted to PSDs and ensemble averaged. Using a 75% overlap in conjunction with the Hanning window causes successive overlapped segments to become correlated by 65.9%, so the number of averages in the ensemble average was scaled by 52.0%. The empirical PSDs are compared to the spectra computed from the full-scale WERFL data and the von Karman spectra in the form presented in Greenway (1979).

(4-4)

where L_{ux} is the integral length scale computed from the data. It is evident from the figure that the turbulence spectrum in the inertial subrange is captured. As expected, the control system is less effective at recreating fine-scale (dissipation range) turbulence.

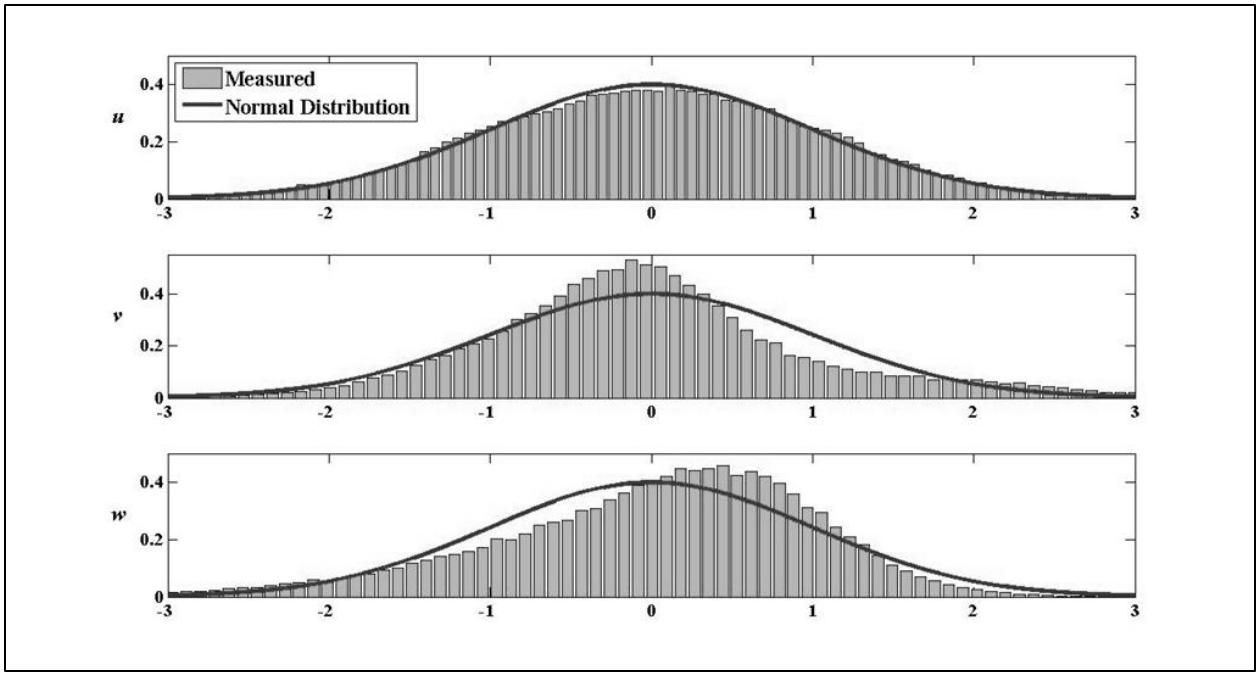

Figure 4-16. Standardized probability densities of the longitudinal, lateral, and vertical components measured at the eave height of a one-story building at the test section

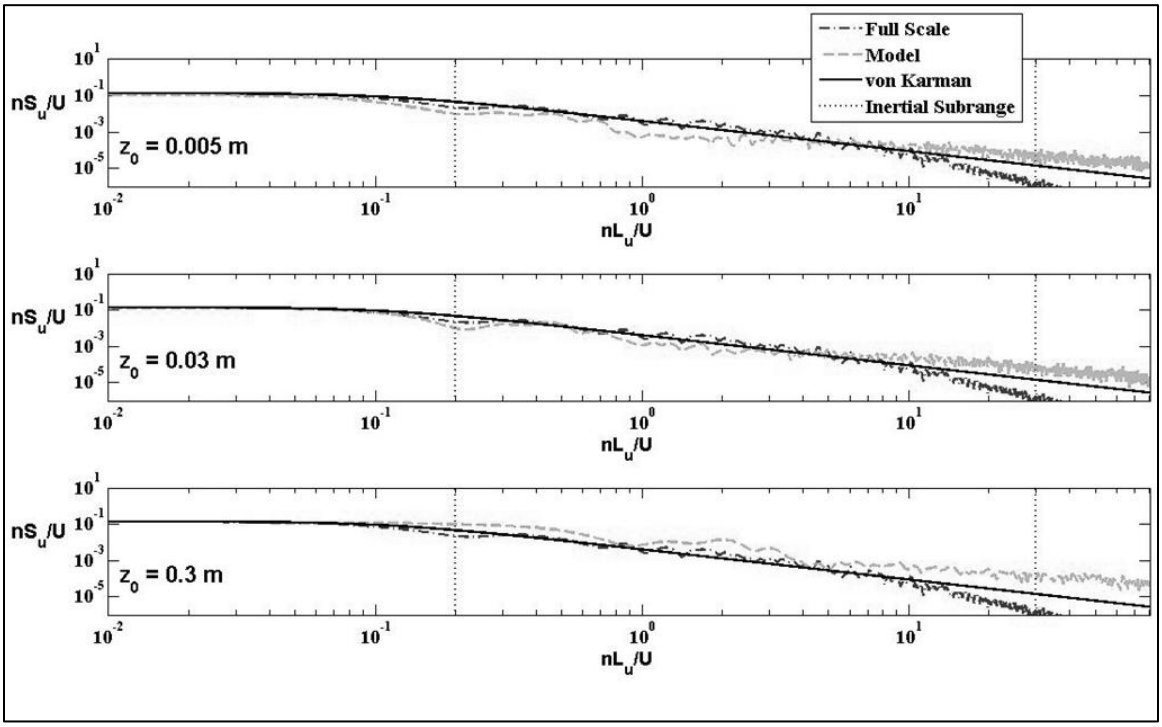

Figure 4-17. Comparison of measured power spectra for marine, open, and suburban terrian conditionat the eave height of a one-story building at the test section to (1) the spectra obtained from the full-scale data and (2) the von Karman model

In Figure 4-18, the measured integral length scales (L_{ux}) are compared to values from Counihan (1975),

(4-5)

where z is the elevation above the ground and C and $1/n$ are empirically derived terms for a specified z_0 value. For marine (z_0 = 0.005 m), open (z_0 = 0.03 m) and suburban (z_0= 0.3 m) exposure, C = 200, 90 and 34 and $1/n$ = 0.08, 0.18 and 0.37, respectively. Measured and modeled values are normalized by their corresponding length scale at z/H = 0.47 to address the difference between the Counihan model values (L_{ux} = 226, 119 and 60 m at z = 5 m in marine, open and suburban terrain, respectively) and the target signal integral length scale (= 68 m, z_0 = 0.01 m). Upon further inspection, we found that the ratios of the modeled length scales (from Eq. 4-5) and the modeled mean wind speeds are nearly identical, which supports the use of the normalization to compare results.

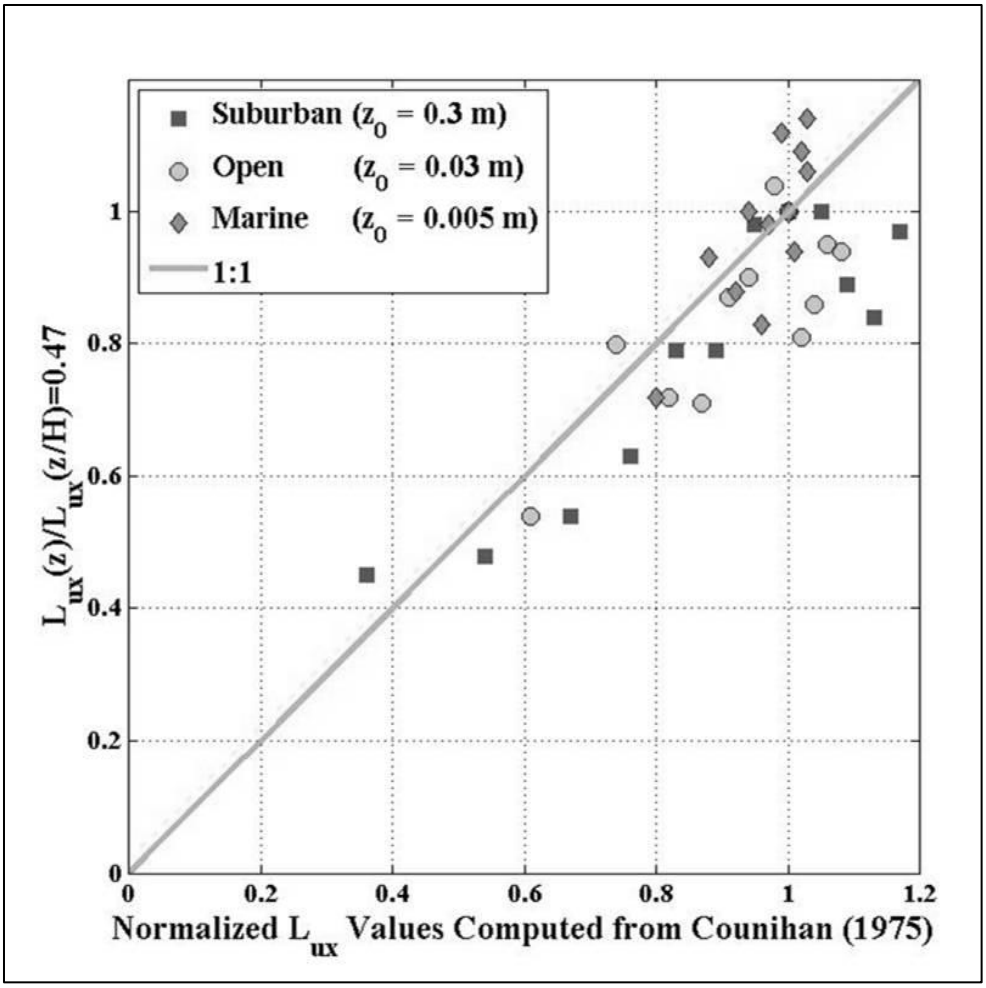

Figure 4-18. Normalized integral length scale values.

At lower elevations, the measured length scales are lower than the modeled values, which we attribute to several factors. First, one *dt* was computed for all fan heights using the mean wind speed at the upper fan height (see Eq. 3-1), which effectively speeds up the fluctuations at the lower levels. This operation artificially reduces *dt* at the lower levels, affecting the integral length scale calculation. Invoking Taylor's hypothesis, L_{ux} is defined as the product of the mean wind speed and the area under the autocorrelation function of the standardized velocity signal computed from the origin to the first zero-crossing point. Speeding up the signal causes the first zero-crossing point to shift toward the origin, which results in a lower L_{ux} value than would be

computed if the time scaling were performed individually for each fan height. Second, Eq. 3-4 applies for integral length scales computed over 1 hr, but a 15-min full-scale record is used in the simulation. 15-min values are on the order of 20% less than their 1 hr counterparts. At z/H = 0.47 (the height of a one-story building model), the length scales are consistent with the modeled values (withstanding the difference between the durations). Above this height, the length scales decrease with height, which can be attributed to shear layer interaction between the jet and the surrounding air in the test chamber.

Summary

A new method to simulate desired approach flow conditions in a MCFWT was presented. A case study was also presented using a 1:10 scale model of the Institute for Business & Home Safety Research Center Full-Scale Test Facility. This chapter included the methodology to produce desired flow characteristics for which a validation study was conducted and presented in Chapter 5.

CHAPTER 5
COMPARISON OF SCALE MODEL AND FULL-SCALE PRESSURE DISTRIBUTIONS

In the last chapter, a control system was successfully implemented in a multiple controlled fan wind tunnel (MCFWT) to simulate prescribed boundary layer profile characteristics typical of marine, open country and suburban terrains. This chapter focuses on the resultant pressure distributions on buildings immersed in the boundary layer. The goal of this research is to substantiate that the accurate simulation of the mean velocity and turbulence profiles, spectral content and integral length scales was sufficient to produce realistic pressure loading characteristics on simplified building shapes. One major consideration was the distance from the jet to the test subject, which dictates the extent of turbulence dissipation. The MCFWT also employs movable vanes to impart directionality, at the tradeoff of introducing small-scale coherent structures that may alter the flow separation around the building. For this study, the validation data was pressure and velocity measurements taken at the Texas Tech Wind Engineering Research Field Laboratory (WERFL), which was discussed in Chapter 2. Validation will provide accurate wind loading scenarios on scaled models that can be tested in the full-scale IBHS Research Center Full-Scale Test Facility. Within this chapter is the approach that will be taken to accurately produce comparable pressure distributions on the 1:10 scaled WERFL building. These results presented herein were only used for a preliminary evaluation. IBHS has subsequently performed full-scale experiments in the facility to validate similitude; these results are not discussed herein.

1:10 Scaled Wind Engineering Research Field Laboratory (WERFL) Test Building and Pressure Distribution Data Acquisition

The WERFL subject model was a 1:10 scaled building replica constructed from 6.35 mm thick sheets of acrylic plastic, and shown on the turntable within the test

section in Figure 5-1. A total of 102 pressure taps were installed on the model throughout one half of the roof and wall surfaces due to symmetry. Model tap locations correspond to their full-scale test counterpart, and are shown with their respective five digit designation on the exploded view of the model in Figure 5-2.

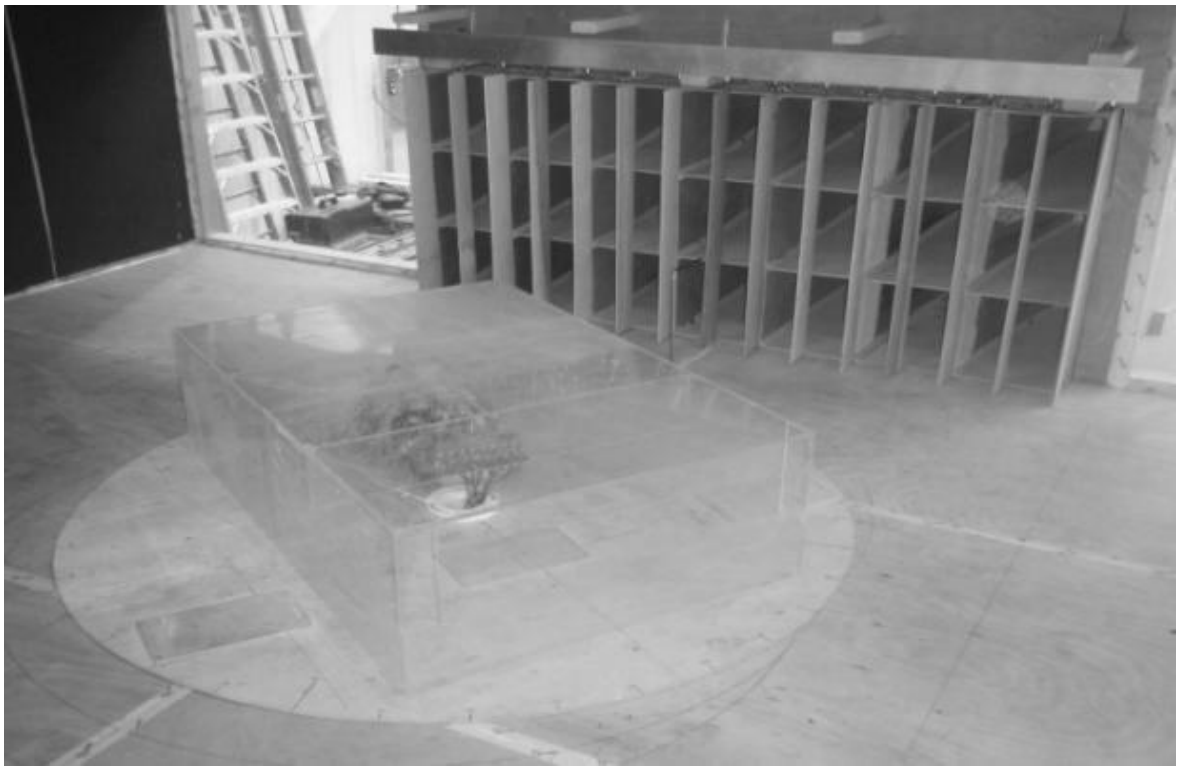

Figure 5-1. 1:10 scaled model of the Texas Tech University's Wind Engineering Research Field Laboratory (WERFL) Test Building

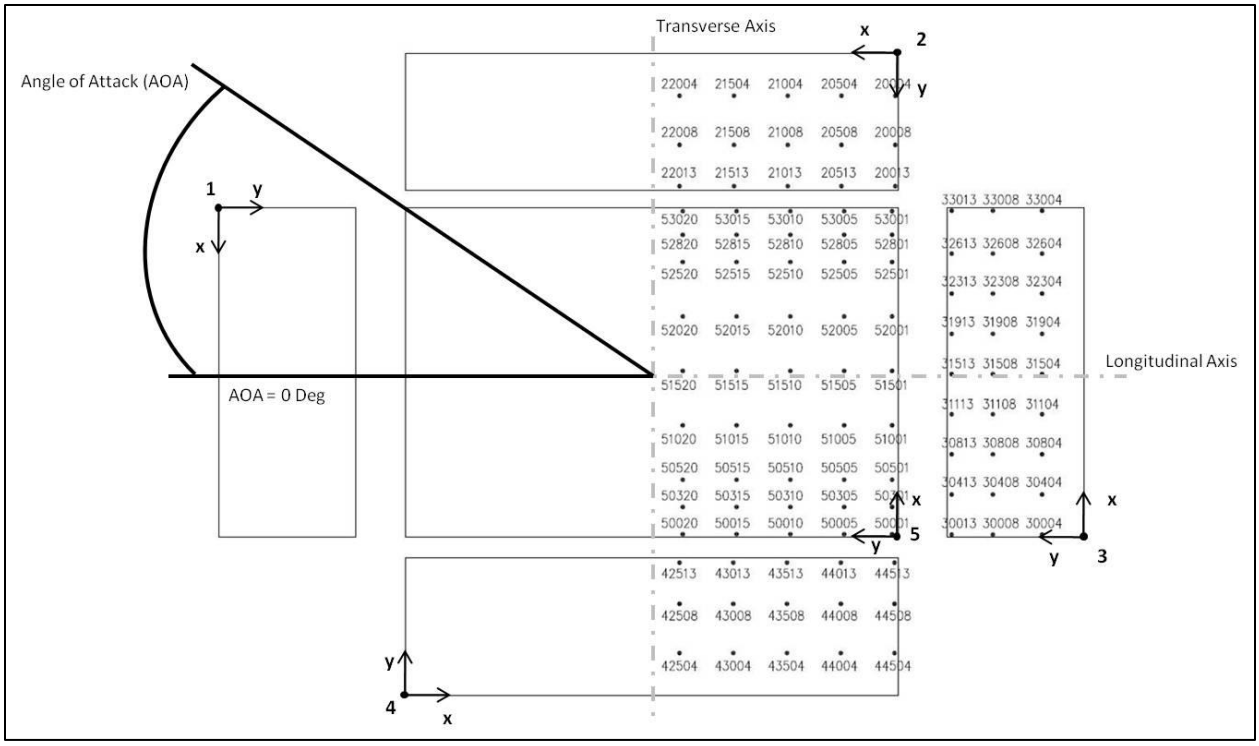

Figure 5-2. Exploded view of 1:10 scaled model Texas Tech University's Wind Engineering Research Field Laboratory (WERFL) test building with pressure tap location and angle of attack reference

Each tap was connected with a 450 mm length flexible vinyl tubing with an internal diameter of 1.5 mm to a Scanivalve mechanical pressure scanner containing eight differential pressure transducers. The dynamic amplification of the tubing length to each tap was removed through calibrated graphic equalizers (Monroe, 1996). A Microsoft disk operating system (MS-DOS) program was used to communicate with the Scanivalve digital interface units that controlled the mechanical solenoid switching device. A Digital I/O card and data acquisition program then sampled 8 pressure taps at a time from eight differential pressure transducers simultaneously at 2000 Hz and low-pass filtered to 500 Hz. Scaled 3 minute time histories (Chapter 3) were continually looped to ensure each pressure tap accurately captured the 15 minute full-scale time

history. The data acquisition program calculates non-dimensional pressure coefficients through Eq. 4-2:

$$\frac{\quad}{\quad} \qquad (4\text{-}2)$$

where is a statistical component of entire differential pressure record (i.e. mean, minimum, or maximum), is the density of air and, is the mean wind speed of the 3 minute time history measured at mean roof height (.39 m) from a pitot tube located 0.3 m from the airfoil array on the centerline (CL) of the test section(Figure 5-3a). The Scanivalve data acquisition system only provided pressure coefficient files that included summary Cp_{mean}, Cp_{min}, Cp_{max}, and Cp_{rms}, for each taps' locations which confines comparisons between full and model scale pressure distributions (Note: tap time histories were not available for this study). This varies from WERFL site time histories that provided pressure coefficient time histories at 30 Hz at each tap.

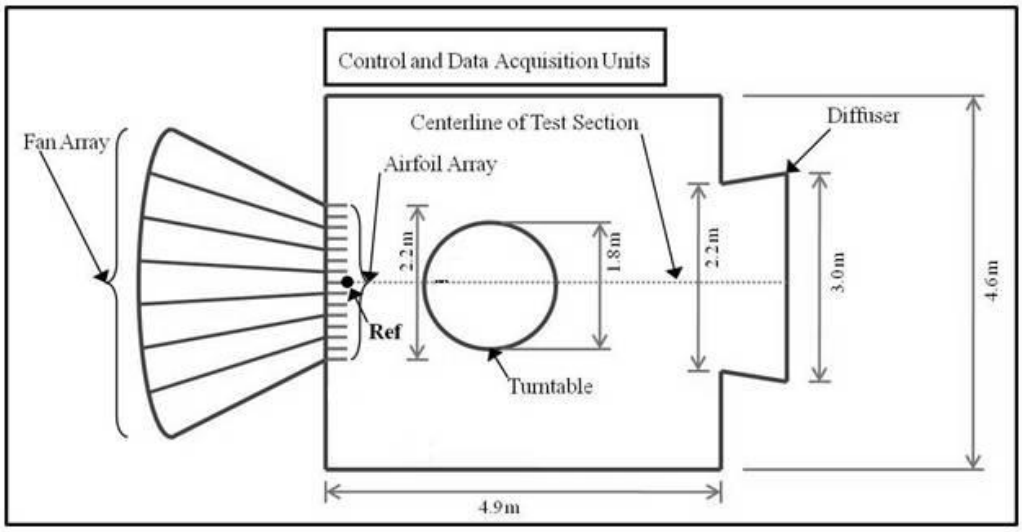

Figure 5-3. Plan view of 1:10 scale model of the Insurance Institute for Business & Home Safety Research Center Full-Scale Test Facility

The data acquisition system is also limited by the fact that it can only sample 8 channels simultaneously greatly increasing the experiment duration. For example, with a total of 102 pressure taps and 3 minute time histories (representative of full-scale data) it took approximately 40 minutes for a single pressure scan of the 102 taps.

Simulation of 1:10 Wind Engineering Research Field Laboratory (WERFL) Site Time Histories

Site conditions for selected data sets were stationary in wind speed and direction with a mean wind speed at 3.9 m greater than 6.7 m/s. A mean wind speed at a height 3.9 m and greater than 6.7 m/s insured that turbulence was mechanically generated and not from thermal convection. Three 15 minute records were used for validation with AOA of 0, 45, and 90 degrees corresponding runs designated 620, 4482 and 2781 (Appendix B). The records represent flow parallel to the longitudinal axis, 45^o from the longitudinal axis, and parallel to the transverse axis (AOA = 0^o, 45^o, & 90^o respectively).

The prescribed 15 minute full-scale site wind time histories were scaled 1:10 through the reduced frequency relationship and site up wind aerodynamic roughness length (z_0 = 0.013 m) with Eqs. 3-1 through 3-5. Model mean wind speeds were adjusted to ensure that the full-scale 15 minute records could be simulated during 3 minute records for smooth transition into the controllers of Chapter 3. The scaled time histories, with respect to height, were simulated within the 1:10 scaled model's test section (following the methodology within Chapter 3). Implementing minor adjustments to the controller inputs, from the open terrain condition of z_0 = 0.03 m (from Chapter 3), to achieve a z_0 = 0.013 m for each the three selected time histories was accomplished (Appendix B). Once site flow conditions were satisfied, the test section was prepared

for 1:10 scaled WERFL test building to be immersed into the simulated flow for comparison of pressure distributions.

Pressure Distributions of the 1:10 Wind Engineering Research Field Laboratory (WERFL) Test Building Immersed in Prescribed Flow Conditions

Comparison of statistical components of full-scale and model-scale pressure distributions were critical for the ability to develop conclusions of atmospheric boundary layer wind load simulations. With the half symmetry of the model being used to reduce the numbers of taps, each of the three full-scale AOAs that were tested required the model to be tested at two AOAs 180^{o} out of phase to accurately simulate one full-scale pressure scan of all the taps. For example (per Figure 5-3), when the scaled time history of the flow was parallel to the longitudinal axis, Surface 1 was the windward wall for the first scan, then the model was rotated 180^{o} and tested again so that Surface 3 was the windward wall for the second scan to account for the 204 full-scale tap locations. Each of the three full-scale AOAs were simulated eight times (16 model-scale scans) to obtain an ensemble average of time domain statistical components. The Cp_{mean}, Cp_{min}, $Cp_{max,\ and}$ Cp_{rms} distributions are the primary characteristics for comparison between the WERFL data and the1:10 scaled model. All pressure coefficients tap data were interpreted between taps using the built-in MATLAB® 4 griddata method, which applied a polynomial interpolation between taps. This interpolation method provided a smoother translation among taps used for all pressure distribution contour figures presented herein.

Flow Distribution Comparison of Flow Simulated Parallel to the Longitudinal Axis (AOA = 0 deg, WERFL Run 620)

With model flow conditions for WERFL site run 620 established within the test section, the 1:10 WERFL test building was centered on the turntable with the windward

wall 1.07 m from the airfoil array as shown in Figure 5-3. A pressure scan was then conducted 8 times on 102 pressure taps at AOAs of 0 and 180 degrees and compared with WERFL test building data. The ensemble averages of the model's two AOA pressure scans were combined to recreate all respective 204 full-scale taps. Model and full-Scale pressure distributions characteristics are shown in Figure 5-4 through Figure 5-11. Comparing 1:10 model and full-scale Cp_{mean} distributions (Figure 5-4 and Figure 5-5) showed favorable agreement on the windward wall (surface 1) with variations increasing closer to the eave height. Amplitude of suction at the windward eave of the roof and sidewall windward corners coincided between the model and full-scale data, though means converged on the 1:10 model 1/2 of the length of the roof while full-scale mean converged within 1/3 of the length of the roof. Cp_{mean} distributions on the leeward wall were uniform in distribution and magnitude between the 1:10 model and full-scale. Figure 5-6 and Figure 5-7 show the variation between the Cp_{min} distributions. Minimum amplitudes and variations of were favorable between the windward, roof, and sidewalls between the 1:10 model and full scale. However, the leeward wall of the 1:10 model had a uniform distribution 30% higher than full-scale.Figure 5-8 and Figure 5-9 compare Cp_{max} distributions. Full-scale maxima have consistent variation on the windward wall from the center to the corners and eave, while the 1:10 model scale maximums are lower in amplitude and did not follow any trend. The 1:10 model had higher amplitude maximums on the leeward edge of the roof and leeward wall. Figure 5-10 and Figure 5-11 display the variation of the Cp_{rms} between the 1:10 model and full-scale. The 1:10 rms distributions were uniform on the windward and leeward walls. Full-scale data had a consistent variation on the windward wall decreasing from the center to the corners

and eave with a sudden increase on the roof at the windward eave that decreased until it converges at 50% of the length of the roof. This trend was also seen on the 1:10 though the amplitude of the converged Cp_{rms} model was 200% higher than full-scale.

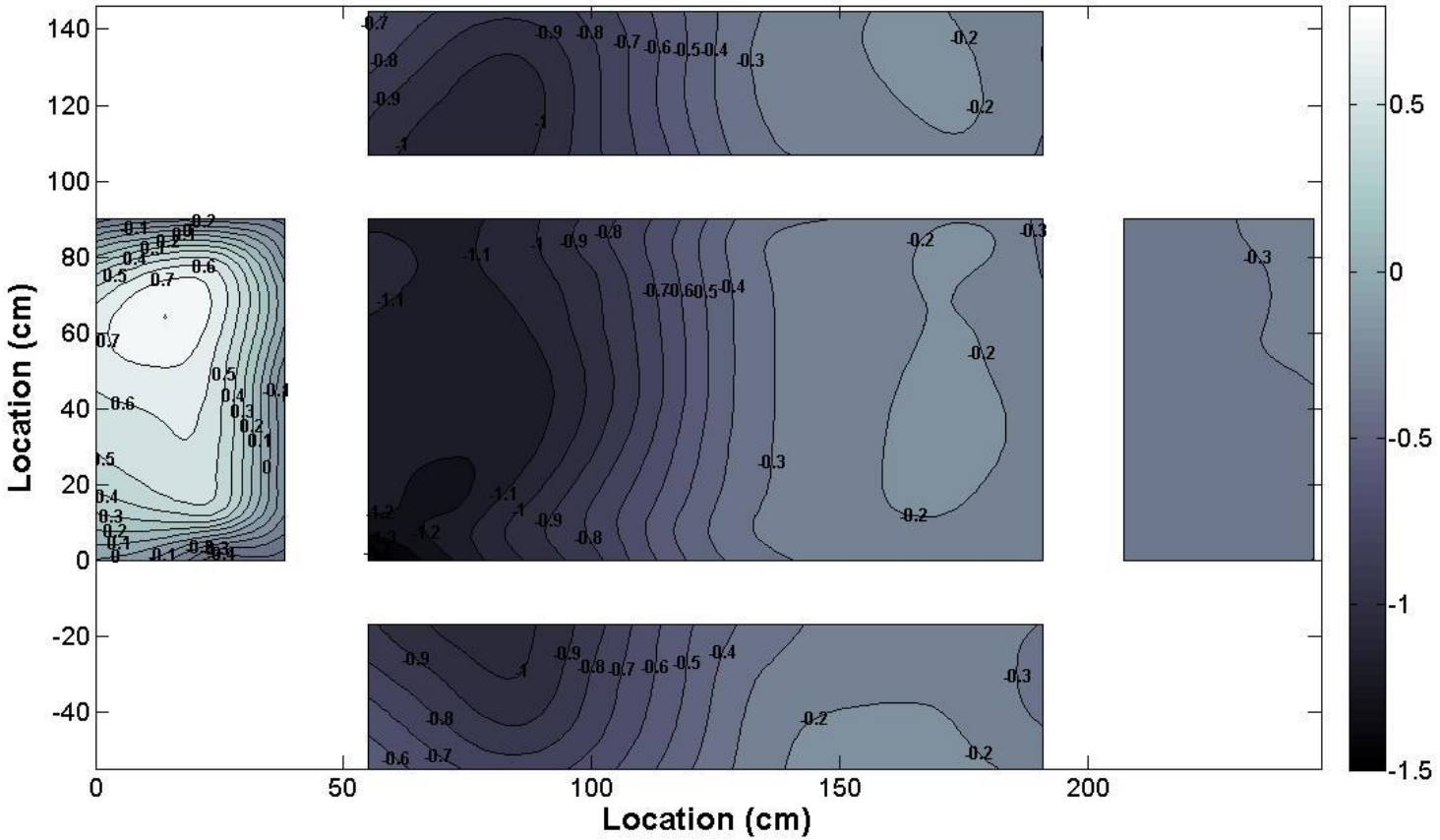

Figure 5-4. Exploded view of the 1:10 scaled model Wind Engineering Research Field Laboratory (WERFL) Test Building's mean Cps with flow simulated parallel to the longitudinal axis (AOA = 0^{o})

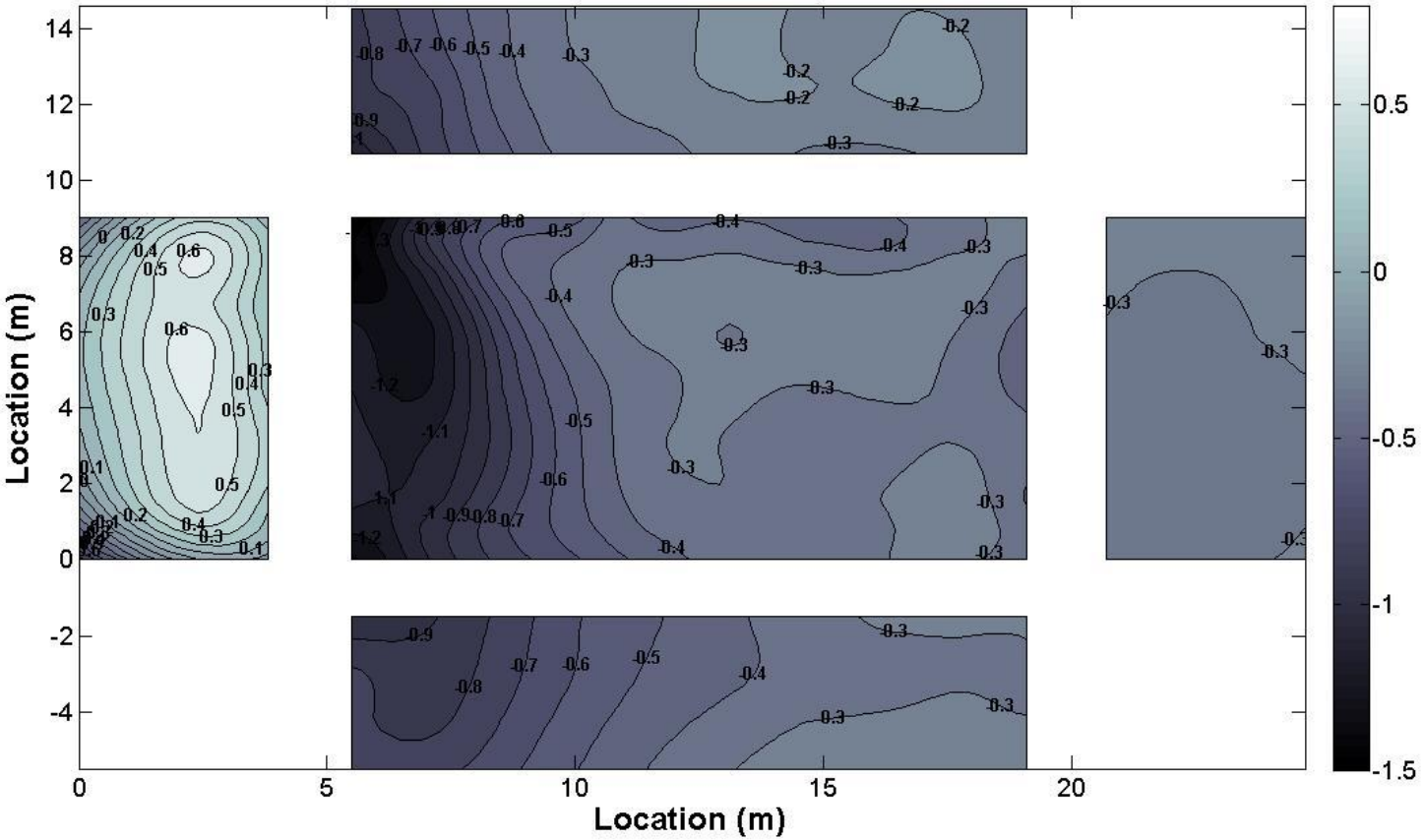

Figure 5-5. Exploded view of the Wind Engineering Research Field Laboratory (WERFL) Test Building's mean Cps with flow simulated parallel to the longitudinal axis (AOA = 0^{o})

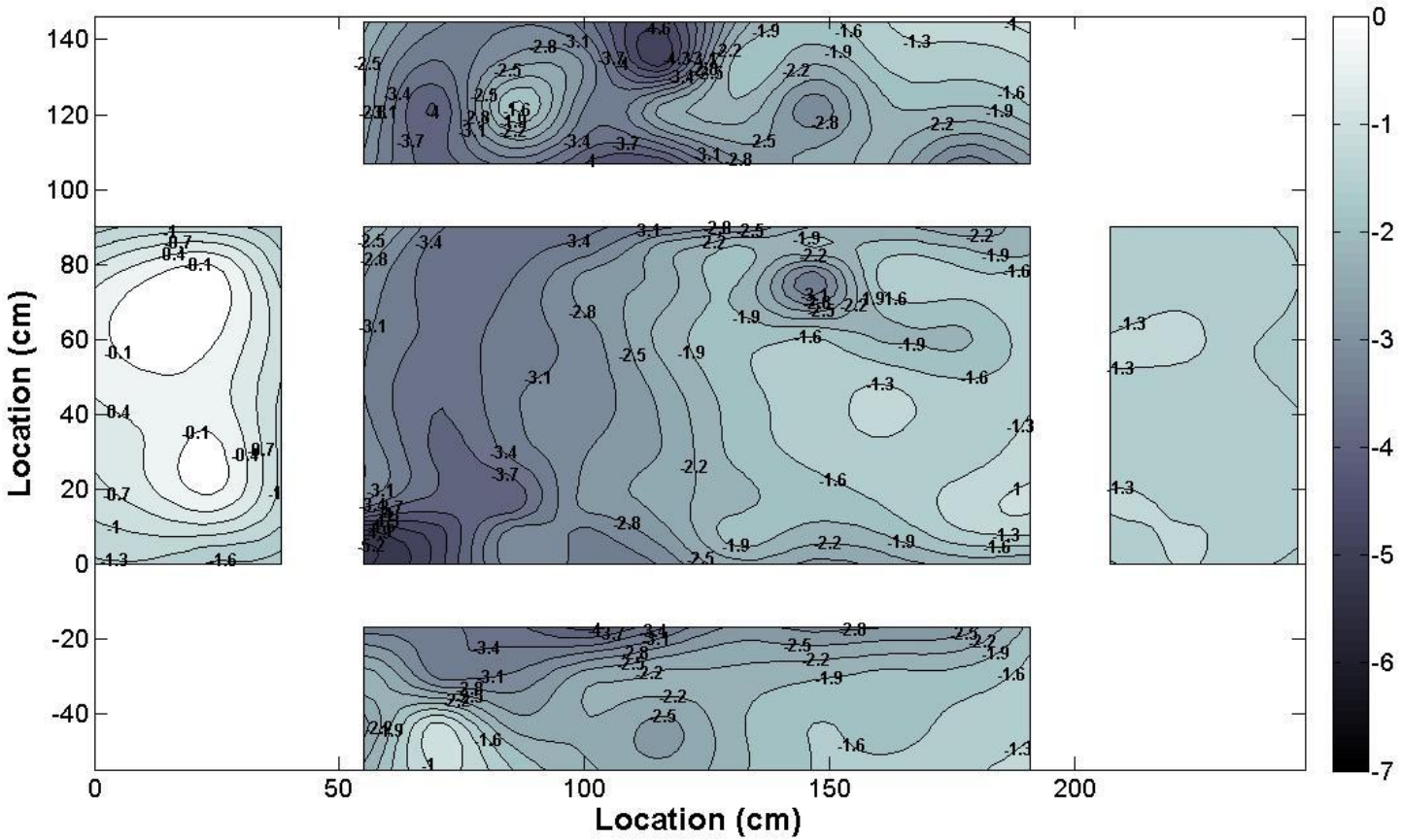

Figure 5-6. Exploded view of the 1:10 scaled model Wind Engineering Research Field Laboratory (WERFL) Test Building's minimum Cps with flow simulated parallel to the longitudinal axis (AOA = 0^{o})

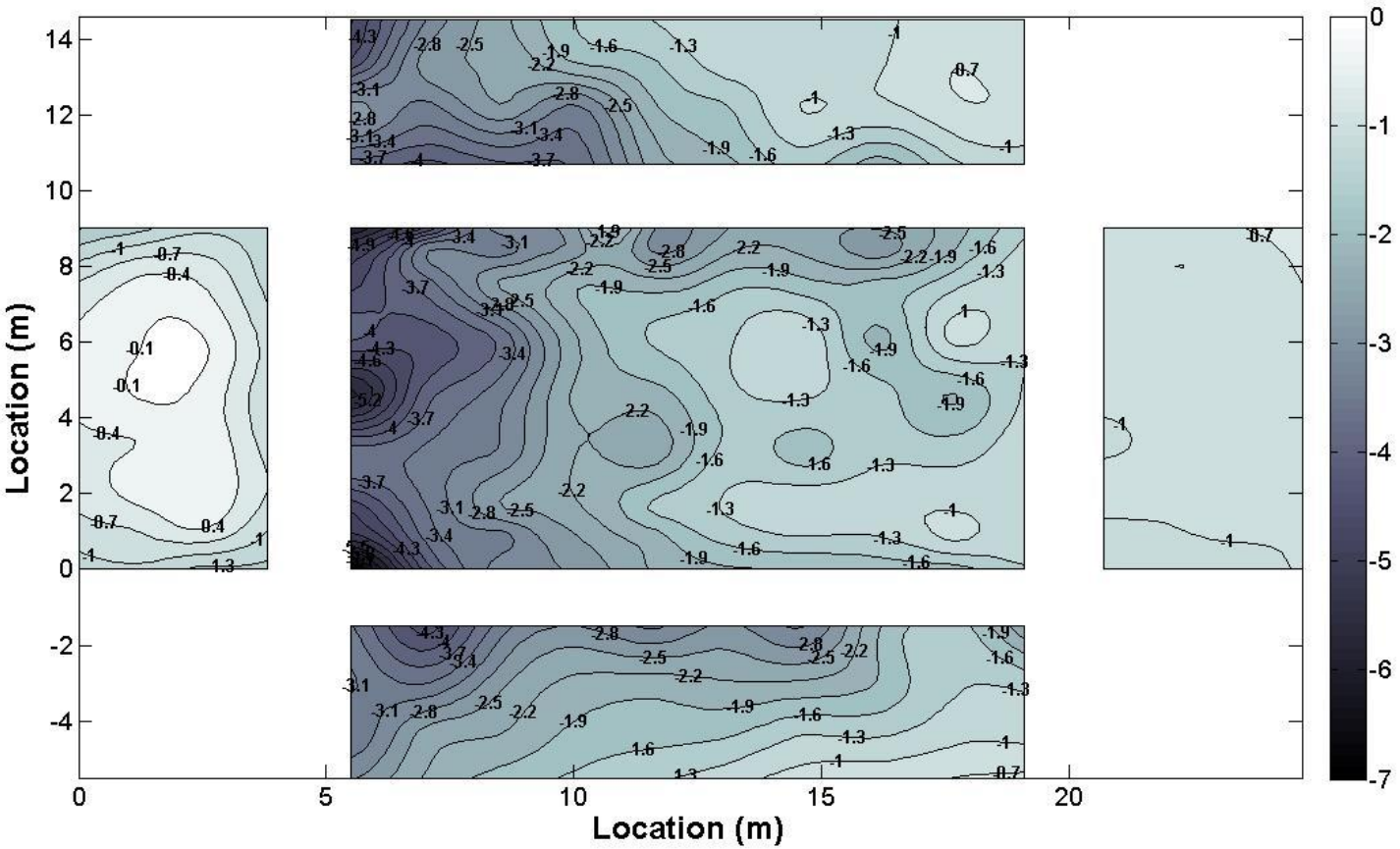

Figure 5-7. Exploded view of the Wind Engineering Research Field Laboratory (WERFL)Test Building's minimum Cps with flow simulated parallel to the longitudinal axis (AOA = 0^{o})

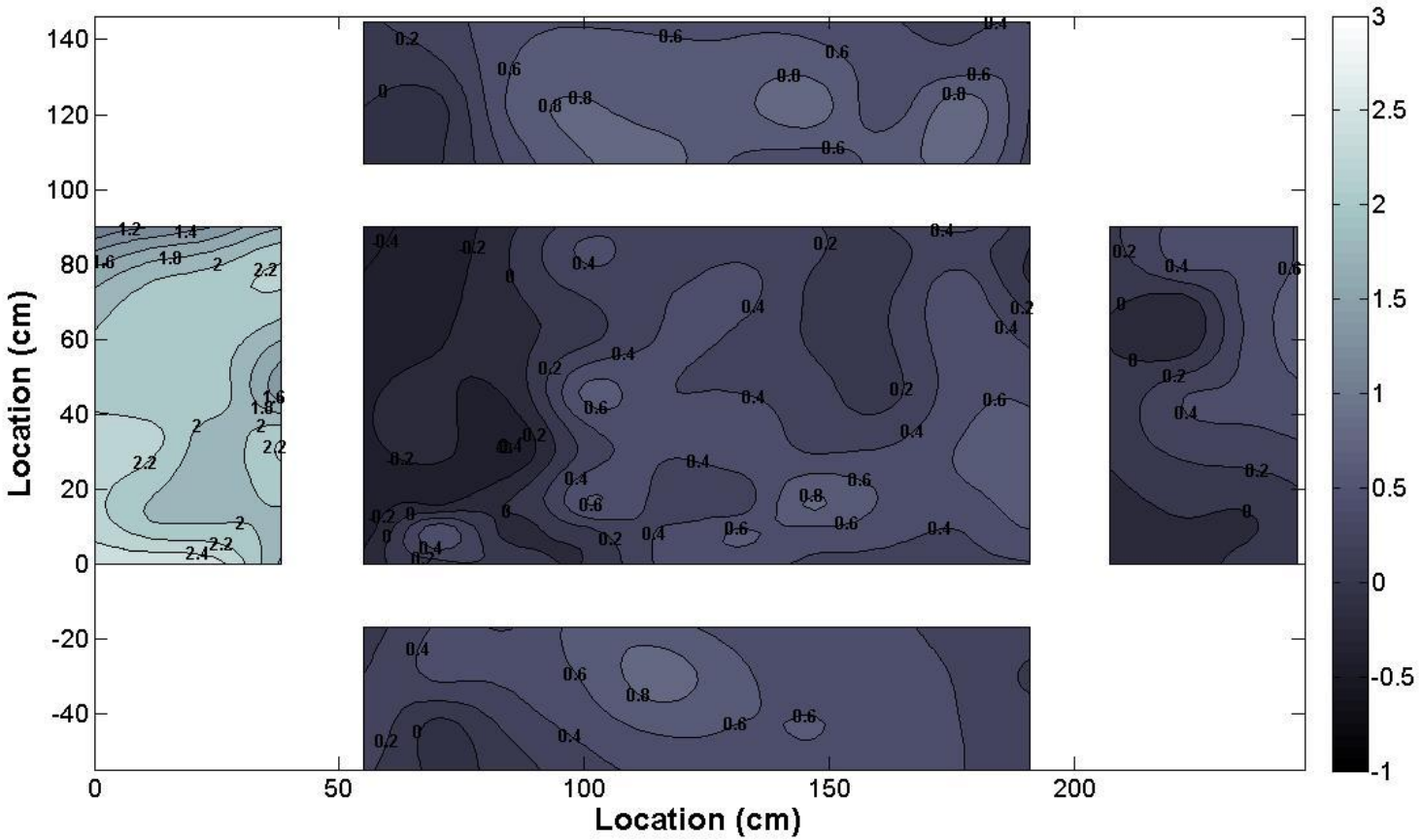

Figure 5-8. Exploded view of the 1:10 scaled model Wind Engineering Research Field Laboratory (WERFL)Test Building's maximum Cps with flow simulated parallel to the longitudinal axis (AOA = 0^{o})

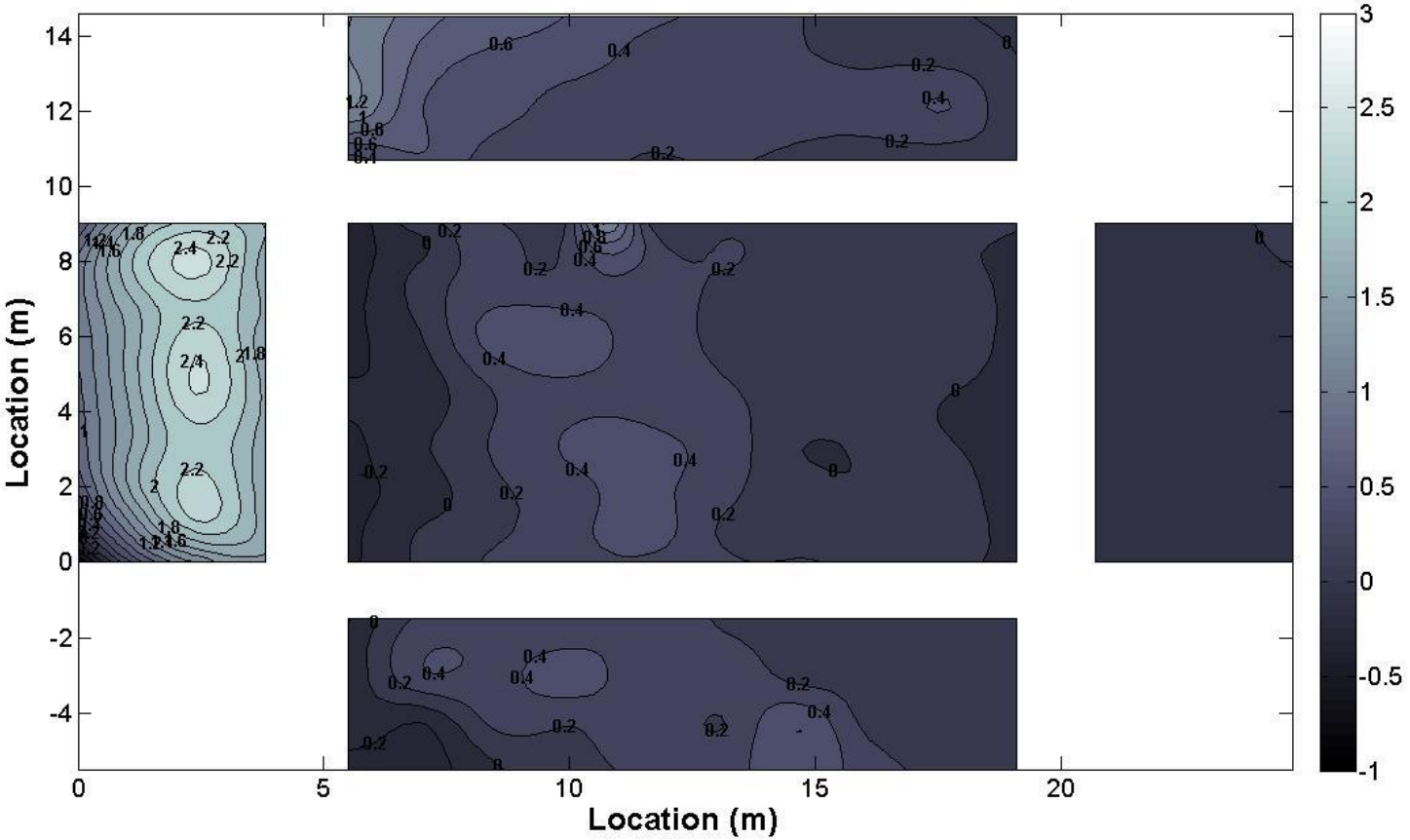

Figure 5-9. Exploded view of the Wind Engineering Research Field Laboratory (WERFL)Test Building's maximum Cps with flow simulated parallel to the longitudinal axis (AOA = 0^{o})

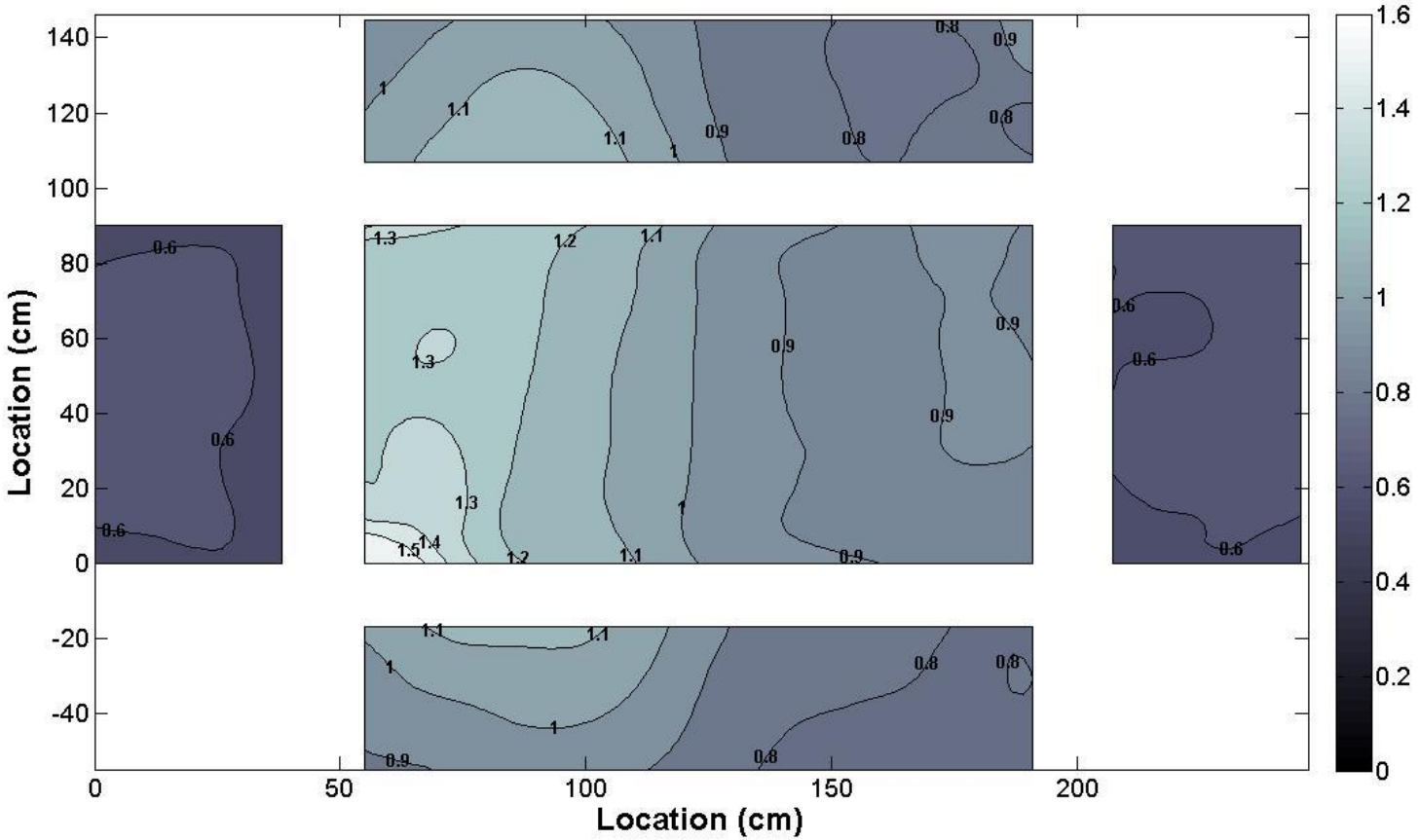

Figure 5-10. Exploded view of the 1:10 scaled model Wind Engineering Research Field Laboratory (WERFL)Test Building's RMS Cps with flow simulated parallel to the longitudinal axis (AOA = 0^{o})

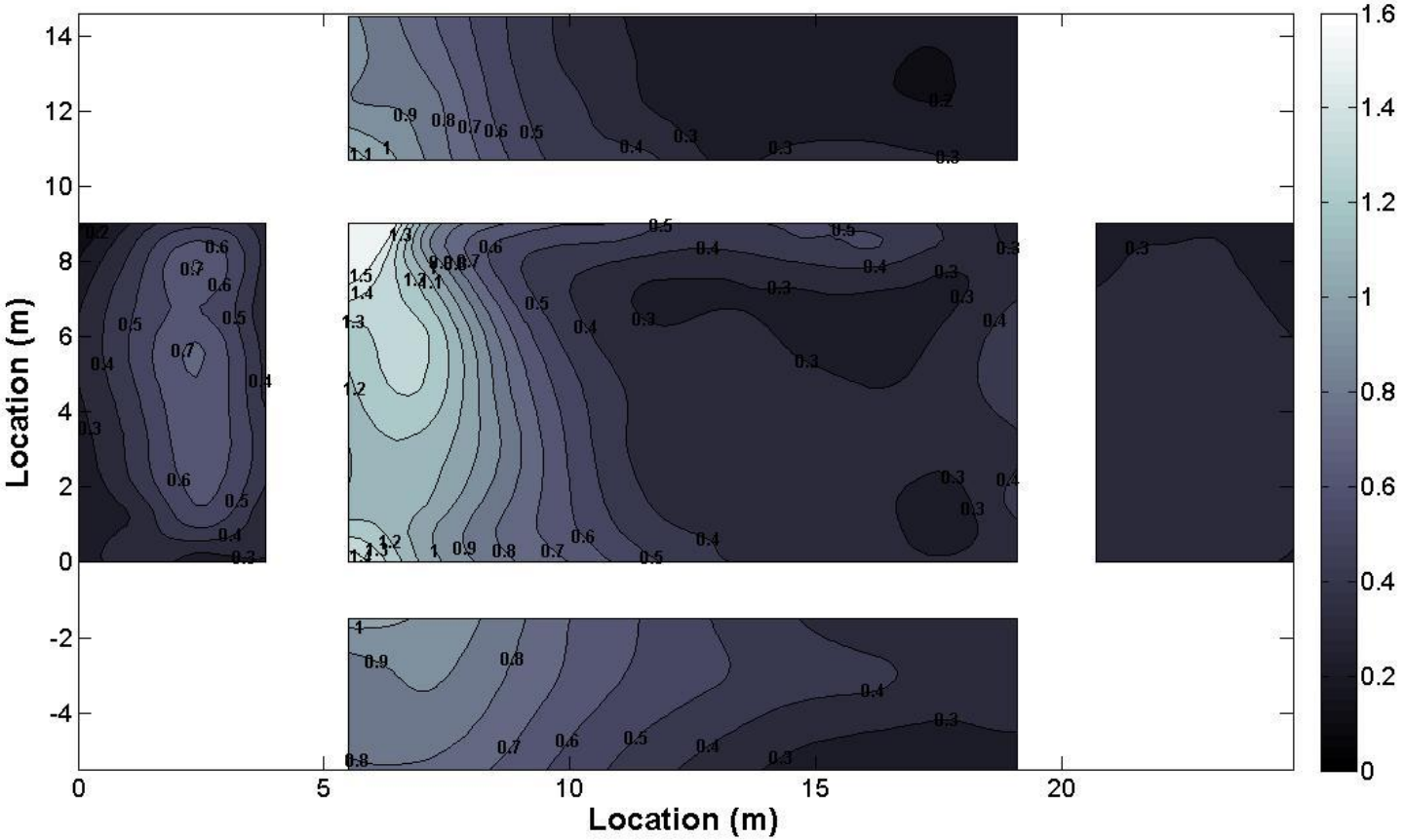

Figure 5-11. Exploded view of the Wind Engineering Research Field Laboratory (WERFL)Test Building's RMS Cps with flow simulated parallel to the longitudinal axis (AOA = 0^{o})

Flow Distribution Comparison of Flow Simulated Parallel to the Longitudinal Axis (AOA = 45 deg, WERFL Run 4482)

Model flow conditions for WERFL site run 4482 were established within the test section, the 1:10 WERFL test building was centered on the turntable with the windward corner 0.9 m from the airfoil array as shown in Figure 5-12. A pressure scan was then conducted 8 times on 102 pressure taps at AOAs of 45 and 225 degrees and compared with WERFL test building data. The ensemble averages of the model's two AOAs pressure scans were combined to recreate all respective 204 full-scale taps.

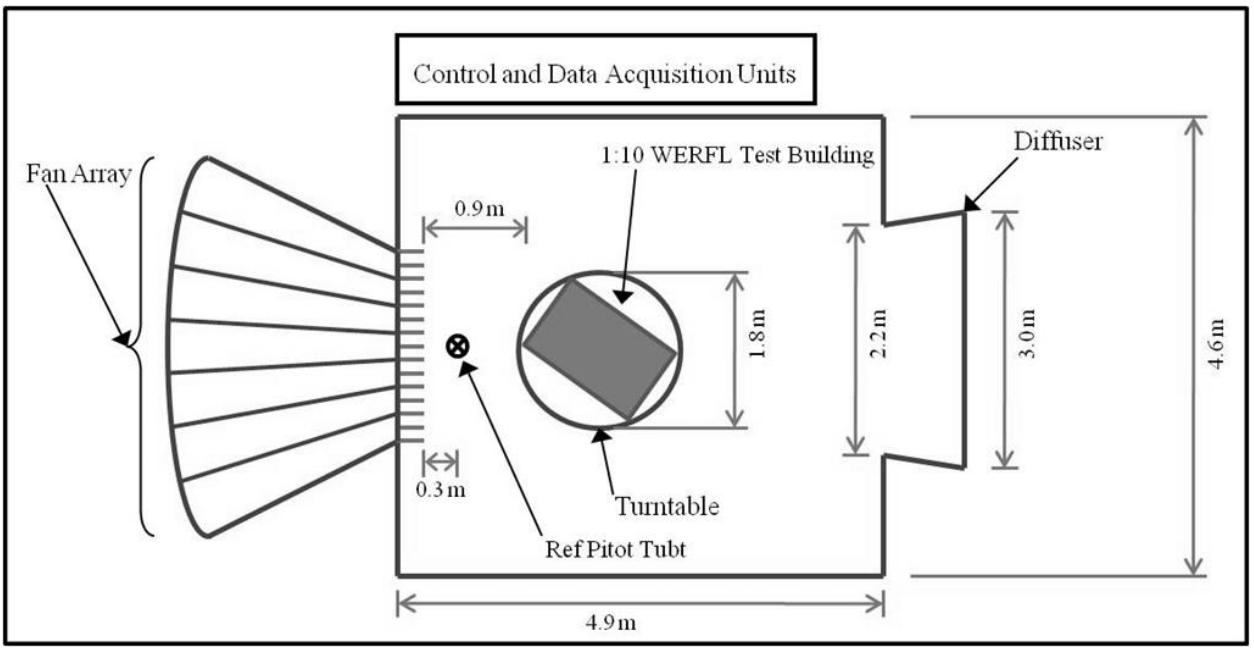

Figure 5-12. Plan view of 1:10 scale model of the Insurance Institute of Business & Home Safety Research Center Full-Scale Test Facility

1:10 model and full-scale pressure distributions characteristics are shown on Figure 5-13 to Figure 5-20. Comparing 1:10 model and full-scale Cp_{mean} distributions (Figure 5-13 and Figure 5-14) showed favorable agreement among amplitudes and variation along the surfaces with a decreased suction observed at the eave of surface 2 and the roofs windward edge. Figure 5-15 and Figure 5-16 show the variation between

the Cp_{min} distributions. The full-scale amplitudes have higher amplitude minimums concentrated at the windward corner. 1:10 model and full-scale variations converged 15 % the length of the roof away from the corner, though full-scale amplitudes were greater. Sidewall and leeward wall amplitudes were favorable as between the 1:10 model and full-scale distributions.Figure 5-17 and Figure 5-18 compare Cp_{max} distributions. Full-scale maximums followed variation from the center of the windward corner decreasing along the length of the windward walls. While the 1:10 model's highest amplitude maximums are at the windward corner they do not follow any trend along the length of the windward walls. The roof and leeward walls of the 1:10 model and full-scale followed a similar trend of variation, though the 1:10 had greater magnitudes.Figure 5-19 and Figure 5-20 display the variation of Cp_{rms} between the 1:10 model and full-scale. The 1:10 distributions are somewhat uniform for all walls. The 1:10 distributions on the roof followed a trend similar to full-scale, but converge much sooner from the windward corner and with higher amplitude than full-scale. Full-scale sidewalls' distributions decreased the same along the length of the building.

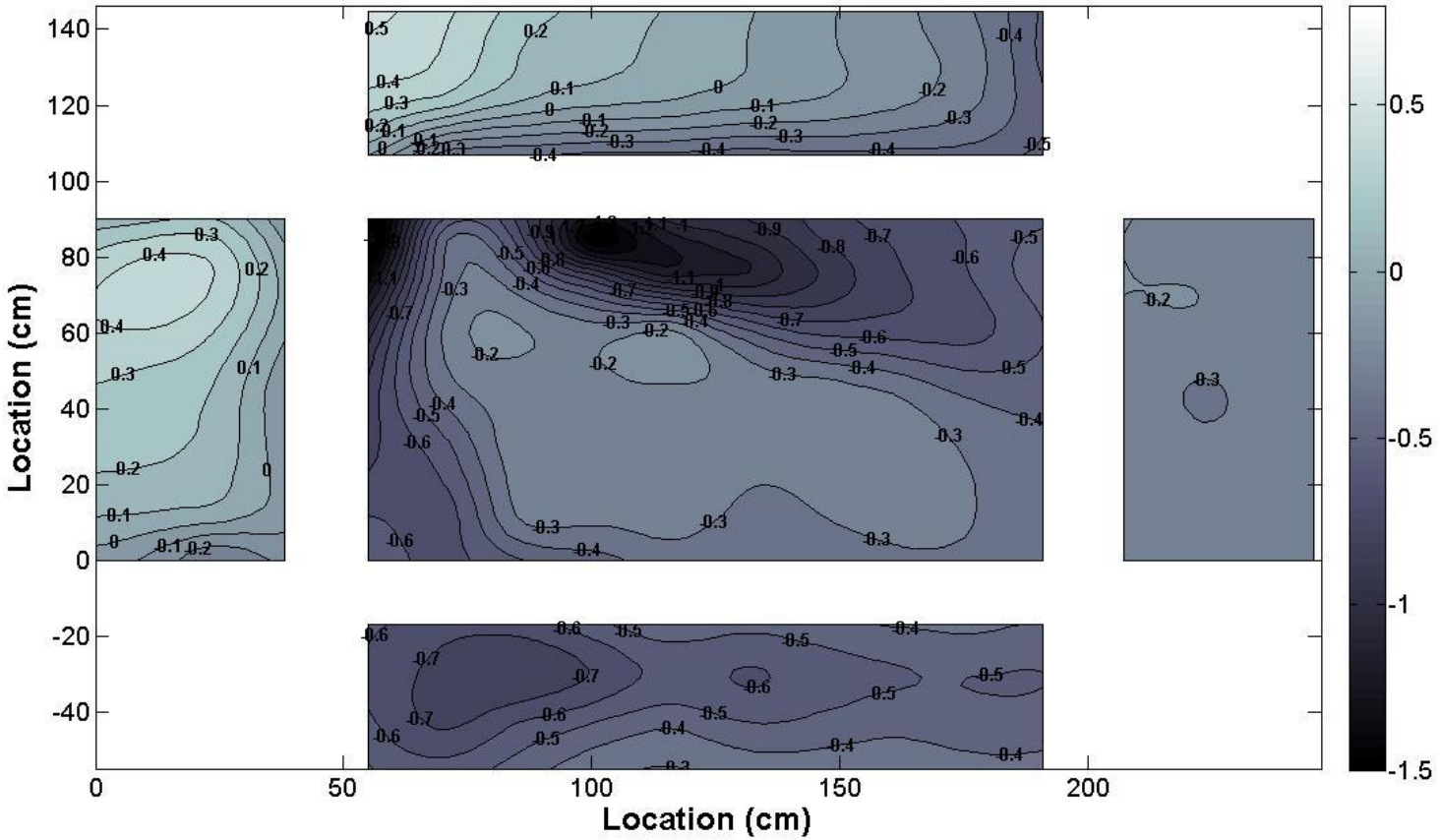

Figure 5-13. Exploded view of 1:10 scaled model Wind Engineering Research Field Laboratory (WERFL)Test Building's mean Cps with flow simulated 45 degrees from the longitudinal axis (AOA = 45^{o})

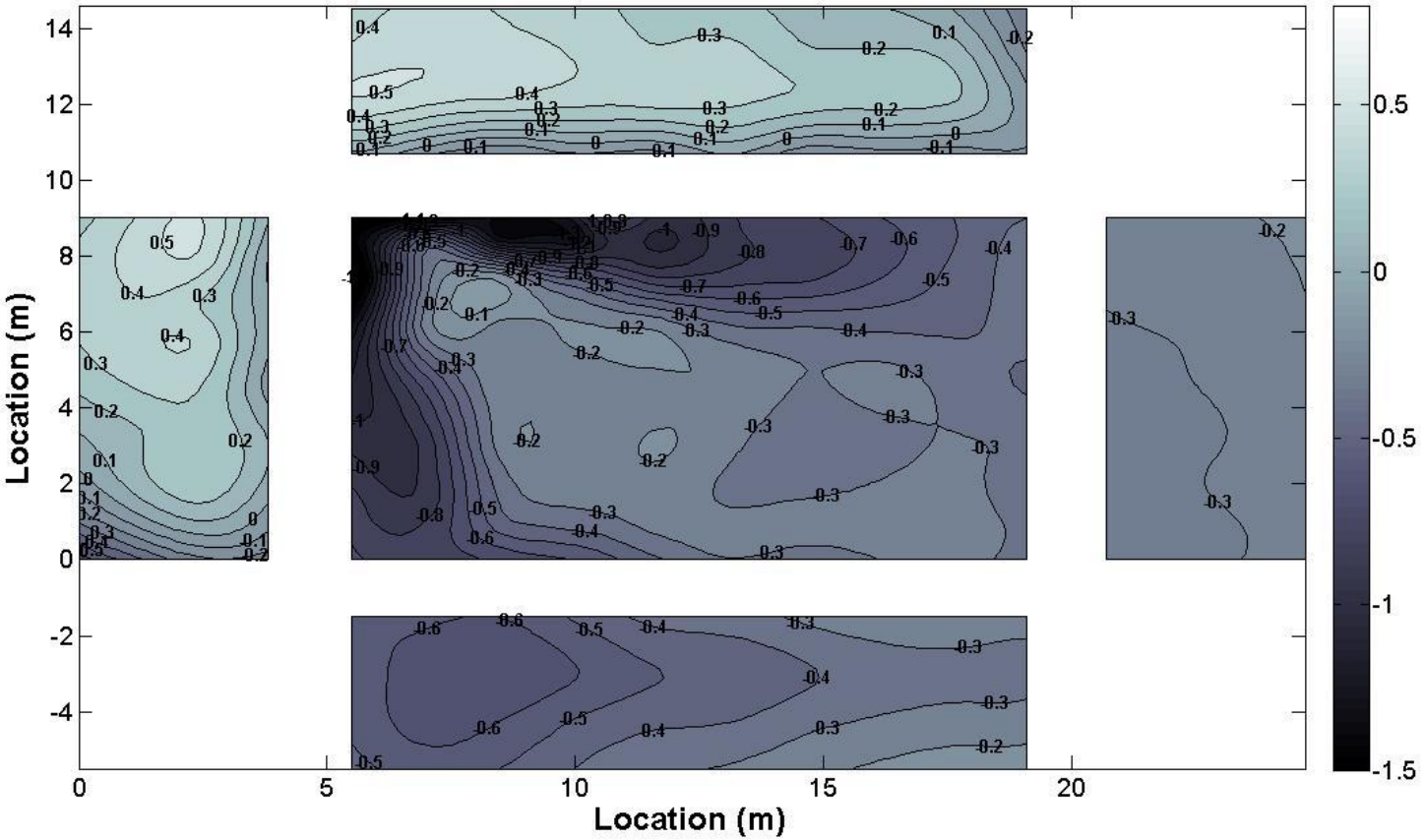

Figure 5-14. Exploded view of the Wind Engineering Research Field Laboratory (WERFL)Test Building's mean Cps with flow simulated 45 degrees from the longitudinal axis (AOA = 45^{o})

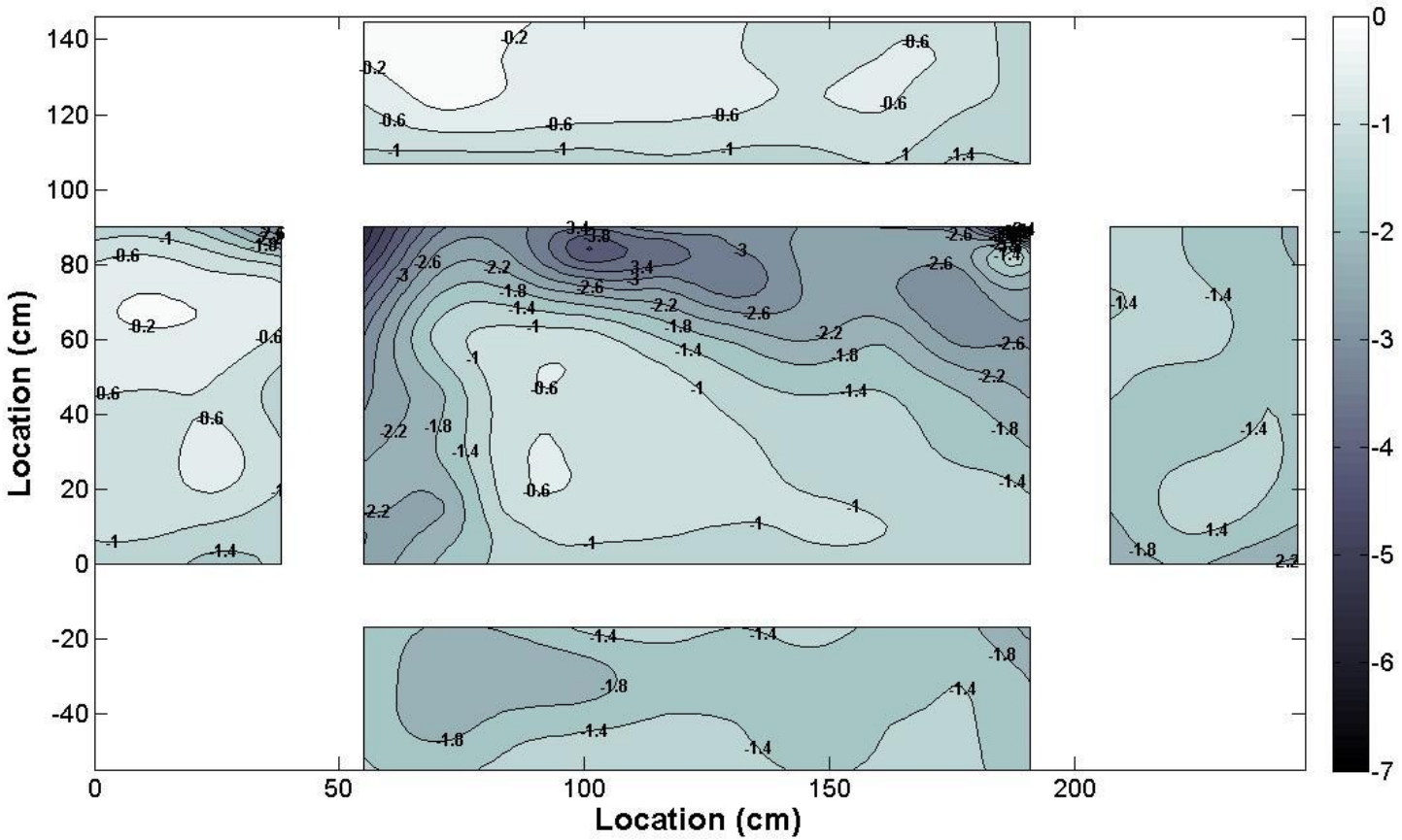

Figure 5-15. Exploded view of 1:10 scaled model Wind Engineering Research Field Laboratory (WERFL)Test Building's minimum Cps with flow simulated 45 degrees from the longitudinal axis (AOA = 45^{o})

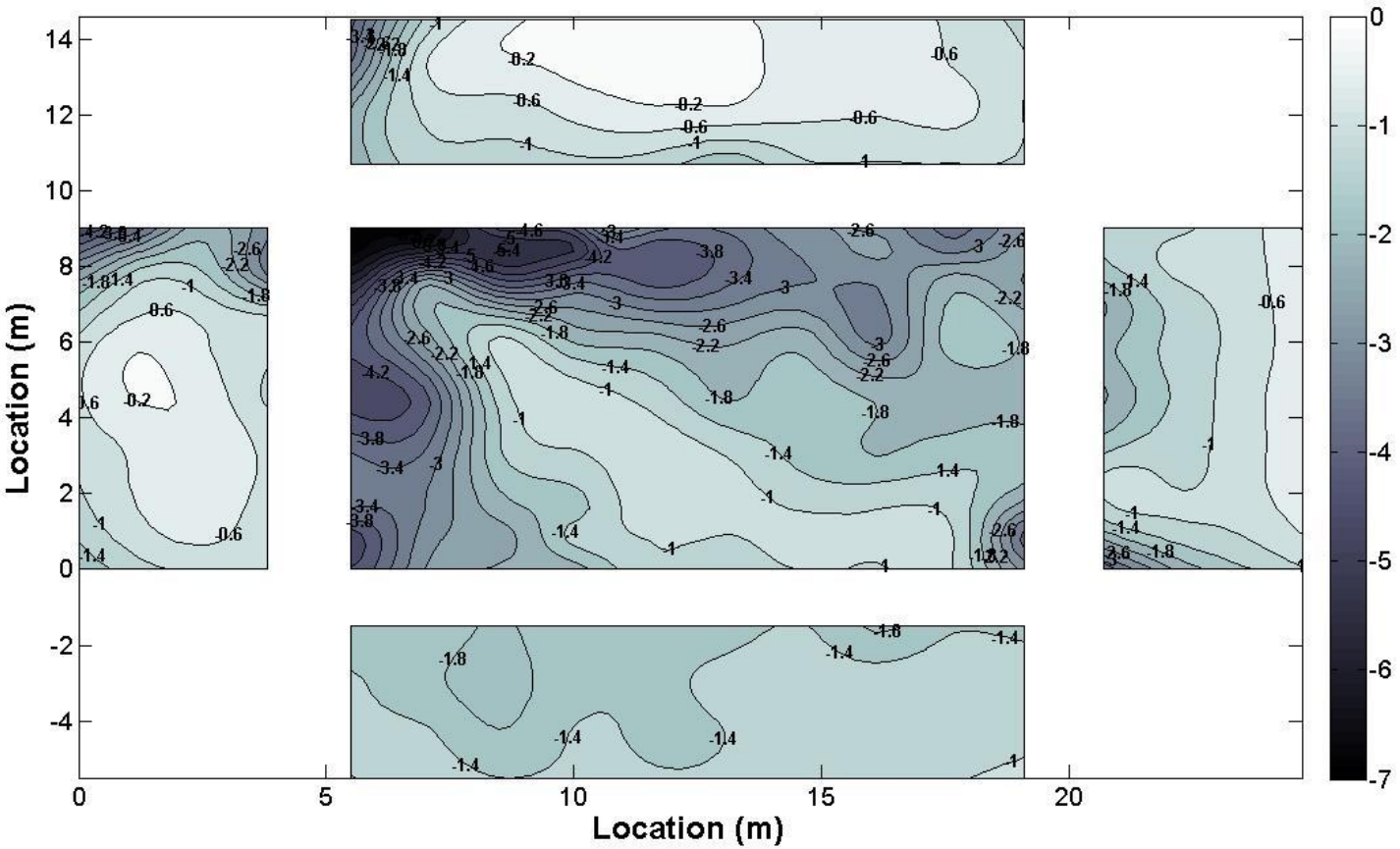

Figure 5-16. Exploded view of the Wind Engineering Research Field Laboratory (WERFL)Test Building's minimum Cps with flow simulated 45 degrees from the longitudinal axis (AOA = 45^{o})

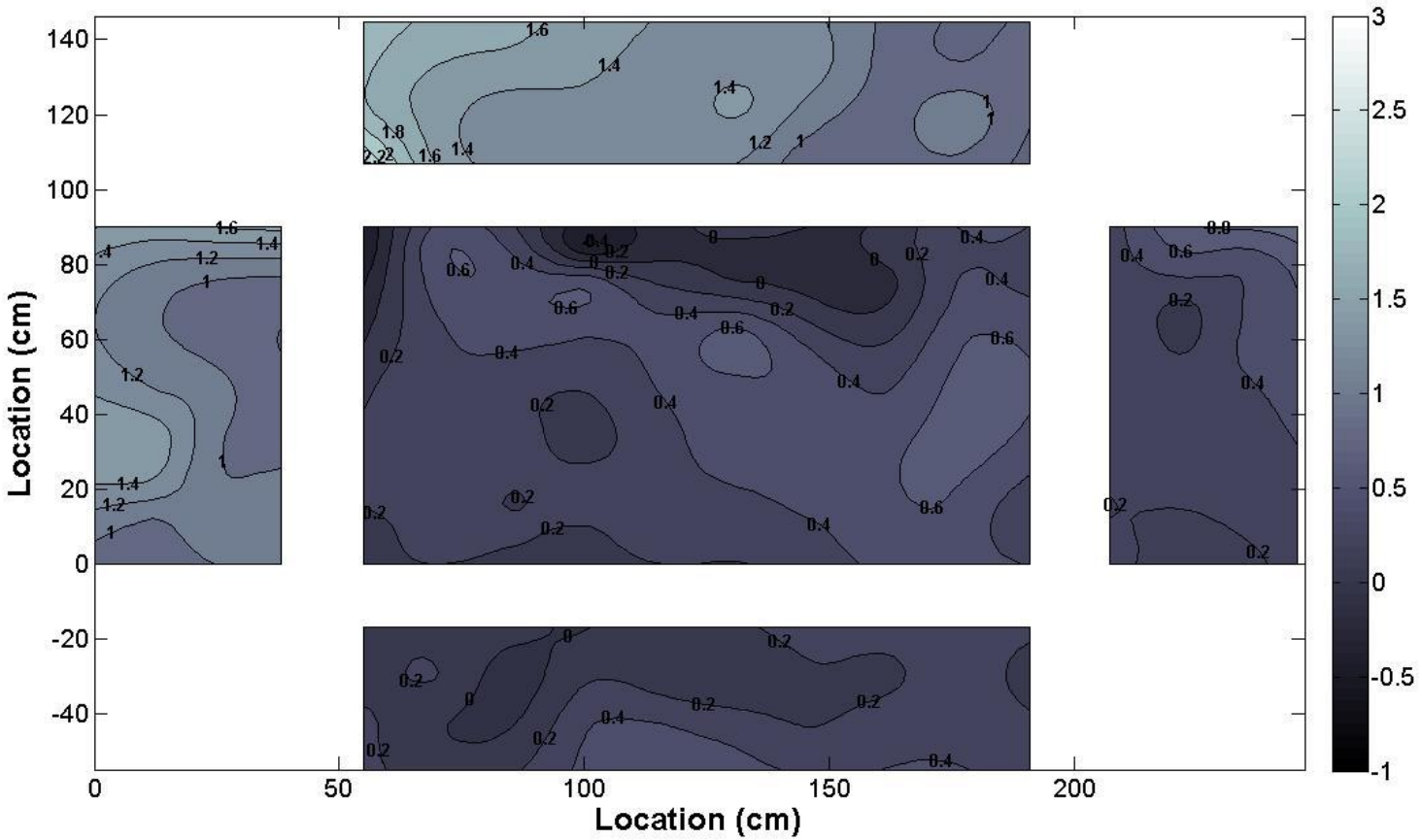

Figure 5-17. Exploded view of 1:10 scaled model Wind Engineering Research Field Laboratory (WERFL)Test Building's maximum Cps with flow simulated 45 degrees from the longitudinal axis (AOA = 45^{o})

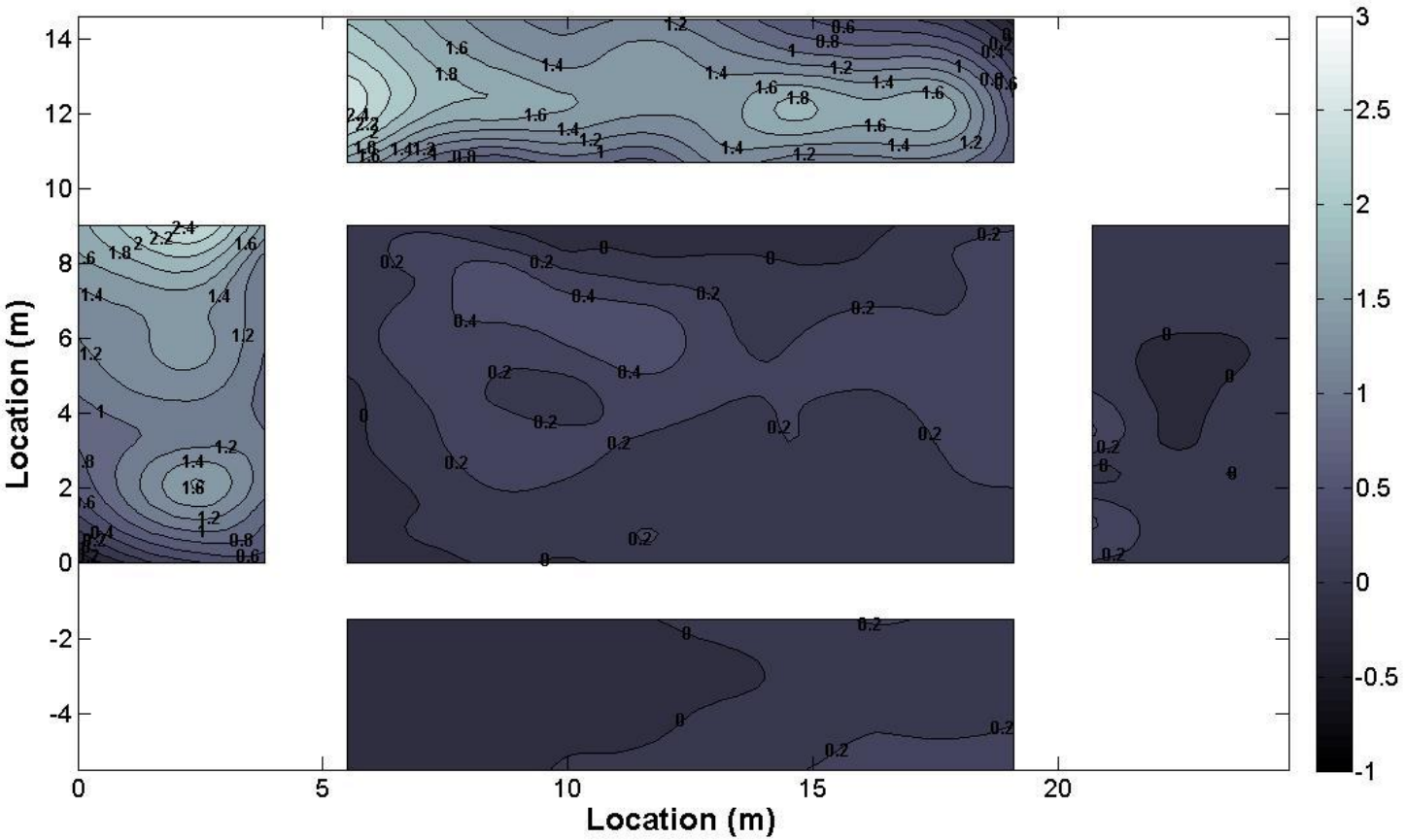

Figure 5-18. Exploded view of the Wind Engineering Research Field Laboratory (WERFL)Test Building's maximum Cps with flow simulated 45 degrees from the longitudinal axis (AOA = 45^{o})

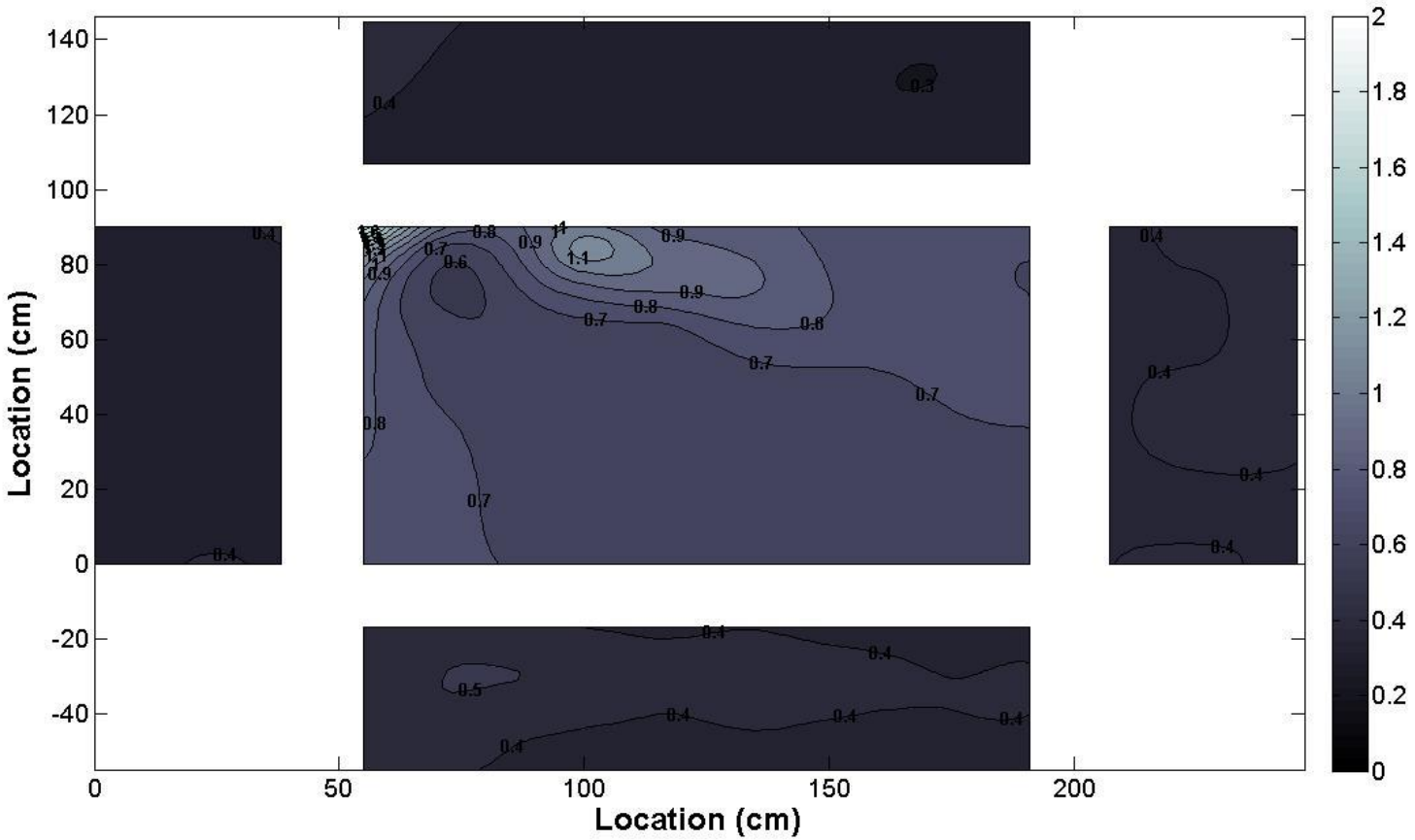

Figure 5-19. Exploded view of 1:10 scaled model Wind Engineering Research Field Laboratory (WERFL)Test Building's RMS Cps with flow simulated 45 degrees from the longitudinal axis (AOA = 45^{o})

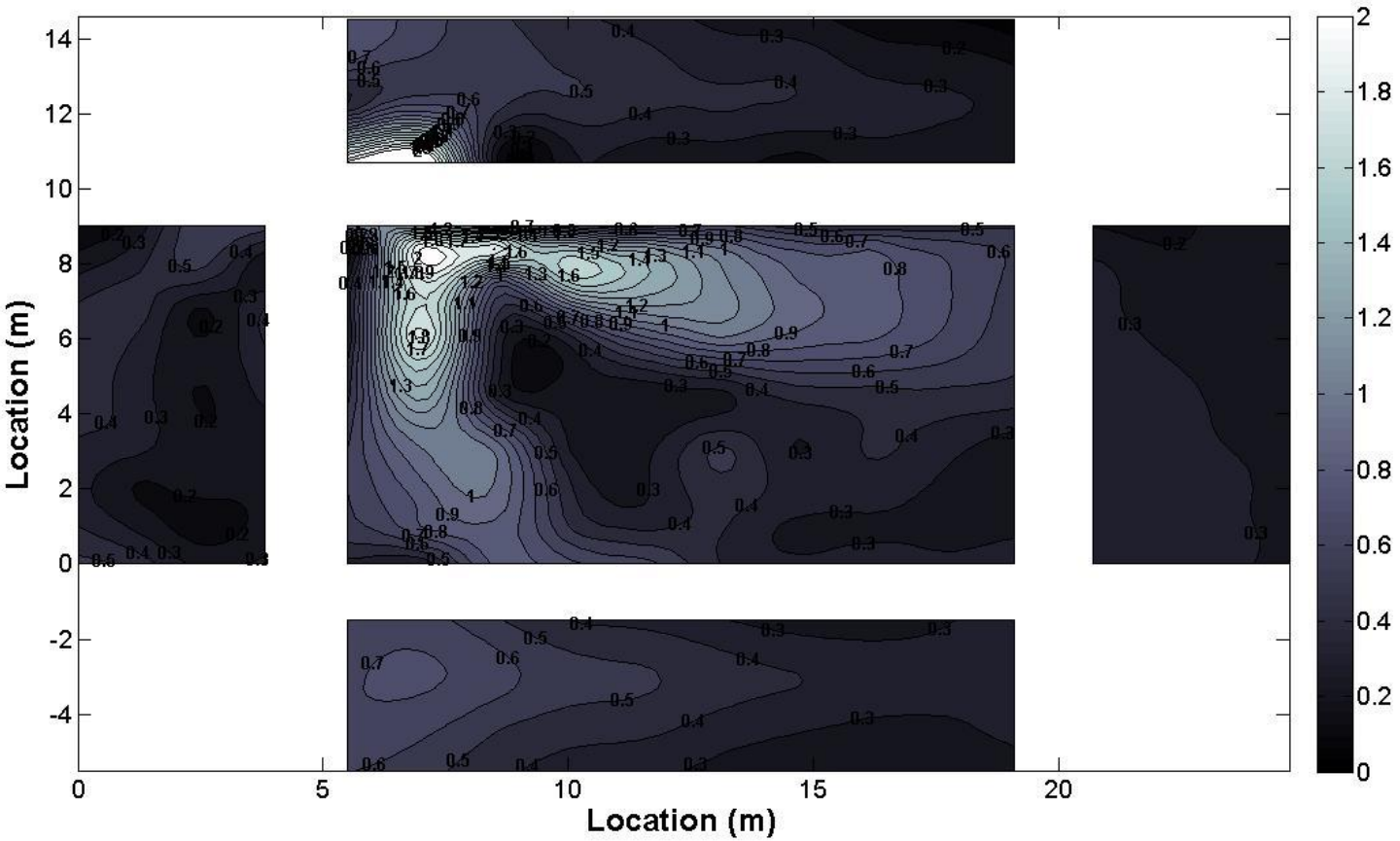

Figure 5-20. Exploded view of the Wind Engineering Research Field Laboratory (WERFL)Test Building's RMS Cps with flow simulated 45 degrees from the longitudinal axis (AOA = 45^0)

Flow Distribution Comparison of Flow Simulated Parallel to the Longitudinal Axis (AOA = 90 deg, WERFL Run 2181)

Model flow conditions for WERFL site run 2181 were established within the test section, the 1:10 WERFL test building was centered on the turntable with the windward wall 1.3 m from the airfoil array as shown in Figure 5-21. A pressure scan was then conducted 8 times on 102 pressure taps at AOAs of 90 and 270 degrees and compared with WERFL test building data. The ensemble averages of the model's two AOAs pressure scans were combined to recreate all respective 204 full-scale taps.

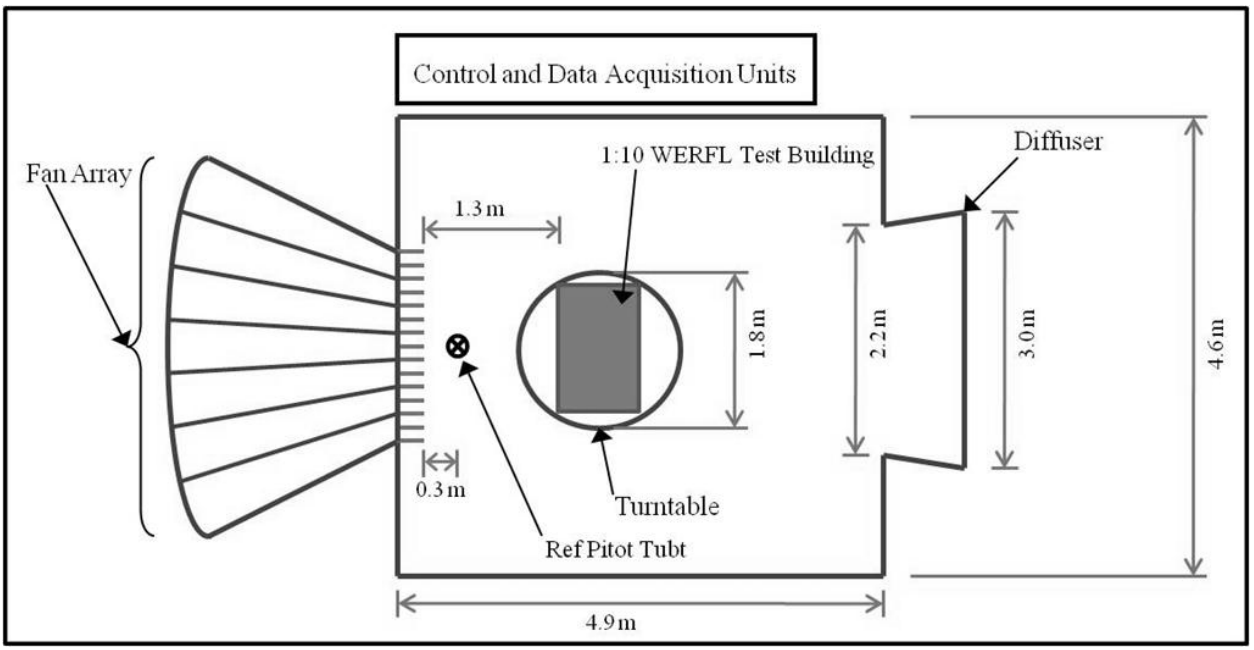

Figure 5-21. Plan view of 1:10 scale model of the Insurance Institute for Business & Home Safety Research Center Full-Scale Test Facility

Model- and full-scale pressure distributions' characteristics are shown in Figure 5-22 through Figure 5-29. Comparing 1:10 model and full-scale Cp_{mean} distributions (Figure 5-22 and Figure 5-23) showed favorable agreement on the windward wall (surface 2) were variations increased closer to the eave height. Amplitude of suction at the windward eave of the roof varied by 30% between the model and full-scale data,

while flow converges on the 1:10 model 85% of the width of the roof and full-scale pressures converge within 70% of the width of the roof. Pressures on the leeward wall were uniform in distribution and magnitude between the 1:10 model and full-scale. Figure 5-24 and Figure 5-25 show the variation between the Cp_{min} distributions. Overall minimum distributions on the 1:10 model were less in amplitude than full-scale. Full-scale distributions also had more variation then the 1:10 model. Figure 5-26 and Figure 5-27 compare Cp_{max} distributions. Full-scale maximums have consistent variation on the windward wall from the center to the corners and eave, while the 1:10 model scale maximums are lower in amplitude and do not follow any trend. The 1:10 model has higher amplitude maximums on the leeward edge of the roof and leeward wall. Sidewall distributions agreed well between the 1:10 model and full-scale. Figure 5-28 and Figure 5-29 display the variation of Cp_{rms} between the 1:10 model and full-scale. The 1:10 rms distributions are uniform on the windward and leeward walls. Full-scale data has a consistent variation on the windward wall decreased from the center to the corners and eave with a sudden increase on the roof at the windward eave that decreases until it converges at 75% of the length of the roof. Convergence was also shown on the 1:10 though the amplitude of the converged model is 200% higher than full-scale.

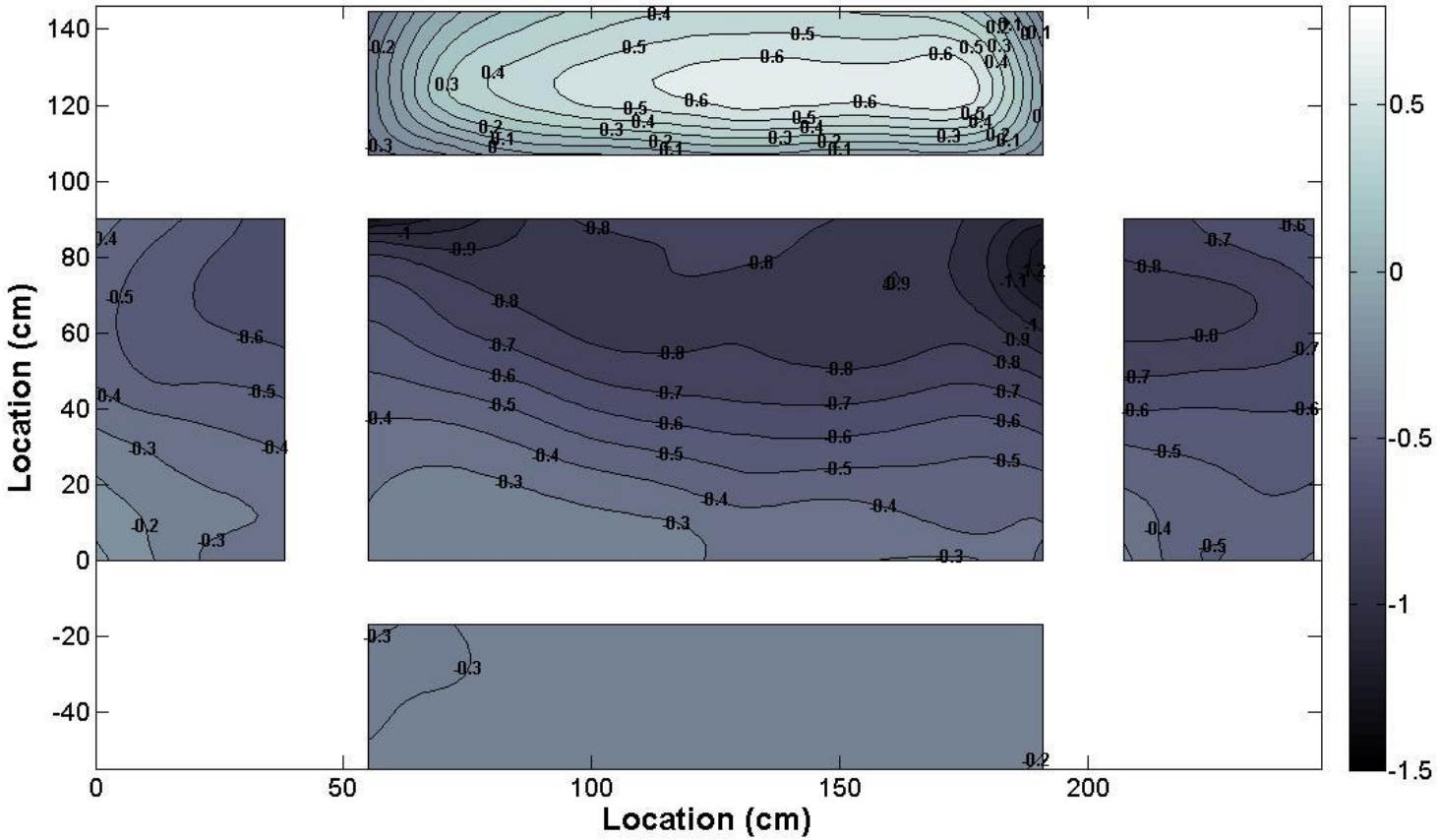

Figure 5-22. Exploded view of 1:10 scaled model Wind Engineering Research Field Laboratory (WERFL)Test Building's mean Cps with flow simulated parallel to the transverse axis (AOA = 90^{o})

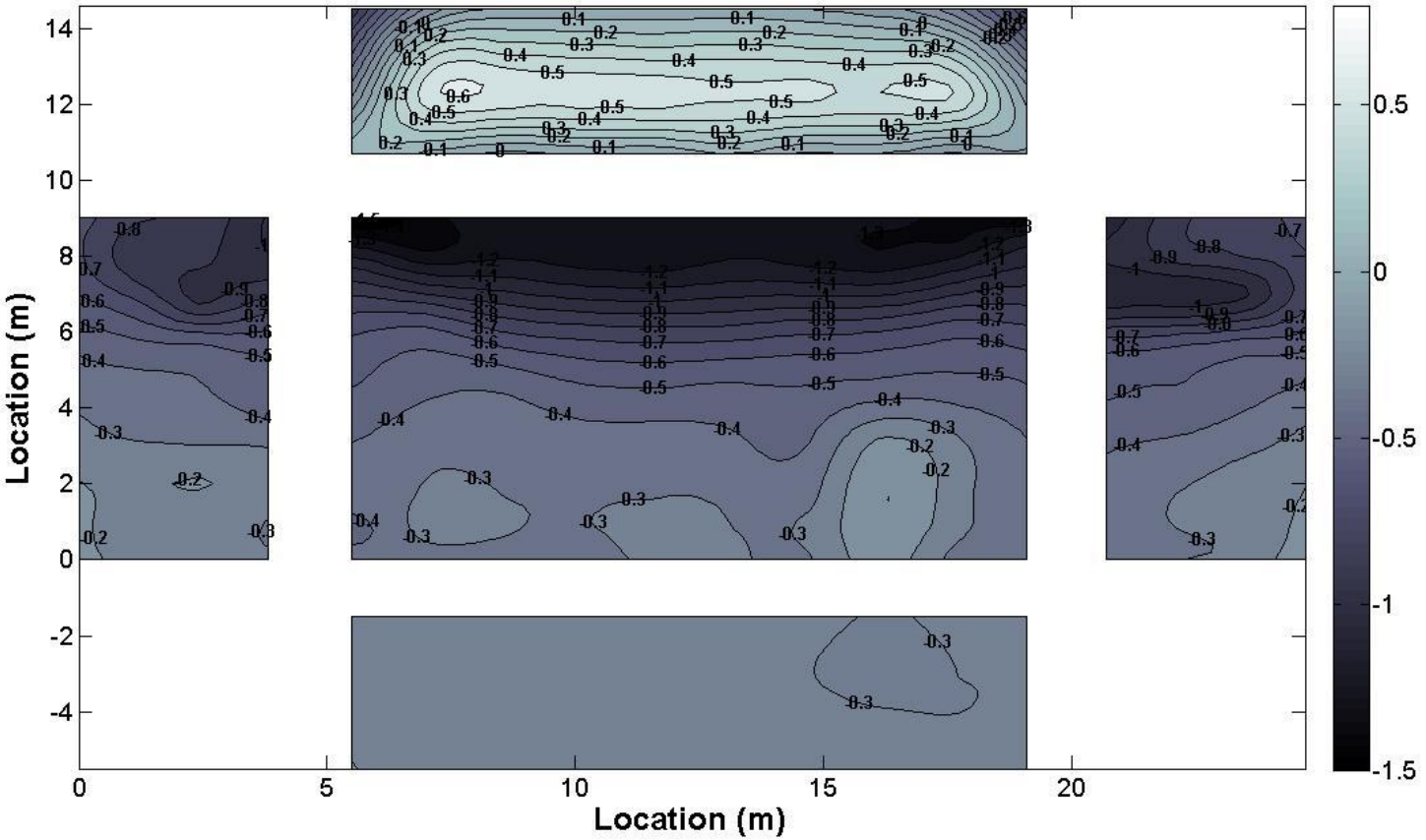

Figure 5-23. Exploded view of the Wind Engineering Research Field Laboratory (WERFL)Test Building's mean Cps with flow simulated parallel to the transverse axis (AOA = 90^{o})

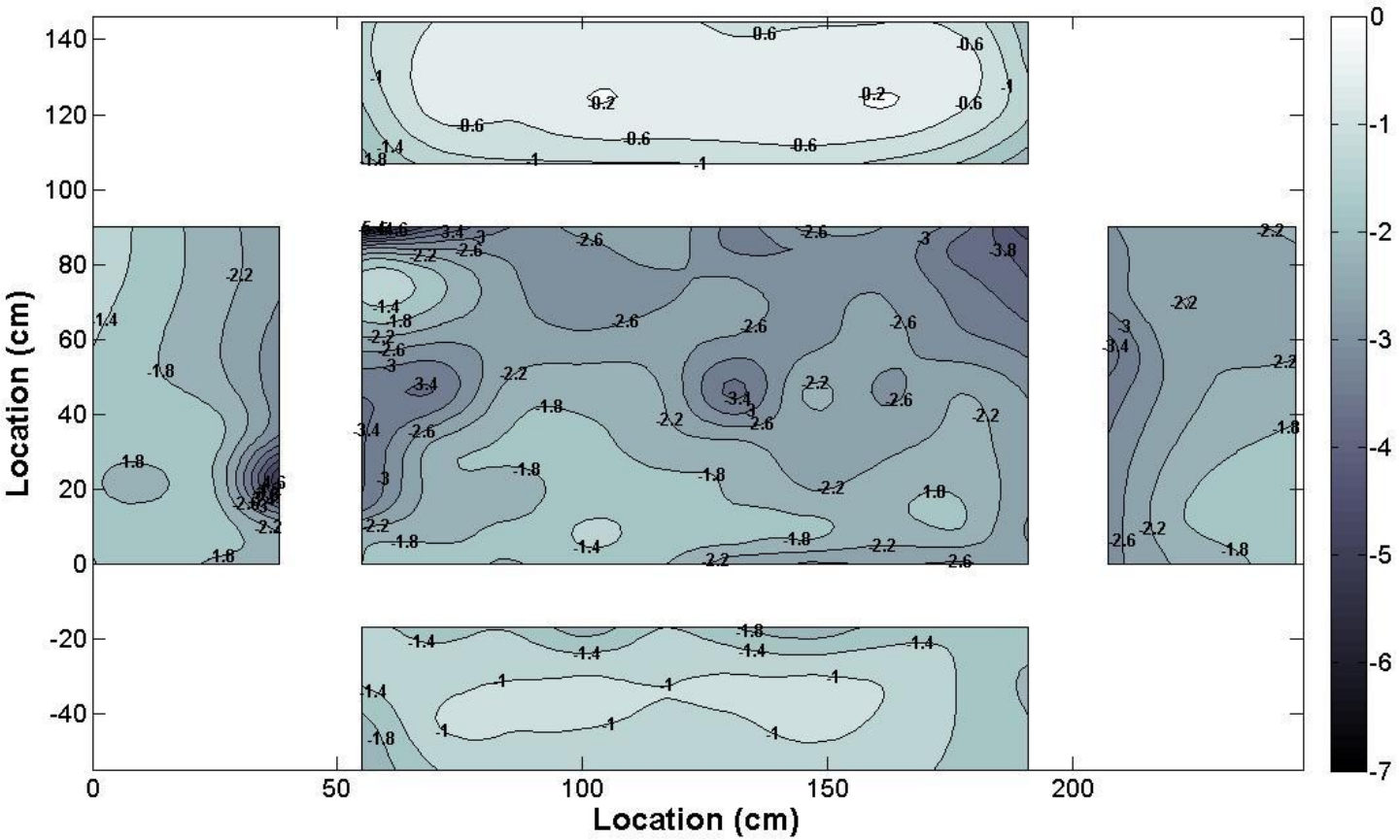

Figure 5-24. Exploded view of 1:10 scaled model Wind Engineering Research Field Laboratory (WERFL)Test Building's minimum Cps with flow simulated parallel to the transverse axis (AOA = 90^{o})

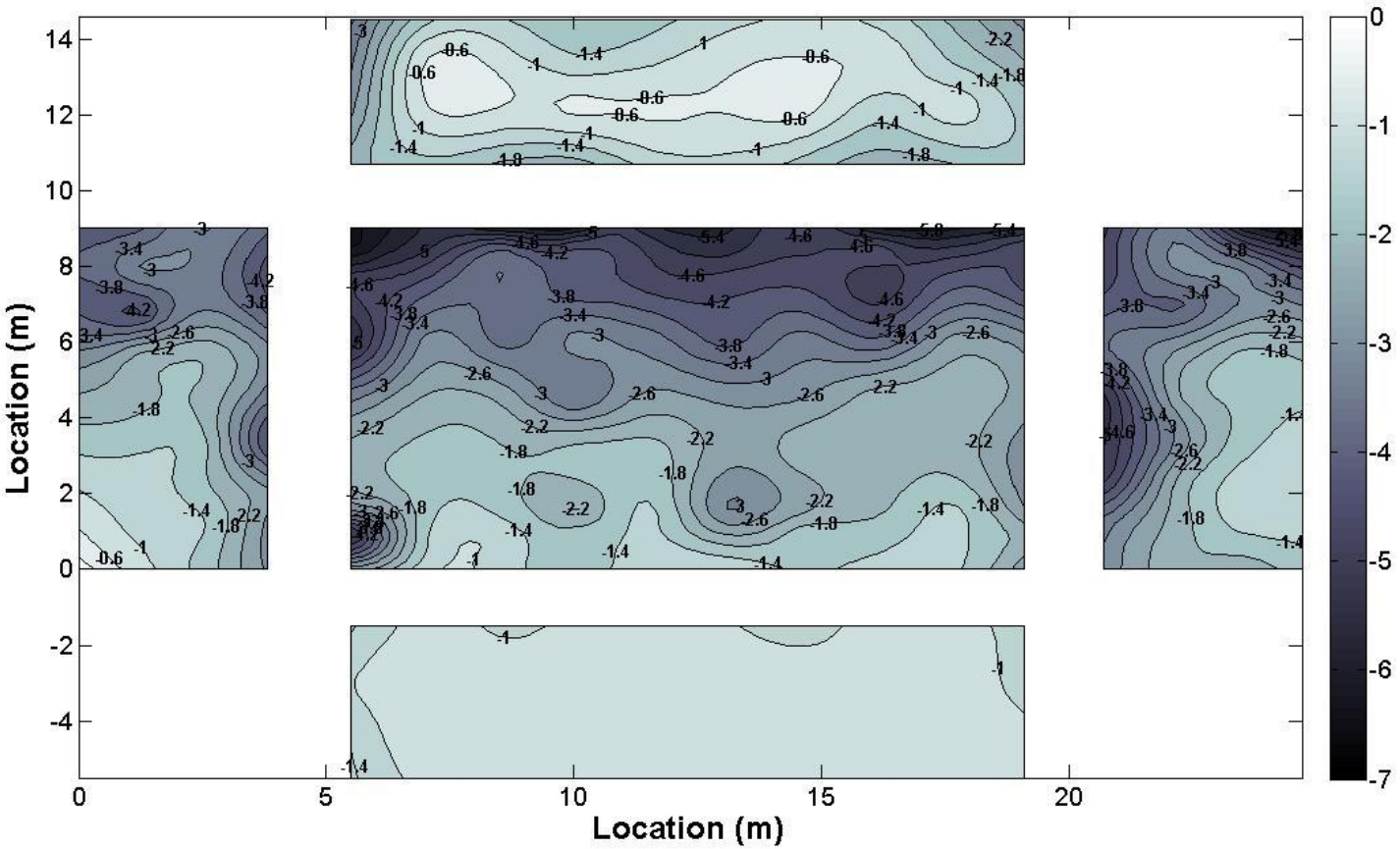

Figure 5-25. Exploded view of the Wind Engineering Research Field Laboratory (WERFL)Test Building's minimum Cps with flow simulated parallel to the transverse axis (AOA = 90^{o})

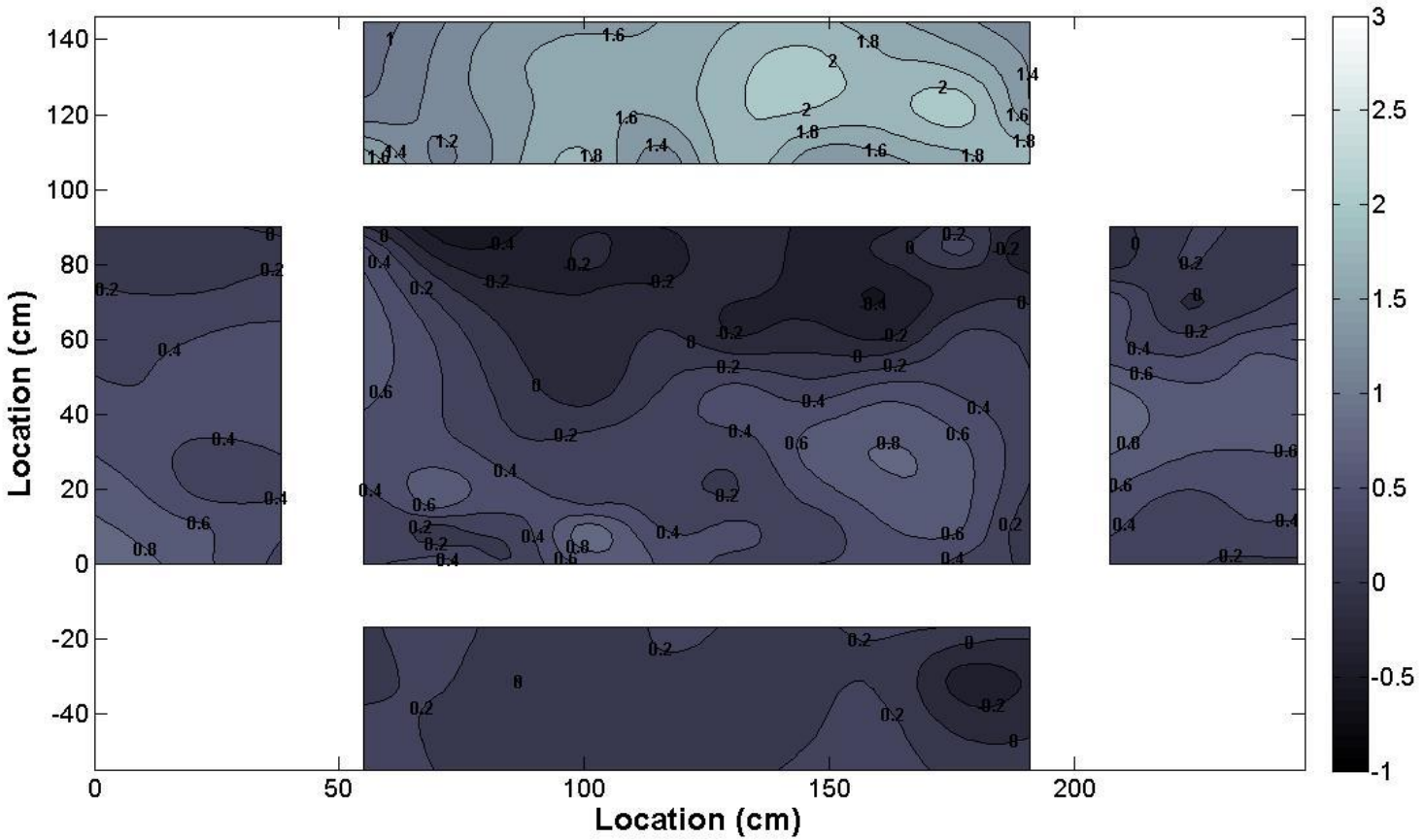

Figure 5-26 . Exploded view of 1:10 scaled model Wind Engineering Research Field Laboratory (WERFL)Test Building's maximum Cps with flow simulated parallel to the transverse axis (AOA = 90^{o})

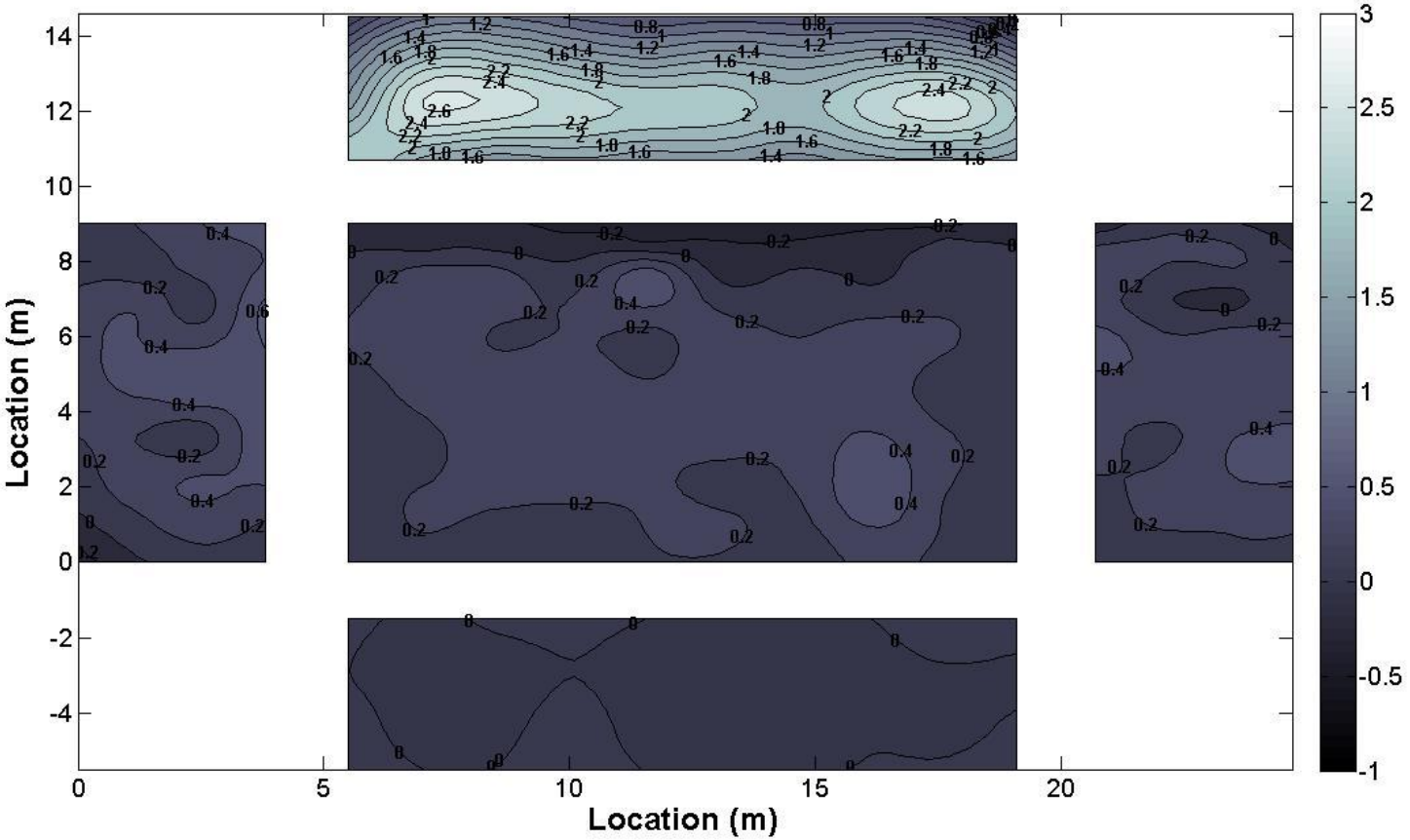

Figure 5-27. Exploded view of the Wind Engineering Research Field Laboratory (WERFL)Test Building's maximum Cps with flow simulated parallel to the transverse axis (AOA = 90^{o})

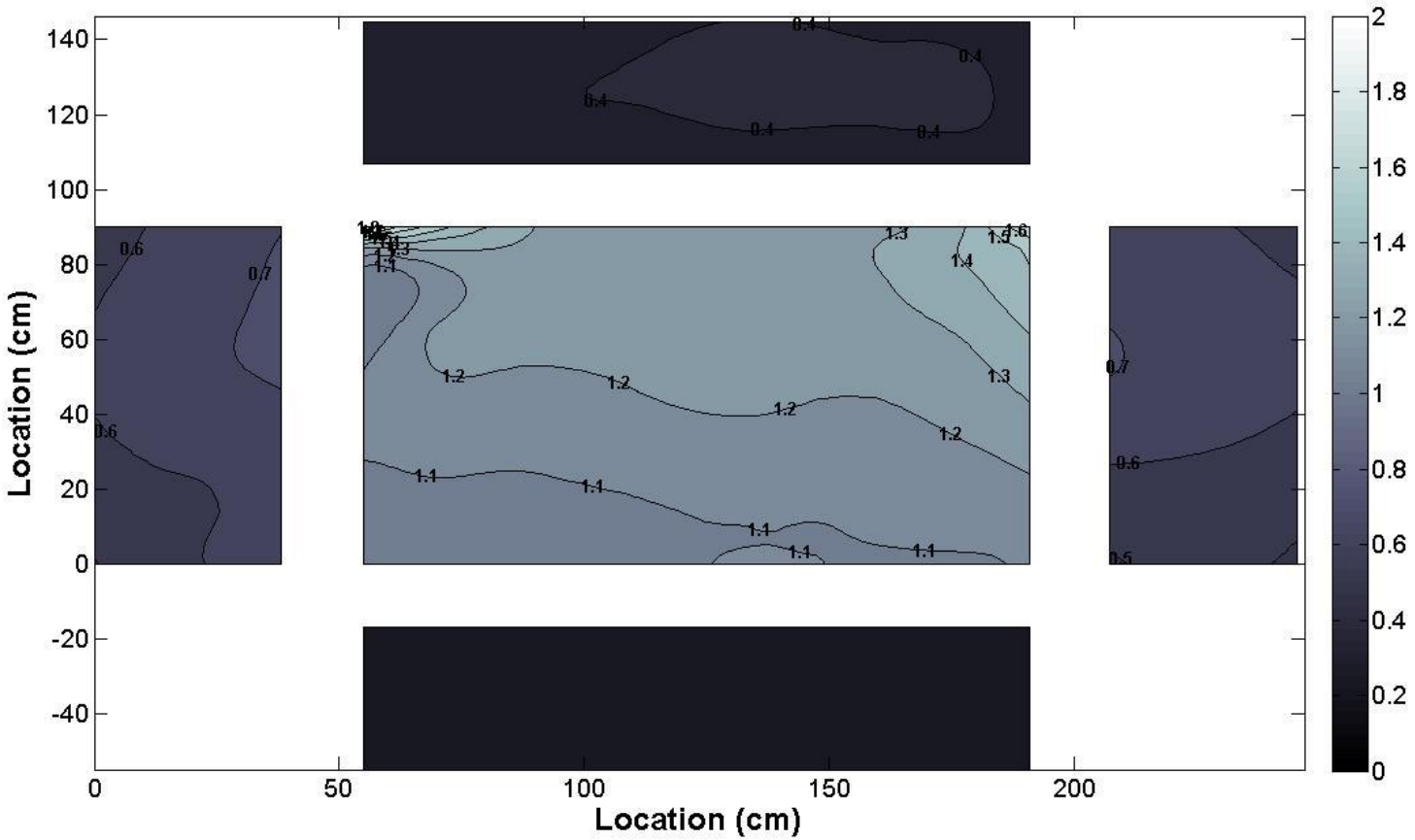

Figure 5-28. Exploded view of 1:10 scaled model Wind Engineering Research Field Laboratory (WERFL)Test Building's RMS Cps with flow simulated parallel to the transverse axis (AOA = 90^{o})

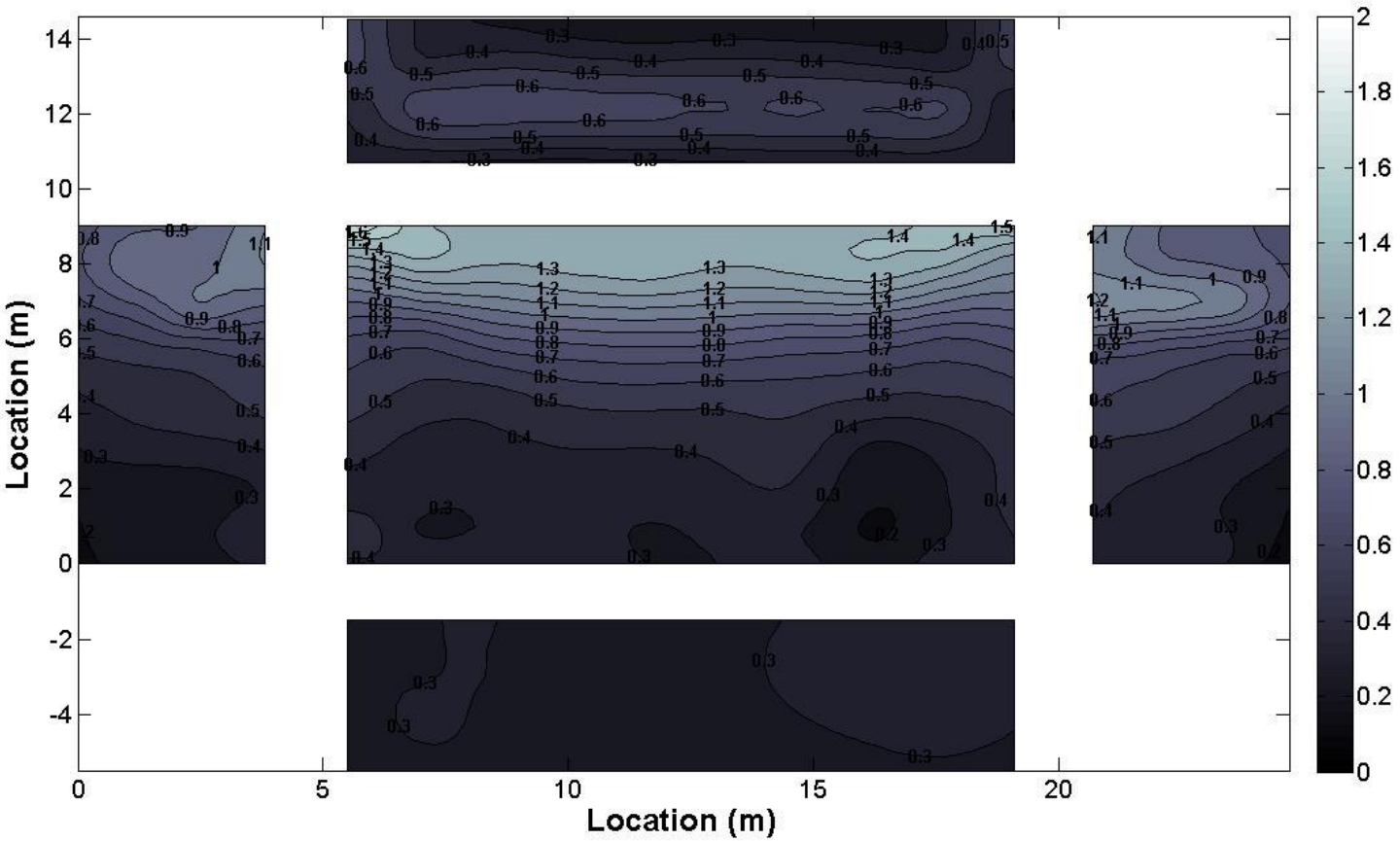

Figure 5-29. Exploded view of the Wind Engineering Research Field Laboratory (WERFL)Test Building's RMS Cps with flow simulated parallel to the transverse axis (AOA = 90^{o})

Discussion of Variations between Model and Full-Scale Pressure Distributions

Sources of the variations between pressure distributions of the 1:10 model and WERFL test building may be attributed to the following factors. First was the effect of the high frequency component of simulated time histories shown in Figure 3-19 associated with the vortices produced by the propeller and/or vanes. It was assumed the effect of the higher frequencies was negligible due to minimal energy associated with them. Large local variations of maximum pressure coefficients occur due to flow separation, which was shown within the Cp_{max} comparisons over the roof in which the 1:10 model exhibits higher amplitude distribution toward the leeward wall. Uncertainties between the eight model scales measurements are compared to full-scale data in Appendix A.

Second, it has been proven that small-scale turbulence has an influence on the development of shear layers and vortices that adversely affect the mean and fluctuating surface pressure (Gartshore, 1973). However, due to the incomplete understanding of vortex formation and the development of shear layers, previous studies were based only upon model and full-scale comparisons. The majority of past wind tunnel testing has successfully modeled mean pressure coefficients of full-scale and model testing (Tieleman, H. et al., 2003; Surry, D., 1991). However, accurate simulation of high suction pressure near roof corners and leading edges of the roof have proved highly difficult. The difficulty of adequately modeling corner pressures can be attributing to an inadequate simulation of longitudinal and lateral turbulence characteristics, particularly at smaller spatial scales. Previous studies have shown that an increase in model size results in improved simulation of the fluctuating pressure on corner vortices on the roof (Tieleman, 2003). For this study, a large model and accurate modeling of the lateral and longitudinal turbulence were obtained, thus we assume effects of shear layer mixing and vortices were negligible when the model was immersed in the flow.

Third, the use of vanes and an active fan system has produced the simple mechanical properties of a turbulent boundary layer flow from a minimal development length. This was accomplished at the expense of the longitudinal length scale. However, Stathopoulos (1983) determined that precise modeling of the desired integral length scale could be relaxed by a factor of two without adversely affecting the magnitudes of the pressure distributions. Tieleman (1998) concluded that the model length scale could be smaller than 20% of the desired value. Both of these conclusions were derived without investigating the effects on the peak pressure coefficients.

Fourth, root mean squared (rms) values are sensitive to fluctuations of wind direction. For example, an increase in wind direction variations would create an increase of rms values. Time domain characteristics of the lateral component of full-scale data were model accurately (per Chapter 4); however variations of the frequency content of the lateral fluctuations were not. Dissimilarities between rms values could be attributed to inaccurate modeling of full-scale fine scale fluctuations.

Summary

A 1:10 scaled model of the TTU WERFL test building was immersed into flow conditions obtained using the procedure presented in Chapter 3. Three angles of attacks were tested, in which flow condition were parallel to the longitudinal axis, 45 degrees from the longitudinal axis, and parallel to the transverse axis. Statistical components of the 1:10 scale model and full-scale pressure distributions were compared.

CHAPTER 6
CONCLUSIONS AND RECOMMENDATIONS FOR FUTURE RESEARCH

This dissertation presents a new technique to calibrate the system to generate mean velocity and turbulence characteristics for a wide range of terrains. A closed-loop control system was implemented to simulate stationary anemometric records converted from full- to model-scale. A case study was presented using a 1:10 scale model of the Insurance Institute for Business & Home Safety (IBHS) Research Center Full-Scale Test Facility in Richburg, South Carolina. Similitude is achieved for the (a) mean velocity profile, (b) longitudinal, lateral and vertical turbulence intensity profiles, (c) the corresponding power spectra, (d) gust factors and (e) integral length scales. An instrumented 1:10 scale model was then immersed into prescribed flow conditions for comparison with full-scale building pressure distributions.

The main contribution of this research is an improvement to existing methods to calibrate approach flows in full-scale test facilities and a new technique to simulate a wide range of atmospheric boundary layer flow conditions in a multiple controlled fan wind tunnel (MCFWT). The following sections summarize contributions and conclusions about the research presented within and suggest recommendation for future research.

Conclusion of the Multiple Controlled Fan Wind Tunnel (MCFWT)

A new method to simulate desired approach flow conditions in a MCFWT was presented. A case study was presented using a 1:10 scale model of the IBHS Research Center Full-Scale Test Facility. Simulations of marine, open, and suburban approach boundary layer flow conditions were in good agreement between model and measured values, including mean velocity, turbulence intensity profiles, integral length scales, and power spectra. Vertical turbulence could not be directly controlled with this method; however, it was observed that similarity in the vertical profiles was achieved once the lateral and longitudinal components

were calibrated. In contrast to other methods that use open loop control (i.e. no feedback), a closed-loop control strategy was implemented to determine the command signals for the fan bank and the airfoil array. Moreover, the proposed approach relies on the direct simulation of scaled wind speed and direction records in lieu of traditional approaches that reshape the desired spectra of the command signals to achieve desire BL characteristics.

A control system was successfully implemented to match simple mechanical turbulence properties of prescribed boundary layer profiles typical of marine, open country and suburban terrains. The research that remained was to determine if these flow configurations reproduced known pressure loading characteristics on buildings immersed in the boundary layer. Overall the 1:10 model pressure distributions conveyed a larger area of flow separation than full-scale distribution; however the source of differences between the 1:10 model and WERFL test building can be attributed to several factors. For example, large local variations of maximum pressure coefficients occurred due to flow separation, which was shown within the Cp_{max} comparisons over the roof in which the 1:10 model exhibits higher amplitude distribution toward the leeward wall. For this study, a large model and accurate modeling of the lateral and longitudinal turbulence were obtained, and effects of shear layer mixing and vortices were negligible when the model was immersed in the flow.

The use of vanes and an active fan system produced the simple mechanical properties of a turbulent boundary layer flow from a minimal development length. Both of these conclusions were derived without investigating the effects on the peak pressure coefficients.

Recommendations for Future Research

To reduce high frequency eddies produced by the propellers, honeycomb grids could be installed within the fan contractions; however this will increase power consumption to maintain

the mean velocities within the test section. Different types of fans (i.e. vane axial) could also aid in the reduction of higher frequency eddies.

Modifications to the control algorithm presented in Chapter 3 could allow for each of the 21 fan cells to have their own input time histories, as oppose to the current configuration only having 3 input time histories for the 3 rows of fans. This would possibly allow for the simulation of prescribed lateral correlations to better model full scale boundary layer fluctuations.

Model scale components such as the cobalt motors used within this study have a higher frequency response characteristic as compared to their full-scale equivalence. The current model configuration could limit the controllers of the motors to model a desired full-scale system's frequency response. This would aid in the investigation of implementing full-scale turbulence mixing devices that could improve energy characteristics within the inertial sub-range of full-scale flow conditions.

APPENDIX A
PRESSURE LOADING COMPARISON

This appendix contains additional information of the simulated pressure loading test conducted within Chapter 4 and Chapter 5.

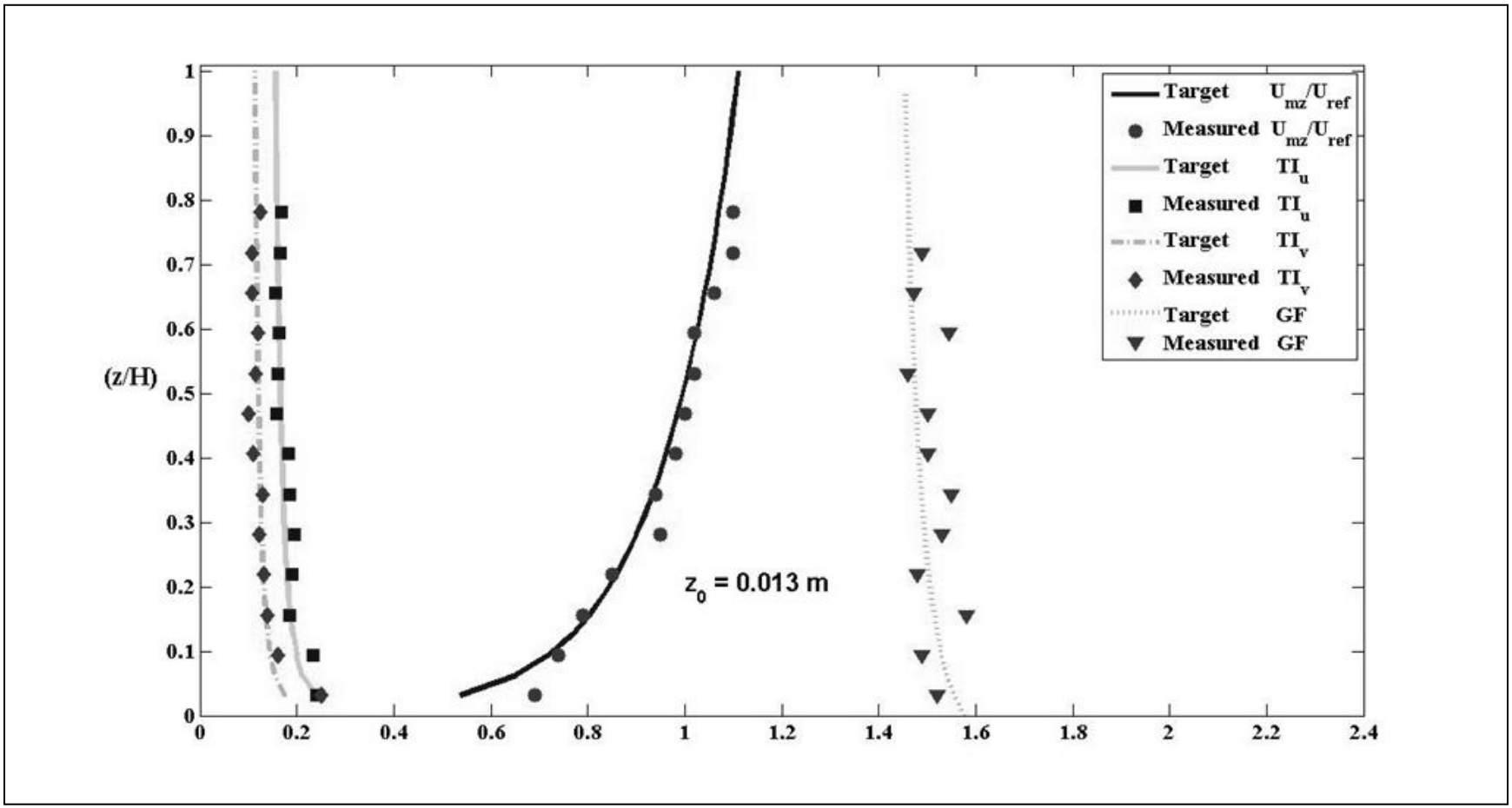

Figure A-1. Wind profile for TTU site exposure (z0 = 0.013 m) Run 620

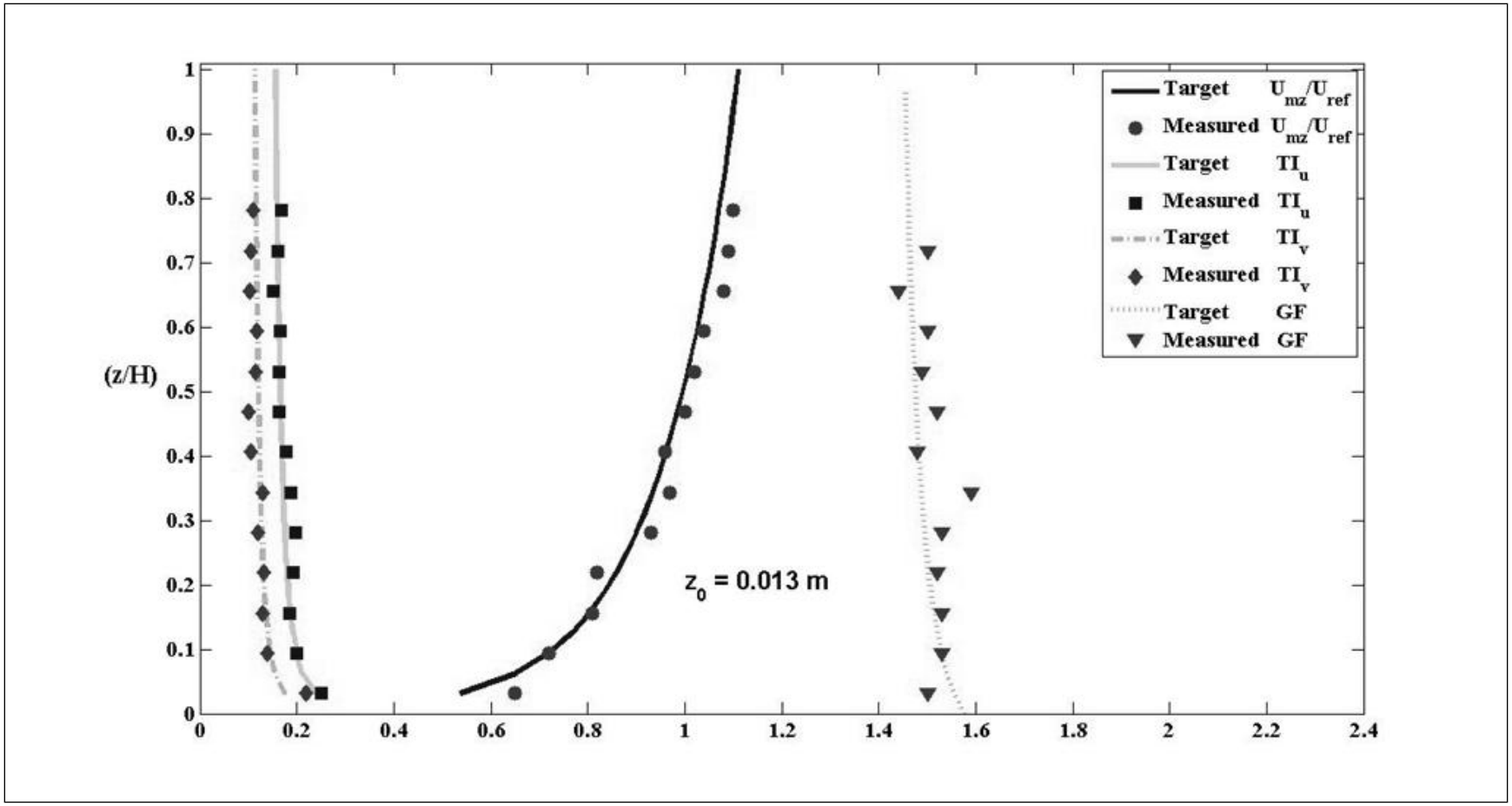

Figure A-2. Wind profile for TTU site exposure (z0 = 0.013 m) Run 4482

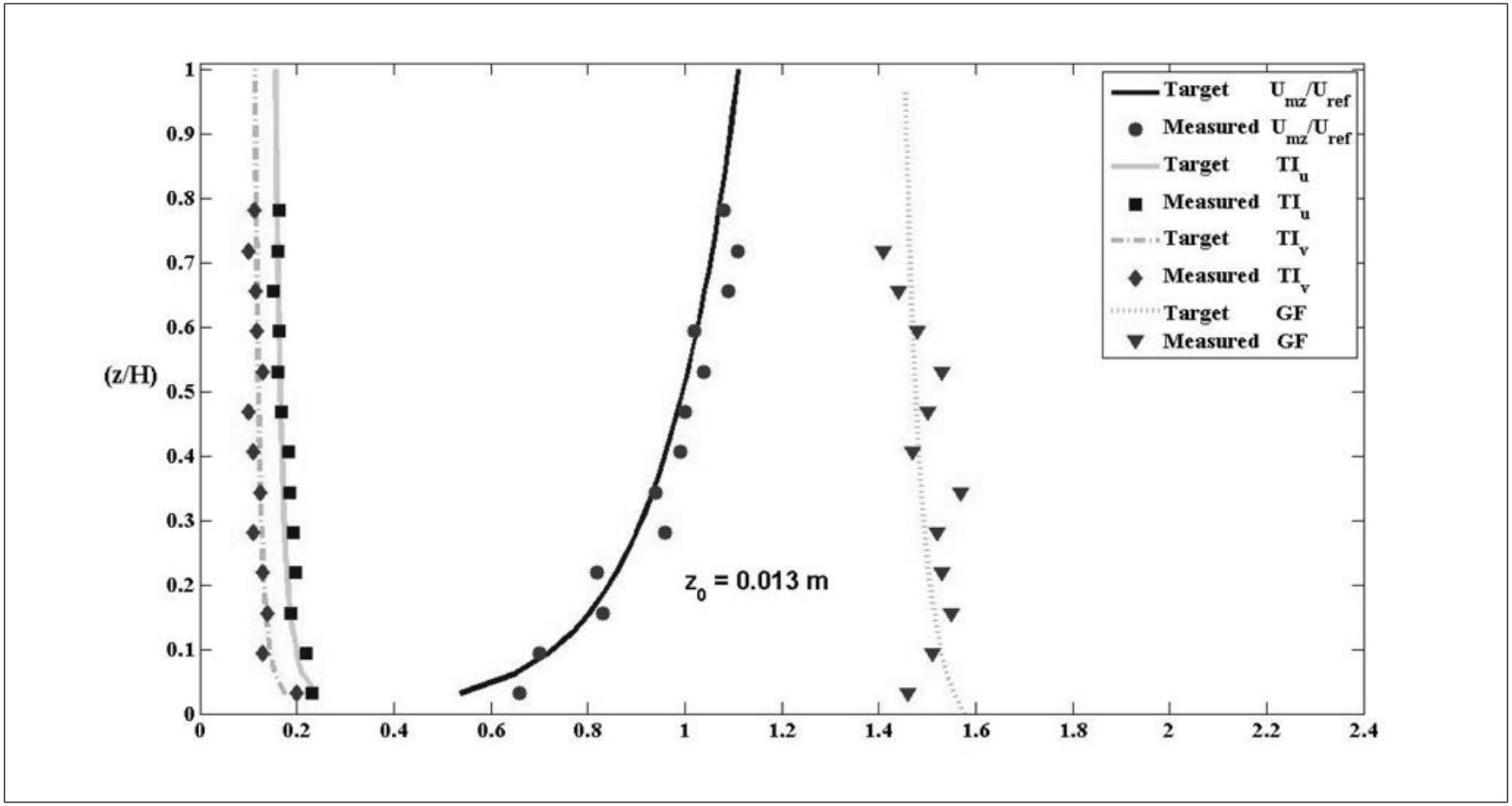

Figure A-3. Wind profile for TTU site exposure (z0 = 0.013 m) Run 2781

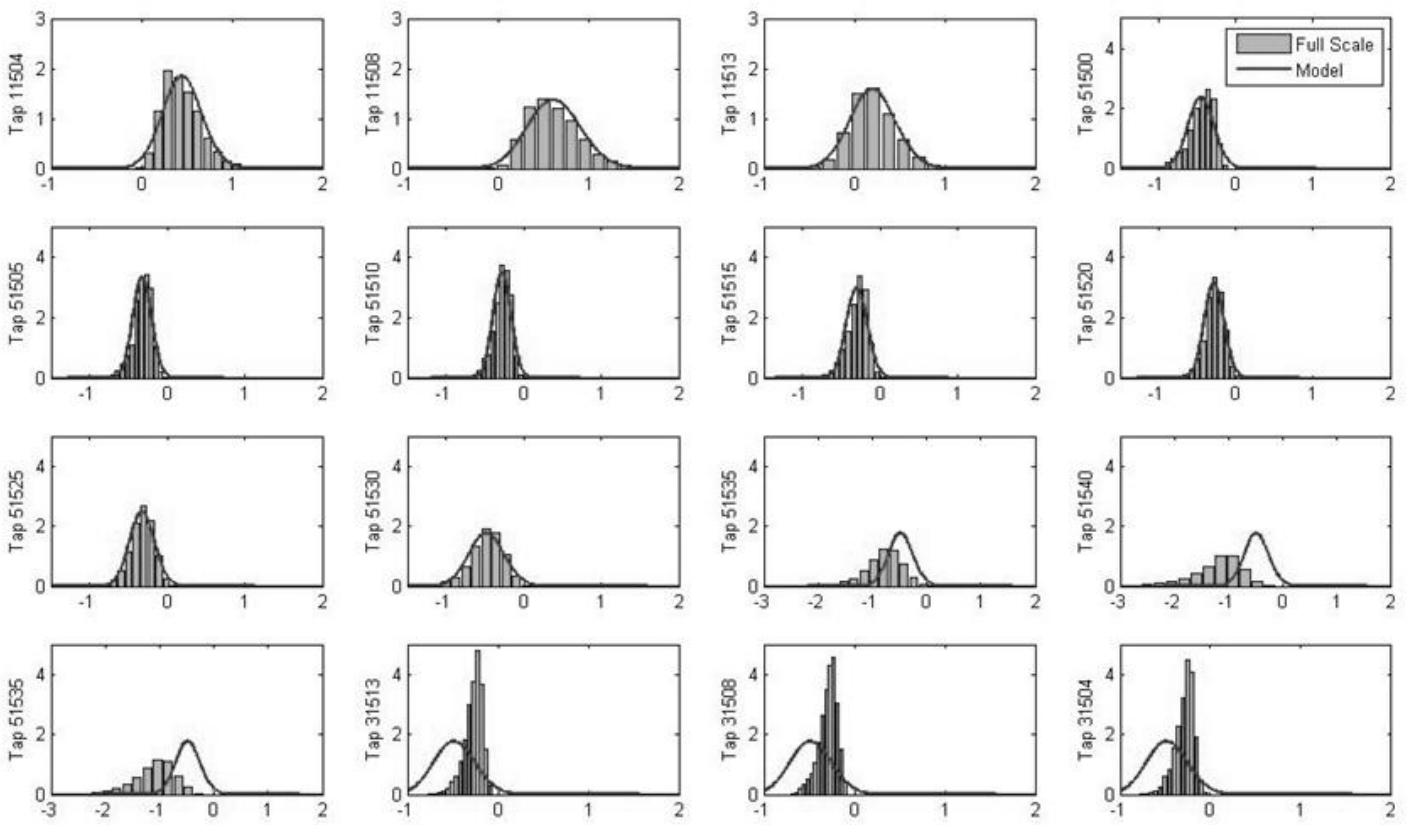

Figure A-4. WERFL Test Building and 1:10 scaled model tap distributions with flow simulated parallel to the longitudinal axis (AOA = 0^{o})

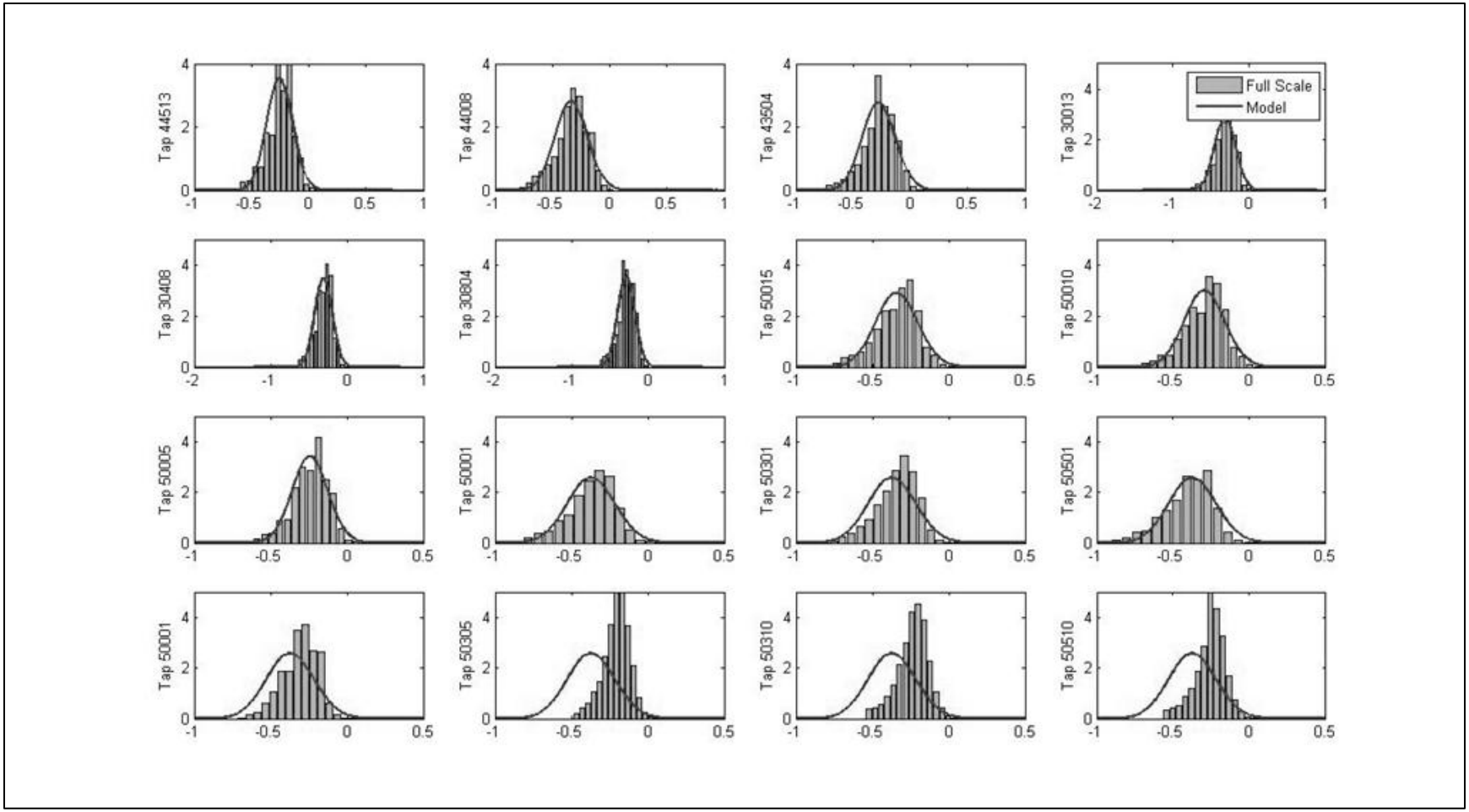

Figure A-5. WERFL Test Building and 1:10 scaled model tap comparison with flow simulated 45 degrees from the longitudinal axis (AOA = 45^{o})

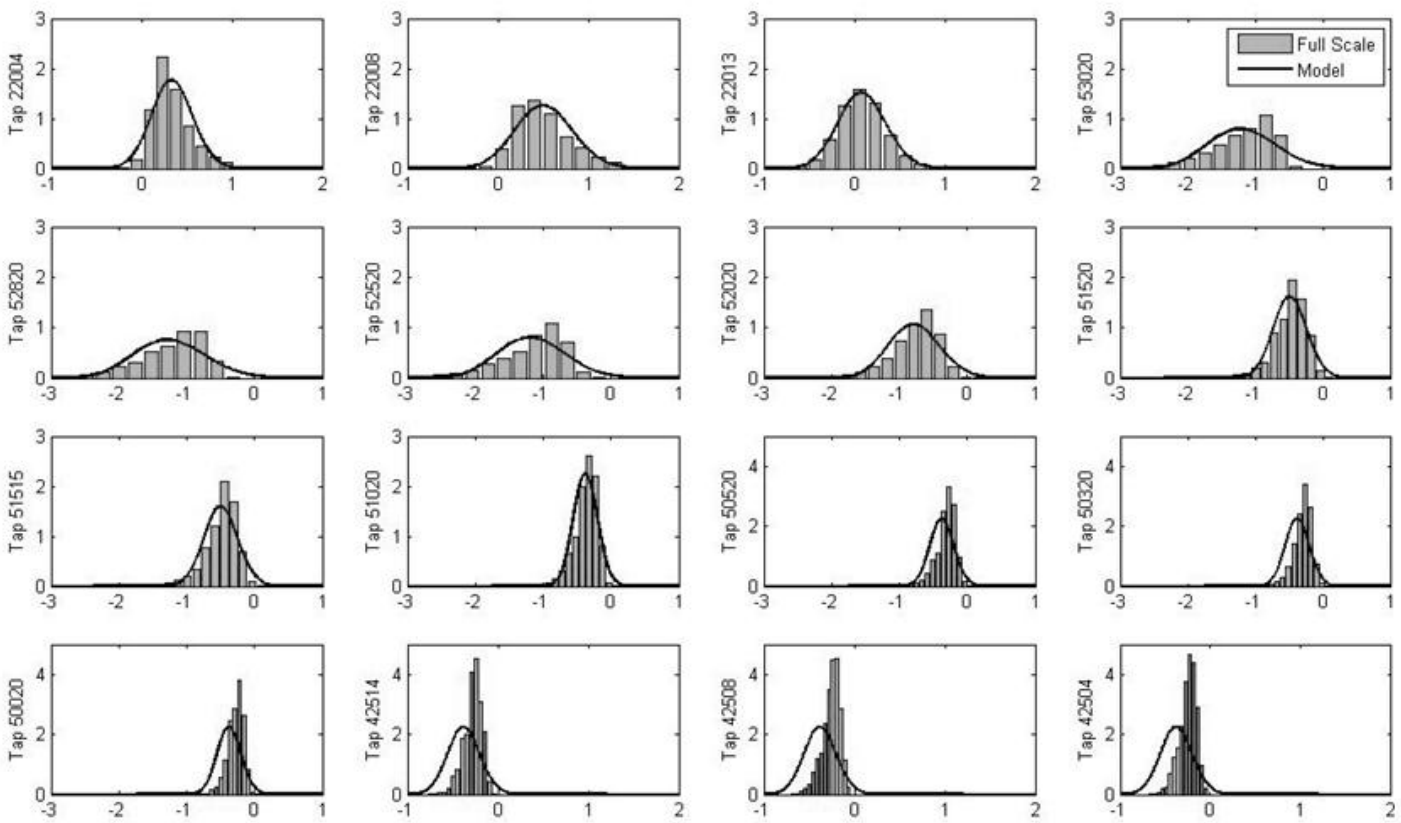

Figure A-6. WERFL Test Building and 1:10 scaled model tap distributions with flow simulated parallel to the transverse axis (AOA = 90^{o})

Table A-1. WERFL Site 15 minute records used for validation with AOA of 0, 45, and 90 degrees (WSERC, 2010)

Run Summary Report -- 620
5/19/2010

Run Description
Experiment Name: Mode 1001.02a
Field Site: WERFL Site
Run Name: 620
Acquisition Date: 02/09/2003
Acquisition Time: 14:41:55
Building Position: 270 deg

Process Description
Computer Name: CE133-01
User Name: w-rcarter
Processing Date: 10/12/2003
Processing Time: 6:06:24 PM
Processing Duration: 5 min 11 sec

Mean Dynamic Reference Pressure
Height: 13.00 ft
Temperature: 58.43 F
Barometric Pressure 26.74 in. Hg
Relative Humidity 19.40 %
Air Density: 0.002127 slugs/ft3
Velocity 25.18 mph STAT
Direction 276.2 deg STAT
Mean Dynamic Pressure 1.450 psf

Profile Parameters
Building Postion: 270.0 deg
Angle of Attack: 6.219 deg

Run Summary Report -- 4482
12/17/2010

Run Description
Experiment Name: Mode 1001.02a
Field Site: WERFL Site
Run Name: 4482
Acquisition Date: 09/13/2003
Acquisition Time: 17:06:59
Building Position: 0 deg

Process Description
Computer Name: CE178-06
User Name: w-jedwards
Processing Date: 10/13/2003
Processing Time: 6:08:51 PM
Processing Duration: 6 min 21 sec

Mean Dynamic Reference Pressure
Height: 13.00 ft
Temperature: 77.81 F
Barometric Pressure 26.83 in. Hg
Relative Humidity 43.18 %
Air Density: 0.002057 slugs/ft3
Velocity 16.32 mph STAT
Direction 45.43 deg STAT
Mean Dynamic Pressure 0.589 psf

Profile Parameters
Building Postion: 0 deg
Angle of Attack: 45.43 deg

Run Summary Report -- 2781
12/17/2010

Run Description
Experiment Name: Mode 1001.02a
Field Site: WERFL Site
Run Name: 2781
Acquisition Date: 05/16/2003
Acquisition Time: 03:13:19
Building Position: 195 deg

Process Description
Computer Name: CE178-04
User Name: w-jedwards
Processing Date: 10/13/2003
Processing Time: 11:50:06 AM
Processing Duration: 6 min 57 sec

Mean Dynamic Reference Pressure
Height: 13.00 ft
Temperature: 70.86 F
Barometric Pressure 26.65 in. Hg
Relative Humidity 27.76 %
Air Density: 0.00207 slugs/ft3
Velocity 15.87 mph STAT
Direction 284.0 deg STAT
Mean Dynamic Pressure 0.561 psf

Profile Parameters
Building Postion: 195.0 deg
Angle of Attack: 88.96 deg

Table A-2. WERFL Test Building and 1:10 scaled model tap comparison with flow simulated

parallel to the longitudinal axis (AOA = 0^o)

Tap	TTU Cp_{mean}	1:10 Cp_{mean}	Resid-ual	TTU Cp_{min}	1:10 Cp_{min}	Resid-ual	TTU Cp_{max}	1:10 Cp_{max}	Resid-ual	TTU Cp_{rms}	1:10 Cp_{rms}	Resid-ual
13004	-0.32	-0.41	0.09	-0.32	-0.41	0.09	-0.32	-0.41	0.09	0.38	0.58	0.20
13008	-0.01	-0.44	0.43	-0.01	-0.44	0.43	-0.01	-0.44	0.43	0.24	0.60	0.36
13013	-0.09	0.37	0.46	-0.09	0.37	0.46	-0.09	0.37	0.46	0.28	0.61	0.33
12604	0.24	0.53	0.29	0.24	0.53	0.29	0.24	0.53	0.29	0.32	0.65	0.33
12608	0.50	-0.18	0.68	0.50	-0.18	0.68	0.50	-0.18	0.68	0.57	0.52	0.05
12613	0.15	0.58	0.43	0.15	0.58	0.43	0.15	0.58	0.43	0.28	0.67	0.39
12304	0.36	0.64	0.28	0.36	0.64	0.28	0.36	0.64	0.28	0.43	0.68	0.25
12308	0.56	0.56	0.00	0.56	0.56	0.00	0.56	0.56	0.00	0.63	0.65	0.02
12313	0.27	-0.37	0.64	0.27	-0.37	0.64	0.27	-0.37	0.64	0.37	0.56	0.19
11904	0.40	0.51	0.11	0.40	0.51	0.11	0.40	0.51	0.11	0.46	0.62	0.17
11908	0.60	-0.36	0.96	0.60	-0.36	0.96	0.60	-0.36	0.96	0.67	0.56	0.11
11913	0.30	0.48	0.18	0.30	0.48	0.18	0.30	0.48	0.18	0.39	0.62	0.23
11501	0.45	-0.55	1.00	0.45	-0.55	1.00	0.45	-0.55	1.00	0.50	0.62	0.12
11508	0.62	-0.30	0.92	0.62	-0.30	0.92	0.62	-0.30	0.92	0.69	0.55	0.15
11513	0.20	-0.48	0.68	0.20	-0.48	0.68	0.20	-0.48	0.68	0.33	0.59	0.27
10404	0.38	0.50	0.12	0.38	0.50	0.12	0.38	0.50	0.12	0.46	0.61	0.15
10413	0.19	-0.28	0.47	0.19	-0.28	0.47	0.19	-0.28	0.47	0.31	0.54	0.23
10408	0.64	-0.27	0.91	0.64	-0.27	0.91	0.64	-0.27	0.91	0.71	0.54	0.17
10004	0.03	0.40	0.37	0.03	0.40	0.37	0.03	0.40	0.37	0.30	0.62	0.31
10008	0.31	0.53	0.23	0.31	0.53	0.23	0.31	0.53	0.23	0.43	0.61	0.18
10013	0.03	-0.27	0.30	0.03	-0.27	0.30	0.03	-0.27	0.30	0.27	0.54	0.28
24504	-0.85	-0.20	0.65	-0.85	-0.20	0.65	-0.85	-0.20	0.65	0.94	0.77	0.17
24508	-0.85	-0.24	0.61	-0.85	-0.24	0.61	-0.85	-0.24	0.61	0.91	0.82	0.09
24513	-1.09	-0.31	0.78	-1.09	-0.31	0.78	-1.09	-0.31	0.78	1.17	0.96	0.22
24008	-0.74	-0.22	0.52	-0.74	-0.22	0.52	-0.74	-0.22	0.52	0.87	0.81	0.06
24013	-0.78	-0.31	0.47	-0.78	-0.31	0.47	-0.78	-0.31	0.47	0.91	0.85	0.06
23504	-0.42	-0.32	0.10	-0.42	-0.32	0.10	-0.42	-0.32	0.10	0.54	0.86	0.32
23508	-0.45	-0.36	0.09	-0.45	-0.36	0.09	-0.45	-0.36	0.09	0.57	0.88	0.31
23004	-0.29	-0.25	0.04	-0.29	-0.25	0.04	-0.29	-0.25	0.04	0.38	0.80	0.42
23008	-0.34	-0.20	0.14	-0.34	-0.20	0.14	-0.34	-0.20	0.14	0.42	0.78	0.36
23013	-0.36	-0.19	0.17	-0.36	-0.19	0.17	-0.36	-0.19	0.17	0.45	0.78	0.33
22504	-0.24	-0.30	0.06	-0.24	-0.30	0.06	-0.24	-0.30	0.06	0.29	0.79	0.51
22508	-0.24	-0.22	0.02	-0.24	-0.22	0.02	-0.24	-0.22	0.02	0.30	0.82	0.53
22513	-0.37	-0.32	0.05	-0.37	-0.32	0.05	-0.37	-0.32	0.05	0.42	0.80	0.38
22004	-0.18	-0.19	0.01	-0.18	-0.19	0.01	-0.18	-0.19	0.01	0.21	0.81	0.60
22008	-0.20	-0.28	0.08	-0.20	-0.28	0.08	-0.20	-0.28	0.08	0.24	0.83	0.58
22013	-0.24	-1.06	0.82	-0.24	-1.06	0.82	-0.24	-1.06	0.82	0.28	1.14	0.86
21504	-0.21	-0.99	0.78	-0.21	-0.99	0.78	-0.21	-0.99	0.78	0.23	1.09	0.86
21508	-0.20	-0.81	0.61	-0.20	-0.81	0.61	-0.20	-0.81	0.61	0.23	1.06	0.83
21513	-0.32	-0.94	0.63	-0.32	-0.94	0.63	-0.32	-0.94	0.63	0.34	1.04	0.70
21004	-0.20	-0.56	0.36	-0.20	-0.56	0.36	-0.20	-0.56	0.36	0.22	0.96	0.74
21008	-0.20	-0.55	0.35	-0.20	-0.55	0.35	-0.20	-0.55	0.35	0.22	0.98	0.77
21013	-0.32	-1.07	0.75	-0.32	-1.07	0.75	-0.32	-1.07	0.75	0.35	1.13	0.78
20504	-0.18	-0.82	0.64	-0.18	-0.82	0.64	-0.18	-0.82	0.64	0.20	1.10	0.91
20508	-0.18	-0.60	0.42	-0.18	-0.60	0.42	-0.18	-0.60	0.42	0.20	1.03	0.83
20513	-0.29	-0.82	0.54	-0.29	-0.82	0.54	-0.29	-0.82	0.54	0.31	1.15	0.84
20004	-0.29	-1.00	0.71	-0.29	-1.00	0.71	-0.29	-1.00	0.71	0.31	1.07	0.77
20008	-0.26	-0.86	0.60	-0.26	-0.86	0.60	-0.26	-0.86	0.60	0.27	0.99	0.72
20013	-0.27	-0.74	0.47	-0.27	-0.74	0.47	-0.27	-0.74	0.47	0.29	0.95	0.66
33004	-0.26	-0.33	0.07	-0.26	-0.33	0.07	-0.26	-0.33	0.07	0.28	0.61	0.33
33008	-0.27	-0.31	0.04	-0.27	-0.31	0.04	-0.27	-0.31	0.04	0.28	0.59	0.31
33013	-0.25	-0.30	0.05	-0.25	-0.30	0.05	-0.25	-0.30	0.05	0.27	0.64	0.37
32604	-0.28	-0.31	0.03	-0.28	-0.31	0.03	-0.28	-0.31	0.03	0.30	0.64	0.34
32608	-0.29	-0.34	0.05	-0.29	-0.34	0.05	-0.29	-0.34	0.05	0.31	0.59	0.28
32613	-0.27	-0.30	0.03	-0.27	-0.30	0.03	-0.27	-0.30	0.03	0.29	0.63	0.35
32304	-0.30	-0.33	0.04	-0.30	-0.33	0.04	-0.30	-0.33	0.04	0.31	0.64	0.33
32308	-0.32	-0.34	0.02	-0.32	-0.34	0.02	-0.32	-0.34	0.02	0.34	0.65	0.31

32313	-0.29	-0.35	0.06	-0.29	-0.35	0.06	-0.29	-0.35	0.06	0.31	0.60	0.29
31904	-0.31	-0.36	0.05	-0.31	-0.36	0.05	-0.31	-0.36	0.05	0.33	0.60	0.27
31908	-0.34	-0.33	0.01	-0.34	-0.33	0.01	-0.34	-0.33	0.01	0.36	0.59	0.23
31913	-0.31	-0.37	0.06	-0.31	-0.37	0.06	-0.31	-0.37	0.06	0.33	0.60	0.27
31504	-0.33	-0.33	0.01	-0.33	-0.33	0.01	-0.33	-0.33	0.01	0.35	0.60	0.25
31508	-0.34	-0.35	0.01	-0.34	-0.35	0.01	-0.34	-0.35	0.01	0.36	0.60	0.24
31513	-0.33	-0.30	0.03	-0.33	-0.30	0.03	-0.33	-0.30	0.03	0.35	0.64	0.29
30404	-0.34	-0.37	0.03	-0.34	-0.37	0.03	-0.34	-0.37	0.03	0.36	0.59	0.23
30408	-0.33	-0.35	0.02	-0.33	-0.35	0.02	-0.33	-0.35	0.02	0.36	0.60	0.25
30413	-0.33	-0.35	0.02	-0.33	-0.35	0.02	-0.33	-0.35	0.02	0.35	0.60	0.25
30004	-0.32	-0.32	0.00	-0.32	-0.32	0.00	-0.32	-0.32	0.00	0.35	0.64	0.30
30008	-0.33	-0.37	0.04	-0.33	-0.37	0.04	-0.33	-0.37	0.04	0.35	0.59	0.24
30013	-0.31	-0.34	0.03	-0.31	-0.34	0.03	-0.31	-0.34	0.03	0.34	0.60	0.26
44504	-0.29	-0.24	0.05	-0.29	-0.24	0.05	-0.29	-0.24	0.05	0.32	0.81	0.49
44508	-0.31	-0.17	0.14	-0.31	-0.17	0.14	-0.31	-0.17	0.14	0.34	0.78	0.44
44513	-0.29	-0.19	0.10	-0.29	-0.19	0.10	-0.29	-0.19	0.10	0.31	0.80	0.48
44008	-0.31	-0.30	0.01	-0.31	-0.30	0.01	-0.31	-0.30	0.01	0.37	0.79	0.42
44013	-0.29	-0.29	0.01	-0.29	-0.29	0.01	-0.29	-0.29	0.01	0.32	0.83	0.52
43504	-0.28	-0.32	0.04	-0.28	-0.32	0.04	-0.28	-0.32	0.04	0.32	0.85	0.53
43508	-0.36	-0.28	0.08	-0.36	-0.28	0.08	-0.36	-0.28	0.08	0.42	0.80	0.38
43004	-0.30	-0.26	0.04	-0.30	-0.26	0.04	-0.30	-0.26	0.04	0.35	0.82	0.47
43008	-0.37	-0.39	0.02	-0.37	-0.39	0.02	-0.37	-0.39	0.02	0.44	0.89	0.45
43013	-0.35	-0.29	0.06	-0.35	-0.29	0.06	-0.35	-0.29	0.06	0.40	0.83	0.43
42504	-0.37	-0.24	0.13	-0.37	-0.24	0.13	-0.37	-0.24	0.13	0.43	0.79	0.37
42508	-0.42	-0.34	0.08	-0.42	-0.34	0.08	-0.42	-0.34	0.08	0.50	0.80	0.29
42513	-0.42	-0.31	0.11	-0.42	-0.31	0.11	-0.42	-0.31	0.11	0.48	0.79	0.30
42004	-0.44	-0.80	0.36	-0.44	-0.80	0.36	-0.44	-0.80	0.36	0.51	0.95	0.44
42008	-0.48	-0.78	0.30	-0.48	-0.78	0.30	-0.48	-0.78	0.30	0.57	1.05	0.48
42013	-0.51	-0.63	0.12	-0.51	-0.63	0.12	-0.51	-0.63	0.12	0.59	0.93	0.35
41504	-0.55	-0.74	0.20	-0.55	-0.74	0.20	-0.55	-0.74	0.20	0.62	1.00	0.38
41508	-0.59	-0.52	0.07	-0.59	-0.52	0.07	-0.59	-0.52	0.07	0.68	0.93	0.26
41513	-0.61	-0.55	0.06	-0.61	-0.55	0.06	-0.61	-0.55	0.06	0.69	0.97	0.28
41004	-0.69	-0.57	0.12	-0.69	-0.57	0.12	-0.69	-0.57	0.12	0.76	1.01	0.25
41008	-0.74	-1.03	0.29	-0.74	-1.03	0.29	-0.74	-1.03	0.29	0.81	1.14	0.33
41013	-0.77	-1.00	0.23	-0.77	-1.00	0.23	-0.77	-1.00	0.23	0.86	1.05	0.18
40504	-0.83	-0.91	0.09	-0.83	-0.91	0.09	-0.83	-0.91	0.09	0.87	1.00	0.13
40508	-0.86	-0.76	0.10	-0.86	-0.76	0.10	-0.86	-0.76	0.10	0.92	0.95	0.03
40513	-0.92	-1.03	0.11	-0.92	-1.03	0.11	-0.92	-1.03	0.11	0.98	1.12	0.13
40004	-0.78	-0.89	0.11	-0.78	-0.89	0.11	-0.78	-0.89	0.11	0.84	1.02	0.19
40008	-0.78	-0.91	0.13	-0.78	-0.91	0.13	-0.78	-0.91	0.13	0.82	1.04	0.21
40013	-0.97	-0.84	0.13	-0.97	-0.84	0.13	-0.97	-0.84	0.13	1.03	1.12	0.10
50045	-1.31	-0.29	1.02	-1.31	-0.29	1.02	-1.31	-0.29	1.02	1.47	0.89	0.58
50345	-1.16	-0.28	0.88	-1.16	-0.28	0.88	-1.16	-0.28	0.88	1.24	0.88	0.36
50545	-1.08	-0.20	0.88	-1.08	-0.20	0.88	-1.08	-0.20	0.88	1.14	0.87	0.27
50040	-1.01	-0.21	0.80	-1.01	-0.21	0.80	-1.01	-0.21	0.80	1.08	0.87	0.21
50340	-0.98	-0.21	0.77	-0.98	-0.21	0.77	-0.98	-0.21	0.77	1.04	0.87	0.17
50540	-1.05	-0.23	0.82	-1.05	-0.23	0.82	-1.05	-0.23	0.82	1.11	0.88	0.23
51040	-1.10	-0.26	0.84	-1.10	-0.26	0.84	-1.10	-0.26	0.84	1.17	0.89	0.27
50035	-0.77	-0.39	0.38	-0.77	-0.39	0.38	-0.77	-0.39	0.38	0.84	0.97	0.13
50335	-0.72	-0.26	0.46	-0.72	-0.26	0.46	-0.72	-0.26	0.46	0.79	0.89	0.10
50532	-0.76	-0.34	0.42	-0.76	-0.34	0.42	-0.76	-0.34	0.42	0.83	0.94	0.10
51035	-0.84	-0.22	0.62	-0.84	-0.22	0.62	-0.84	-0.22	0.62	0.91	0.88	0.04
50030	-0.61	-0.18	0.43	-0.61	-0.18	0.43	-0.61	-0.18	0.43	0.69	0.91	0.21
50330	-0.53	-0.35	0.18	-0.53	-0.35	0.18	-0.53	-0.35	0.18	0.61	0.93	0.32
50530	-0.52	-0.28	0.24	-0.52	-0.28	0.24	-0.52	-0.28	0.24	0.60	0.91	0.32
51030	-0.51	-0.19	0.32	-0.51	-0.19	0.32	-0.51	-0.19	0.32	0.57	0.91	0.34
50025	-0.46	-0.25	0.21	-0.46	-0.25	0.21	-0.46	-0.25	0.21	0.52	0.89	0.37
50325	-0.38	-0.36	0.02	-0.38	-0.36	0.02	-0.38	-0.36	0.02	0.44	0.93	0.50
50525	-0.35	-0.36	0.01	-0.35	-0.36	0.01	-0.35	-0.36	0.01	0.40	0.95	0.55
51025	-0.31	-0.20	0.11	-0.31	-0.20	0.11	-0.31	-0.20	0.11	0.36	0.91	0.55
52845	-1.42	-0.36	1.06	-1.42	-0.36	1.06	-1.42	-0.36	1.06	2.02	0.93	1.09
53045	-1.56	-0.31	1.25	-1.56	-0.31	1.25	-1.56	-0.31	1.25	2.47	0.92	1.55
51540	-1.21	-0.20	1.01	-1.21	-0.20	1.01	-1.21	-0.20	1.01	1.29	0.91	0.38
52040	-1.23	-0.25	0.98	-1.23	-0.25	0.98	-1.23	-0.25	0.98	1.32	0.89	0.43
52840	-0.89	-0.35	0.54	-0.89	-0.35	0.54	-0.89	-0.35	0.54	0.97	0.94	0.03

53040	-1.03	-0.23	0.80	-1.03	-0.23	0.80	-1.03	-0.23	0.80	1.13	0.89	0.24
51535	-0.80	-0.16	0.64	-0.80	-0.16	0.64	-0.80	-0.16	0.64	0.87	0.95	0.07
51530	-0.48	-0.25	0.23	-0.48	-0.25	0.23	-0.48	-0.25	0.23	0.53	0.89	0.36
52030	-0.39	-0.33	0.06	-0.39	-0.33	0.06	-0.39	-0.33	0.06	0.45	0.93	0.48
52530	-0.36	-0.24	0.12	-0.36	-0.24	0.12	-0.36	-0.24	0.12	0.40	0.93	0.52
52830	-0.43	-0.26	0.17	-0.43	-0.26	0.17	-0.43	-0.26	0.17	0.51	0.89	0.38
53030	-0.56	-0.31	0.25	-0.56	-0.31	0.25	-0.56	-0.31	0.25	0.64	0.90	0.26
51525	-0.33	-0.24	0.09	-0.33	-0.24	0.09	-0.33	-0.24	0.09	0.37	0.89	0.53
52025	-0.28	-0.32	0.04	-0.28	-0.32	0.04	-0.28	-0.32	0.04	0.31	0.92	0.61
52525	-0.28	-0.25	0.03	-0.28	-0.25	0.03	-0.28	-0.25	0.03	0.31	0.90	0.59
52825	-0.38	-0.30	0.08	-0.38	-0.30	0.08	-0.38	-0.30	0.08	0.47	0.88	0.42
53025	-0.47	-0.29	0.18	-0.47	-0.29	0.18	-0.47	-0.29	0.18	0.54	0.88	0.34
51520	-0.28	-1.15	0.87	-0.28	-1.15	0.87	-0.28	-1.15	0.87	0.31	1.46	1.15
52020	-0.30	-1.09	0.79	-0.30	-1.09	0.79	-0.30	-1.09	0.79	0.33	1.28	0.95
52520	-0.27	-1.17	0.90	-0.27	-1.17	0.90	-0.27	-1.17	0.90	0.30	1.22	0.91
52820	-0.35	-1.15	0.81	-0.35	-1.15	0.81	-0.35	-1.15	0.81	0.43	1.20	0.77
53028	-0.40	-1.03	0.63	-0.40	-1.03	0.63	-0.40	-1.03	0.63	0.64	1.17	0.53
51515	-0.30	-0.96	0.66	-0.30	-0.96	0.66	-0.30	-0.96	0.66	0.33	1.17	0.84
52015	-0.26	-1.01	0.75	-0.26	-1.01	0.75	-0.26	-1.01	0.75	0.29	1.22	0.93
52515	-0.29	-0.55	0.26	-0.29	-0.55	0.26	-0.29	-0.55	0.26	0.33	1.05	0.72
52815	-0.42	-1.13	0.71	-0.42	-1.13	0.71	-0.42	-1.13	0.71	0.49	1.30	0.81
53015	-0.45	-0.51	0.06	-0.45	-0.51	0.06	-0.45	-0.51	0.06	0.51	1.03	0.52
51510	-0.28	-1.12	0.84	-0.28	-1.12	0.84	-0.28	-1.12	0.84	0.30	1.27	0.96
52010	-0.25	-1.15	0.90	-0.25	-1.15	0.90	-0.25	-1.15	0.90	0.27	1.31	1.03
52510	-0.31	-0.55	0.24	-0.31	-0.55	0.24	-0.31	-0.55	0.24	0.35	1.03	0.68
52810	-0.44	-0.87	0.43	-0.44	-0.87	0.43	-0.44	-0.87	0.43	0.52	1.21	0.69
53010	-0.40	-1.15	0.75	-0.40	-1.15	0.75	-0.40	-1.15	0.75	0.45	1.29	0.84
51505	-0.32	-0.97	0.65	-0.32	-0.97	0.65	-0.32	-0.97	0.65	0.34	1.12	0.78
52005	-0.30	-0.62	0.32	-0.30	-0.62	0.32	-0.30	-0.62	0.32	0.32	1.04	0.72
52505	-0.25	-0.65	0.40	-0.25	-0.65	0.40	-0.25	-0.65	0.40	0.29	1.11	0.82
52805	-0.34	-1.18	0.84	-0.34	-1.18	0.84	-0.34	-1.18	0.84	0.39	1.32	0.93
53005	-0.33	-0.67	0.34	-0.33	-0.67	0.34	-0.33	-0.67	0.34	0.37	1.04	0.67
52500	-0.34	-0.61	0.27	-0.34	-0.61	0.27	-0.34	-0.61	0.27	0.36	1.07	0.70
52800	-0.26	-1.24	0.98	-0.26	-1.24	0.98	-0.26	-1.24	0.98	0.28	1.37	1.08
53000	-0.25	-0.91	0.66	-0.25	-0.91	0.66	-0.25	-0.91	0.66	0.27	1.12	0.84
50020	-0.35	-0.66	0.31	-0.35	-0.66	0.31	-0.35	-0.66	0.31	0.40	1.05	0.65
50320	-0.35	-0.83	0.48	-0.35	-0.83	0.48	-0.35	-0.83	0.48	0.39	1.17	0.78
50520	-0.31	-1.16	0.85	-0.31	-1.16	0.85	-0.31	-1.16	0.85	0.35	1.35	1.01
51020	-0.31	-0.79	0.48	-0.31	-0.79	0.48	-0.31	-0.79	0.48	0.34	1.11	0.77
50015	-0.35	-0.63	0.28	-0.35	-0.63	0.28	-0.35	-0.63	0.28	0.39	1.06	0.67
50315	-0.30	-1.23	0.93	-0.30	-1.23	0.93	-0.30	-1.23	0.93	0.33	1.43	1.10
50515	-0.32	-0.77	0.46	-0.32	-0.77	0.46	-0.32	-0.77	0.46	0.34	1.12	0.78
51015	-0.36	-1.49	1.14	-0.36	-1.49	1.14	-0.36	-1.49	1.14	0.39	1.79	1.40
50005	-0.29	-0.90	0.62	-0.29	-0.90	0.62	-0.29	-0.90	0.62	0.31	1.16	0.85
50305	-0.24	-0.83	0.59	-0.24	-0.83	0.59	-0.24	-0.83	0.59	0.26	1.17	0.91
51055	-0.26	-0.93	0.67	-0.26	-0.93	0.67	-0.26	-0.93	0.67	0.28	1.14	0.85
50000	-0.36	-1.25	0.89	-0.36	-1.25	0.89	-0.36	-1.25	0.89	0.39	1.47	1.08
50300	-0.36	-1.18	0.82	-0.36	-1.18	0.82	-0.36	-1.18	0.82	0.39	1.34	0.95

Table A-3. WERFL Test Building and 1:10 scaled model tap comparison with flow simulated

45 degrees from the longitudinal axis (AOA = 45^{o})

Tap	TTU Cp_{mean}	1:10 Cp_{mean}	Resid-ual	TTU Cp_{min}	1:10 Cp_{min}	Resid-ual	TTU Cp_{max}	1:10 Cp_{max}	Resid-ual	TTU Cp_{rms}	1:10 Cp_{rms}	Resid-ual
13004	-0.42	-0.25	0.17	-1.16	-1.47	0.31	0.09	0.93	0.84	0.46	0.41	0.06
13008	-0.23	-0.16	0.07	-0.91	-3.61	2.70	0.38	1.75	1.37	0.28	0.49	0.21
13013	-0.29	0.09	0.38	-1.03	-0.83	0.20	0.43	1.00	0.57	0.34	0.32	0.02
12604	0.15	0.18	0.03	-0.40	-0.75	0.35	1.23	1.36	0.14	0.15	0.30	0.16
12608	-0.07	-0.01	0.06	-0.91	-1.04	0.13	0.77	1.09	0.32	0.24	0.34	0.10
12613	0.17	0.22	0.05	-0.54	-0.75	0.21	1.18	1.52	0.34	0.20	0.30	0.11
12304	0.28	0.25	0.03	-0.35	-0.62	0.27	1.63	1.22	0.41	0.25	0.31	0.06
12308	0.19	0.19	0.00	-0.50	-0.64	0.14	0.99	1.10	0.11	0.35	0.30	0.05
12313	0.28	0.16	0.12	-0.22	-1.93	1.71	1.09	1.68	0.59	0.21	0.31	0.10
11904	0.05	0.38	0.33	-0.81	-0.69	0.12	0.99	1.10	0.11	0.26	0.33	0.06
11908	0.31	0.14	0.17	-0.17	-1.42	1.25	1.21	1.59	0.38	0.35	0.32	0.03
11913	0.30	0.42	0.12	-0.32	-0.42	0.10	1.26	1.17	0.09	0.19	0.33	0.14
11501	-0.09	-0.23	0.14	-1.15	-1.34	0.19	0.88	0.90	0.02	0.36	0.39	0.03
11508	0.38	-0.12	0.50	-0.21	-1.30	1.09	1.36	0.81	0.55	0.37	0.36	0.01
11513	0.39	-0.30	0.69	-0.55	-1.51	0.96	1.48	1.00	0.48	0.21	0.42	0.20
10404	0.48	0.13	0.35	-1.40	-0.52	0.88	1.85	1.03	0.82	0.52	0.31	0.21
10413	0.40	-0.07	0.47	-3.85	-1.04	2.81	2.17	1.07	1.10	0.23	0.35	0.12
10408	0.50	-0.11	0.61	-2.10	-1.08	1.02	2.46	0.88	1.58	0.57	0.36	0.21
10004	0.05	0.06	0.01	-3.00	-0.94	2.06	1.49	1.15	0.34	0.58	0.33	0.25
10008	0.41	0.17	0.24	-3.46	-0.51	2.95	2.28	1.05	1.23	0.71	0.30	0.41
10013	0.50	-0.06	0.56	-2.23	-1.32	0.91	2.56	1.12	1.44	0.42	0.35	0.07
24504	0.48	-0.26	0.74	-0.61	-0.68	0.08	1.84	0.80	1.04	0.59	0.31	0.28
24508	0.45	-0.10	0.55	-0.90	-0.63	0.27	1.91	1.13	0.78	0.71	0.32	0.39
24513	-0.09	-0.55	0.46	-1.21	-1.34	0.13	0.93	0.87	0.05	2.39	0.38	2.01
24008	0.42	-0.08	0.50	-0.78	-0.67	0.11	1.78	1.30	0.48	0.53	0.32	0.21
24013	-0.22	0.00	0.22	-1.18	-0.58	0.60	0.61	1.34	0.73	0.20	0.34	0.13
23504	0.39	-0.05	0.44	-0.06	-0.56	0.50	1.33	1.43	0.10	0.48	0.33	0.15
23508	0.35	-0.46	0.81	-0.42	-1.24	0.82	1.61	1.20	0.41	0.48	0.35	0.13
23004	0.31	-0.44	0.75	-0.12	-1.01	0.90	1.55	0.89	0.66	0.43	0.34	0.09
23008	0.36	-0.17	0.53	-0.22	-0.59	0.37	1.48	0.93	0.55	0.42	0.30	0.11
23013	-0.15	-0.17	0.02	-1.24	-0.59	0.65	0.73	0.94	0.21	0.21	0.30	0.09
22504	0.33	-0.51	0.84	-0.14	-1.12	0.98	1.31	0.80	0.51	0.35	0.36	0.01
22508	0.33	-0.45	0.78	-0.21	-1.50	1.29	1.49	0.96	0.53	0.41	0.36	0.05
22513	0.00	-0.55	0.55	-1.71	-1.38	0.33	1.23	0.69	0.54	0.23	0.37	0.14
22004	0.21	-0.28	0.49	-0.28	-0.97	0.69	1.13	1.10	0.03	0.36	0.32	0.04
22008	0.28	-0.43	0.71	-0.47	-1.23	0.76	1.89	0.85	1.04	0.39	0.34	0.05
22013	-0.18	0.12	0.30	-1.08	-0.30	0.78	1.04	1.32	0.28	0.16	0.35	0.20
21504	0.20	0.20	0.00	-0.22	-0.24	0.02	1.02	1.55	0.53	0.26	0.37	0.11
21508	0.26	0.13	0.13	-0.53	-0.30	0.23	1.64	1.45	0.19	0.34	0.35	0.01
21513	-0.14	0.01	0.15	-1.04	-1.17	0.13	1.07	2.40	1.33	0.25	0.37	0.12
21004	0.14	0.07	0.07	-0.64	-0.41	0.23	1.00	1.33	0.33	0.24	0.34	0.10
21008	0.21	0.01	0.20	-0.44	-0.49	0.05	1.70	1.28	0.42	0.31	0.34	0.02
21013	-0.16	-0.35	0.19	-1.02	-1.30	0.28	1.06	1.58	0.52	0.23	0.34	0.11
20504	-0.23	0.05	0.28	-1.01	-0.42	0.59	0.18	1.35	1.18	0.18	0.34	0.16
20508	-0.09	-0.43	0.34	-1.06	-1.13	0.07	0.54	1.20	0.66	0.27	0.34	0.07
20513	-0.14	-0.43	0.29	-1.11	-1.28	0.17	0.51	1.32	0.81	0.23	0.35	0.12
20004	-0.21	0.28	0.49	-0.77	-0.17	0.60	0.10	1.50	1.40	0.26	0.38	0.11
20008	-0.22	0.37	0.59	-1.08	-0.64	0.44	0.10	1.84	1.74	0.14	0.41	0.27
20013	-0.28	0.47	0.75	-1.34	-0.19	1.15	0.11	1.87	1.76	0.18	0.42	0.25
33004	-0.24	-0.20	0.04	-0.77	-1.40	0.63	0.01	1.52	1.51	0.23	0.40	0.17
33008	-0.25	-0.25	0.00	-0.88	-2.20	1.32	0.01	0.22	0.21	0.24	0.40	0.16
33013	-0.28	-0.24	0.04	-1.52	-1.64	0.12	0.04	0.44	0.40	0.31	0.41	0.09
32604	-0.24	-0.25	0.01	-0.83	-1.49	0.66	0.06	0.41	0.35	0.26	0.41	0.15
32608	-0.27	-0.24	0.03	-1.21	-1.84	0.63	0.06	0.20	0.14	0.27	0.39	0.11
32613	-0.29	-0.26	0.03	-2.22	-1.48	0.74	0.08	0.44	0.36	0.31	0.41	0.10
32304	-0.26	-0.27	0.01	-0.88	-1.43	0.55	-0.02	0.36	0.38	0.26	0.41	0.15
32308	-0.30	-0.31	0.01	-1.20	-1.75	0.55	-0.03	0.33	0.36	0.29	0.43	0.14

32313	-0.31	-0.29	0.02	-1.90	-1.73	0.17	0.08	0.15	0.07	0.33	0.41	0.08
31904	-0.27	-0.27	0.00	-0.79	-1.29	0.50	0.02	0.19	0.17	0.28	0.39	0.11
31908	-0.31	-0.28	0.03	-1.29	-2.06	0.77	-0.05	0.17	0.22	0.32	0.40	0.08
31913	-0.31	-0.26	0.05	-2.23	-1.42	0.81	0.20	0.23	0.04	0.34	0.39	0.05
31504	-0.29	-0.18	0.11	-0.82	-1.25	0.43	0.06	0.29	0.23	0.29	0.38	0.09
31508	-0.32	-0.22	0.10	-1.13	-1.37	0.24	-0.03	0.26	0.29	0.33	0.38	0.06
31513	-0.33	-0.18	0.15	-1.62	-1.43	0.19	0.40	0.56	0.16	0.34	0.39	0.05
30404	-0.30	-0.20	0.10	-1.48	-1.26	0.22	0.05	0.19	0.14	0.32	0.37	0.05
30408	-0.32	-0.20	0.12	-2.08	-1.45	0.63	0.09	0.31	0.22	0.34	0.38	0.04
30413	-0.33	-0.22	0.11	-3.63	-1.30	2.33	0.18	0.37	0.19	0.35	0.38	0.03
30004	-0.25	-0.22	0.03	-1.05	-1.38	0.33	0.20	0.50	0.30	0.33	0.40	0.07
30008	-0.32	-0.23	0.09	-1.06	-1.23	0.17	0.09	0.18	0.09	0.35	0.38	0.02
30013	-0.26	-0.20	0.06	-1.55	-1.28	0.27	0.12	0.30	0.18	0.37	0.38	0.01
44504	-0.25	-0.51	0.26	-1.05	-1.68	0.63	0.15	0.16	0.01	0.29	0.41	0.12
44508	-0.34	-0.43	0.09	-1.06	-1.42	0.36	0.04	0.30	0.26	0.35	0.39	0.04
44513	-0.21	-0.47	0.26	-1.45	-1.75	0.30	0.18	0.19	0.01	0.29	0.40	0.11
44008	-0.37	-0.39	0.02	-1.19	-2.45	1.26	0.03	0.25	0.22	0.37	0.38	0.01
44013	-0.22	-0.50	0.28	-1.86	-1.40	0.46	0.21	0.29	0.08	0.24	0.41	0.16
43504	-0.33	-0.61	0.28	-1.10	-1.64	0.54	0.08	0.05	0.03	0.32	0.44	0.11
43508	-0.41	-0.35	0.06	-1.17	-1.71	0.54	0.02	0.30	0.28	0.40	0.37	0.04
43004	-0.40	-0.56	0.16	-1.39	-1.55	0.16	0.06	0.18	0.12	0.36	0.42	0.06
43008	-0.48	-0.44	0.04	-1.29	-1.36	0.07	-0.04	0.19	0.23	0.45	0.39	0.06
43013	-0.34	-0.39	0.05	-1.56	-1.25	0.31	0.05	0.31	0.26	0.31	0.38	0.07
42504	-0.42	-0.50	0.08	-1.47	-1.42	0.05	-0.04	0.31	0.35	0.44	0.40	0.04
42508	-0.51	-0.50	0.01	-1.44	-1.87	0.43	-0.06	0.11	0.17	0.51	0.40	0.11
42513	-0.37	-0.45	0.08	-1.49	-1.74	0.25	-0.01	0.23	0.24	0.37	0.40	0.02
42004	-0.49	-0.72	0.23	-1.37	-1.97	0.60	-0.02	0.02	0.04	0.45	0.48	0.03
42008	-0.60	-0.69	0.09	-1.52	-1.99	0.47	-0.06	0.18	0.24	0.54	0.49	0.06
42013	-0.48	-0.58	0.10	-1.50	-1.51	0.01	-0.02	0.23	0.25	0.40	0.44	0.04
41504	-0.60	-0.50	0.10	-1.79	-1.49	0.30	-0.04	0.38	0.42	0.52	0.41	0.11
41508	-0.67	-0.42	0.25	-1.95	-1.33	0.62	-0.04	0.40	0.44	0.64	0.39	0.26
41513	-0.60	-0.58	0.02	-1.84	-1.59	0.25	-0.04	0.10	0.14	0.51	0.44	0.08
41004	-0.64	-0.39	0.25	-1.35	-1.18	0.17	-0.15	0.17	0.32	0.64	0.37	0.26
41008	-0.64	-0.62	0.02	-1.70	-1.63	0.07	-0.04	0.07	0.11	0.72	0.42	0.30
41013	-0.59	-0.79	0.21	-1.57	-2.11	0.54	-0.04	-0.09	0.05	0.64	0.50	0.14
40504	-0.52	-0.60	0.08	-1.27	-1.60	0.33	-0.03	-0.01	0.02	0.68	0.43	0.25
40508	-0.55	-0.62	0.07	-1.34	-1.48	0.14	-0.02	0.15	0.17	0.69	0.44	0.25
40513	-0.56	-0.64	0.08	-1.57	-1.78	0.21	-0.02	0.13	0.15	0.63	0.46	0.16
40004	-0.73	-0.56	0.17	-4.37	-1.54	2.83	-0.08	0.15	0.23	0.56	0.42	0.14
40008	-0.76	-0.73	0.03	-3.50	-2.09	1.41	-0.11	0.20	0.31	0.59	0.50	0.09
40013	-0.93	-0.50	0.43	-3.37	-1.21	2.16	-0.04	-0.01	0.03	0.60	0.38	0.21
50045	-0.76	-0.36	0.40	-2.58	-1.24	1.34	-0.10	0.40	0.50	0.33	0.67	0.34
50345	-0.78	-0.36	0.42	-2.82	-1.13	1.69	0.04	0.24	0.20	0.79	0.66	0.13
50545	-0.86	-0.33	0.53	-2.98	-1.40	1.58	0.00	0.40	0.40	0.81	0.67	0.15
50040	-0.68	-0.65	0.03	-2.15	-1.92	0.23	0.03	0.16	0.13	0.83	0.76	0.07
50340	-0.44	-0.71	0.27	-2.38	-2.53	0.15	0.10	-0.07	0.17	0.86	0.76	0.10
50540	-0.38	-0.68	0.30	-2.02	-2.33	0.31	0.15	0.11	0.04	0.95	0.76	0.19
51040	-0.25	-0.64	0.40	-1.41	-2.78	1.37	0.29	0.02	0.27	0.98	0.75	0.23
50035	-0.59	-0.88	0.29	-1.96	-2.99	1.03	-0.02	0.11	0.13	0.73	0.84	0.12
50335	-0.37	-0.32	0.05	-1.19	-1.15	0.04	0.10	0.46	0.36	0.50	0.66	0.16
50532	-0.28	-0.97	0.69	-1.54	-2.95	1.41	0.11	-0.04	0.15	0.44	0.88	0.44
51035	-0.26	-0.30	0.04	-1.04	-1.01	0.03	0.26	0.54	0.28	0.29	0.65	0.35
50030	-0.42	-0.32	0.10	-1.07	-1.52	0.45	0.10	0.67	0.57	0.63	0.67	0.04
50330	-0.27	-1.11	0.84	-0.97	-3.33	2.36	0.21	-0.02	0.23	0.40	0.94	0.55
50530	-0.24	-0.36	0.12	-0.76	-1.10	0.34	0.05	0.31	0.26	0.31	0.67	0.36
51030	-0.19	-0.44	0.25	-0.69	-1.80	1.11	0.17	0.67	0.50	0.28	0.72	0.44
50025	-1.09	-0.26	0.83	-4.42	-1.42	3.00	-0.05	0.55	0.60	0.45	0.65	0.20
50325	-1.27	-0.50	0.77	-4.12	-1.97	2.15	0.09	0.67	0.58	0.29	0.76	0.46
50525	-1.70	-0.40	1.30	-5.62	-1.26	4.36	0.02	0.19	0.17	0.26	0.68	0.42
51025	-1.46	-0.64	0.82	-6.80	-2.76	4.04	0.07	0.57	0.50	0.20	0.78	0.57
52845	-0.36	-0.24	0.12	-2.43	-1.21	1.22	0.22	0.53	0.31	1.83	0.64	1.19
53045	-0.61	-0.33	0.28	-5.90	-1.03	4.87	0.34	0.32	0.02	1.95	0.66	1.29
51540	-1.71	-0.59	1.12	-6.70	-2.82	3.88	0.02	0.41	0.39	0.82	0.76	0.06
52040	-0.22	-0.65	0.43	-1.20	-2.28	1.08	0.18	0.30	0.12	0.34	0.78	0.44
52840	-0.26	-0.27	0.02	-4.19	-0.90	3.29	0.55	0.52	0.03	0.86	0.65	0.21

53040	-1.36	-0.31	1.05	-5.41	-0.96	4.45	0.16	0.37	0.21	1.85	0.65	1.19
51535	-1.25	-0.59	0.66	-4.16	-2.42	1.74	-0.07	0.35	0.42	0.25	0.76	0.52
51530	-1.05	-0.89	0.16	-3.75	-2.50	1.25	-0.12	-0.10	0.02	0.28	0.82	0.54
52030	-0.24	-0.31	0.08	-1.17	-0.95	0.22	0.31	0.34	0.03	0.23	0.65	0.43
52530	-0.20	-0.58	0.38	-2.05	-3.24	1.19	0.57	0.43	0.14	0.82	0.79	0.04
52830	-0.87	-0.79	0.08	-3.97	-2.43	1.54	0.16	-0.05	0.21	1.40	0.80	0.60
53030	-1.02	-0.54	0.48	-3.98	-7.40	3.42	-0.07	0.42	0.49	1.13	0.79	0.34
51525	-0.89	-0.29	0.60	-2.97	-0.97	2.00	-0.18	0.44	0.62	0.26	0.65	0.39
52025	-0.21	-0.75	0.54	-1.86	-2.59	0.73	0.22	0.01	0.21	0.28	0.78	0.50
52525	-0.38	-0.25	0.13	-2.31	-1.17	1.14	0.24	0.49	0.25	1.02	0.64	0.38
52825	-0.79	-0.49	0.30	-3.49	-2.00	1.49	0.12	0.37	0.25	1.11	0.72	0.39
53025	-0.83	-0.46	0.37	-3.60	-1.91	1.69	-0.05	0.35	0.40	0.96	0.70	0.26
51520	-0.69	-1.68	1.00	-2.45	-5.43	2.98	-0.04	-0.38	0.34	0.24	1.91	1.67
52020	-0.31	-1.69	1.38	-1.51	-5.06	3.55	0.21	-0.39	0.60	0.45	1.39	0.94
52520	-0.39	-0.25	0.14	-1.98	-0.72	1.26	0.19	0.26	0.07	0.88	0.63	0.25
52820	-0.75	-0.23	0.52	-3.03	-0.70	2.33	0.04	0.28	0.25	0.90	0.63	0.27
53028	-0.76	-0.27	0.49	-2.88	-0.82	2.06	-0.04	0.19	0.23	0.74	0.64	0.10
51515	-0.70	-0.32	0.38	-2.61	-1.15	1.46	-0.05	0.25	0.30	0.34	0.65	0.30
52015	-0.26	-0.51	0.25	-1.86	-1.24	0.62	0.19	0.12	0.07	0.47	0.69	0.22
52515	-0.41	-0.35	0.06	-3.14	-1.24	1.90	0.33	0.20	0.13	0.83	0.66	0.16
52815	-0.62	-1.63	1.01	-2.94	-4.95	2.01	0.05	-0.59	0.64	0.82	1.29	0.47
53015	-0.65	-0.27	0.38	-2.48	-0.93	1.55	-0.01	0.31	0.32	0.75	0.65	0.11
51510	-0.58	-0.44	0.14	-2.82	-2.72	0.10	-0.05	0.55	0.60	0.31	0.73	0.42
52010	-0.33	-0.29	0.04	-2.11	-1.27	0.84	0.26	0.36	0.10	0.48	0.66	0.17
52510	-0.42	-0.24	0.18	-1.53	-0.82	0.71	0.22	0.30	0.08	0.69	0.64	0.05
52810	-0.47	-1.12	0.65	-1.98	-2.99	1.01	0.17	-0.23	0.40	0.71	0.95	0.24
53010	-0.50	-0.35	0.15	-3.24	-1.89	1.35	0.18	0.39	0.22	0.63	0.69	0.05
51505	-0.50	-0.24	0.26	-3.58	-0.70	2.88	0.06	0.20	0.15	0.38	0.63	0.25
52005	-0.42	-0.21	0.21	-2.12	-0.81	1.31	0.20	0.32	0.12	0.46	0.63	0.17
52505	-0.36	-0.93	0.57	-1.90	-2.31	0.41	0.31	-0.08	0.39	0.52	0.85	0.34
52805	-0.35	-0.53	0.18	-2.68	-1.78	0.90	0.24	0.36	0.12	0.56	0.75	0.20
53005	-0.35	-0.21	0.14	-2.35	-0.78	1.57	0.29	0.41	0.12	0.56	0.63	0.07
52500	-0.25	-1.13	0.88	-1.00	-3.65	2.65	0.11	-0.08	0.19	0.41	0.95	0.54
52800	-0.32	-0.64	0.32	-0.80	-2.28	1.48	0.04	0.26	0.22	0.42	0.78	0.36
53000	-0.27	-0.23	0.04	-1.04	-0.69	0.35	0.11	0.16	0.05	0.52	0.63	0.11
50020	-0.35	-0.20	0.15	-0.98	-1.47	0.49	0.04	0.46	0.42	0.33	0.64	0.31
50320	-0.26	-1.49	1.24	-0.72	-4.22	3.50	0.12	-0.42	0.54	0.26	1.17	0.90
50520	-0.29	-0.65	0.36	-1.01	-2.08	1.07	0.10	0.30	0.20	0.34	0.77	0.43
51020	-0.38	-0.25	0.13	-1.54	-0.74	0.80	0.20	0.31	0.12	0.30	0.63	0.34
50015	-0.30	-1.17	0.87	-1.04	-2.92	1.88	0.09	0.14	0.06	0.37	0.96	0.59
50315	-0.24	-0.63	0.39	-0.89	-1.76	0.87	0.15	0.20	0.05	0.27	0.75	0.48
50515	-0.26	-0.30	0.04	-0.97	-0.93	0.04	0.08	0.18	0.11	0.31	0.64	0.33
51015	-0.34	-0.55	0.21	-1.82	-2.49	0.67	0.08	0.10	0.02	0.41	0.72	0.31
50005	-0.35	-0.87	0.52	-3.70	-2.96	0.74	0.12	0.49	0.37	0.28	0.95	0.67
50305	-0.41	-0.44	0.03	-2.71	-1.07	1.64	0.11	0.13	0.02	0.23	0.67	0.44
51055	-0.21	-0.26	0.05	-1.00	-0.87	0.13	0.15	0.41	0.26	0.26	0.64	0.38
50000	-0.23	-0.58	0.35	-1.21	-2.59	1.38	0.14	0.08	0.06	0.28	0.73	0.45
50300	-0.38	-0.63	0.25	-2.87	-2.09	0.78	0.12	0.20	0.08	0.38	0.74	0.37

Table A-4. WERFL Test Building and 1:10 scaled model tap comparison with flow simulated
parallel to the transverse axis (AOA = 90^o)

Tap	TTU Cp_{mean}	1:10 Cp_{mean}	Resid-ual	TTU Cp_{min}	1:10 Cp_{min}	Resid-ual	TTU Cp_{max}	1:10 Cp_{max}	Resid-ual	TTU Cp_{rms}	1:10 Cp_{rms}	Resid-ual
13004	-0.26	-0.25	0.01	-0.81	-2.07	1.26	-0.03	0.70	0.73	0.28	0.58	0.30
13008	-0.23	-0.69	0.46	-1.53	-2.60	1.07	0.12	-0.10	0.22	0.26	0.70	0.43
13013	-0.29	-0.22	0.07	-2.80	-1.55	1.25	0.09	0.67	0.59	0.33	0.58	0.25
12604	-0.22	-0.27	0.05	-1.12	-1.99	0.87	0.18	0.53	0.35	0.26	0.59	0.34
12608	-0.24	-0.68	0.44	-1.32	-2.54	1.22	0.32	0.19	0.13	0.28	0.72	0.44
12613	-0.30	-0.34	0.04	-2.87	-1.47	1.40	0.20	0.45	0.25	0.35	0.62	0.26
12304	-0.20	-0.49	0.29	-1.20	-1.70	0.50	0.31	0.42	0.11	0.25	0.66	0.40
12308	-0.20	-0.49	0.29	-1.67	-1.96	0.29	0.44	0.58	0.14	0.27	0.68	0.41
12313	-0.22	-0.54	0.32	-2.74	-2.00	0.74	0.43	0.01	0.42	0.32	0.63	0.31
11904	-0.32	-0.61	0.29	-1.50	-2.00	0.50	0.20	0.10	0.10	0.38	0.65	0.27
11908	-0.34	-0.45	0.11	-1.61	-1.56	0.05	0.06	0.03	0.03	0.39	0.60	0.21
11913	-0.37	-0.53	0.16	-4.48	-1.56	2.92	0.63	0.12	0.51	0.45	0.62	0.16
11501	-0.37	-0.31	0.06	-1.96	-2.60	0.64	0.43	0.20	0.23	0.44	0.59	0.16
11508	-0.40	-0.53	0.13	-1.88	-3.02	1.14	0.57	0.51	0.06	0.48	0.70	0.23
11513	-0.47	-0.33	0.14	-3.43	-1.86	1.57	0.53	0.60	0.07	0.57	0.60	0.04
10404	-0.87	-0.32	0.55	-3.00	-1.73	1.27	0.11	0.25	0.14	0.97	0.60	0.37
10413	-1.00	-0.37	0.63	-4.54	-5.37	0.83	0.43	0.39	0.04	1.11	0.64	0.47
10408	-0.88	-0.43	0.45	-3.09	-3.29	0.20	0.27	0.44	0.17	0.96	0.67	0.30
10004	-0.77	-0.27	0.50	-4.00	-1.57	2.43	0.22	0.56	0.34	0.86	0.60	0.26
10008	-0.82	-0.39	0.43	-3.00	-1.58	1.42	0.41	0.40	0.01	0.89	0.63	0.26
10013	-1.02	-0.31	0.71	-3.72	-2.82	0.90	0.51	0.41	0.10	1.10	0.61	0.49
24504	-0.54	0.52	1.06	-3.11	-0.35	2.76	0.98	1.71	0.74	0.65	0.41	0.23
24508	-0.21	0.64	0.85	-2.73	-0.26	2.47	1.49	2.01	0.52	0.42	0.44	0.01
24513	0.14	-0.15	0.29	-2.07	-1.59	0.48	2.20	1.35	0.85	0.32	0.34	0.02
24008	0.55	0.56	0.01	-0.64	-0.41	0.23	2.62	2.06	0.56	0.66	0.43	0.23
24013	0.07	0.57	0.51	-1.55	-0.49	1.06	1.73	1.93	0.20	0.29	0.43	0.14
23504	0.37	0.67	0.30	-0.78	-0.22	0.56	1.90	1.97	0.07	0.45	0.44	0.01
23508	0.57	0.08	0.49	-0.61	-1.00	0.39	2.56	1.94	0.62	0.67	0.32	0.35
23004	0.35	0.02	0.33	-1.31	-1.11	0.20	1.59	1.52	0.07	0.42	0.30	0.11
23008	0.56	0.65	0.10	-0.51	-0.19	0.32	2.34	1.94	0.40	0.65	0.43	0.21
23013	0.00	0.55	0.55	-2.01	-0.42	1.59	1.54	1.83	0.29	0.25	0.41	0.16
22504	0.32	-0.08	0.40	-1.06	-1.39	0.33	1.38	1.38	0.00	0.39	0.32	0.08
22508	0.56	0.04	0.52	-0.55	-1.44	0.89	2.19	1.70	0.49	0.64	0.31	0.33
22513	0.00	-0.23	0.23	-1.27	-2.22	0.95	1.40	2.02	0.62	0.26	0.36	0.09
22004	0.34	0.62	0.28	-0.70	-0.55	0.15	1.54	2.10	0.56	0.41	0.45	0.04
22008	0.51	0.02	0.49	-0.58	-0.90	0.32	2.14	1.44	0.70	0.60	0.30	0.30
22013	0.09	0.43	0.34	-1.18	-0.53	0.65	1.43	1.53	0.10	0.28	0.38	0.10
21504	0.32	0.37	0.05	-0.57	-0.44	0.13	1.40	1.57	0.17	0.40	0.37	0.03
21508	0.52	0.47	0.05	-0.46	-0.34	0.12	1.93	1.65	0.28	0.62	0.39	0.23
21513	-0.03	-0.40	0.37	-1.58	-2.02	0.44	1.27	1.80	0.53	0.30	0.39	0.09
21004	0.29	0.54	0.25	-0.71	-0.36	0.35	1.59	1.64	0.05	0.37	0.41	0.03
21008	0.49	0.59	0.10	-1.21	-0.27	0.94	2.32	1.66	0.66	0.60	0.40	0.20
21013	-0.02	-0.22	0.20	-2.06	-1.26	0.80	1.49	1.18	0.31	0.30	0.34	0.04
20504	0.20	0.55	0.35	-1.44	-0.22	1.22	1.59	1.64	0.05	0.33	0.40	0.07
20508	0.49	0.03	0.46	-0.79	-1.03	0.24	2.53	1.26	1.27	0.61	0.31	0.30
20513	-0.13	-0.02	0.11	-1.82	-1.05	0.77	1.52	1.85	0.33	0.32	0.30	0.02
20004	-0.46	0.27	0.73	-2.25	-0.46	1.79	0.91	1.27	0.36	0.55	0.34	0.21
20008	-0.08	-0.28	0.20	-1.66	-1.46	0.20	1.90	1.05	0.85	0.29	0.35	0.06
20013	-0.03	-0.29	0.26	-1.68	-1.14	0.54	1.40	0.94	0.46	0.29	0.35	0.06
33004	-0.76	-0.58	0.18	-5.82	-1.99	3.83	-0.03	0.23	0.26	0.84	0.57	0.27
33008	-0.82	-0.27	0.55	-3.48	-2.75	0.73	0.08	0.30	0.22	0.88	0.49	0.40
33013	-1.08	-0.71	0.37	-4.76	-2.41	2.35	-0.26	0.10	0.36	1.17	0.63	0.54
32604	-0.81	-0.79	0.02	-3.02	-2.54	0.48	0.23	0.10	0.13	0.88	0.65	0.24
32608	-0.86	-0.35	0.51	-2.93	-2.81	0.12	0.19	0.48	0.29	0.94	0.53	0.41
32613	-0.98	-0.76	0.22	-4.49	-2.30	2.19	0.39	0.55	0.16	1.07	0.67	0.39
32304	-1.02	-0.65	0.37	-2.98	-2.09	0.89	-0.07	0.64	0.71	1.08	0.64	0.44
32308	-1.08	-0.65	0.43	-3.86	-2.35	1.51	0.00	0.65	0.65	1.15	0.66	0.48

32313	-1.10	-0.50	0.60	-4.01	-2.12	1.89	0.23	0.23	0.00	1.21	0.53	0.68
31904	-0.59	-0.45	0.14	-1.80	-1.80	0.00	0.37	0.23	0.14	0.65	0.54	0.11
31908	-0.64	-0.45	0.19	-2.56	-1.84	0.72	0.27	0.16	0.11	0.72	0.52	0.20
31913	-0.67	-0.49	0.18	-3.46	-1.64	1.82	0.52	0.40	0.12	0.78	0.54	0.24
31504	-0.45	-0.75	0.31	-1.70	-2.39	0.69	0.23	0.01	0.22	0.51	0.64	0.13
31508	-0.50	-0.67	0.17	-2.19	-3.24	1.05	0.34	0.88	0.54	0.57	0.69	0.11
31513	-0.53	-0.68	0.15	-5.03	-2.33	2.70	0.26	0.13	0.13	0.63	0.60	0.03
30404	-0.26	-0.84	0.58	-1.28	-2.19	0.91	0.24	-0.02	0.26	0.29	0.64	0.34
30408	-0.29	-0.83	0.54	-1.97	-2.87	0.90	0.25	0.53	0.28	0.33	0.68	0.35
30413	-0.34	-0.80	0.46	-3.21	-3.56	0.35	0.14	0.45	0.31	0.40	0.71	0.31
30004	-0.27	-0.75	0.48	-2.00	-2.30	0.30	0.13	0.20	0.08	0.30	0.66	0.37
30008	-0.30	-0.79	0.49	-1.90	-2.31	0.41	0.04	0.32	0.28	0.33	0.66	0.33
30013	-0.31	-0.80	0.49	-2.89	-2.80	0.09	0.09	-0.03	0.12	0.36	0.66	0.30
44504	-0.28	-0.24	0.04	-0.95	-1.04	0.09	0.02	0.16	0.14	0.30	0.23	0.07
44508	-0.29	-0.24	0.05	-1.13	-1.08	0.05	-0.02	0.25	0.27	0.31	0.23	0.08
44513	-0.29	-0.23	0.06	-1.15	-0.91	0.24	0.04	0.18	0.14	0.32	0.23	0.09
44008	-0.30	-0.24	0.06	-0.82	-1.57	0.75	-0.02	0.12	0.14	0.32	0.24	0.08
44013	-0.29	-0.23	0.06	-0.89	-1.05	0.16	0.08	0.14	0.06	0.31	0.23	0.09
43504	-0.29	-0.25	0.04	-0.78	-0.96	0.18	-0.01	0.16	0.17	0.31	0.23	0.08
43508	-0.32	-0.26	0.06	-0.81	-1.50	0.69	-0.05	0.24	0.29	0.34	0.24	0.10
43004	-0.27	-0.26	0.01	-0.73	-0.95	0.22	-0.04	0.16	0.20	0.29	0.23	0.06
43008	-0.30	-0.27	0.03	-0.77	-1.91	1.14	-0.05	0.19	0.24	0.32	0.24	0.07
43013	-0.28	-0.28	0.00	-1.12	-2.21	1.09	-0.01	0.18	0.19	0.30	0.25	0.06
42504	-0.25	-0.25	0.00	-0.68	-1.42	0.74	-0.03	-0.27	0.24	0.27	0.23	0.03
42508	-0.26	-0.22	0.04	-0.69	-1.90	1.21	-0.04	-0.16	0.12	0.28	0.23	0.05
42513	-0.28	-0.21	0.07	-0.96	-1.80	0.84	-0.01	-0.04	0.03	0.29	0.23	0.06
42004	-0.26	-0.26	0.00	-0.74	-1.00	0.27	-0.03	0.16	0.19	0.27	0.23	0.04
42008	-0.27	-0.24	0.03	-0.68	-0.96	0.28	-0.04	0.17	0.21	0.29	0.23	0.05
42013	-0.28	-0.31	0.03	-0.72	-1.95	1.23	0.00	0.27	0.27	0.29	0.27	0.02
41504	-0.25	-0.23	0.02	-0.72	-0.98	0.27	0.03	0.14	0.11	0.27	0.23	0.04
41508	-0.26	-0.21	0.05	-0.70	-1.07	0.37	0.00	0.16	0.16	0.27	0.23	0.05
41513	-0.26	-0.23	0.03	-0.90	-1.02	0.12	0.02	0.18	0.16	0.28	0.23	0.05
41004	-0.26	-0.25	0.01	-0.71	-1.49	0.78	-0.03	0.22	0.25	0.28	0.24	0.05
41008	-0.28	-0.27	0.01	-0.76	-1.51	0.75	-0.05	0.08	0.13	0.30	0.23	0.06
41013	-0.28	-0.27	0.01	-1.06	-1.01	0.05	0.02	0.00	0.02	0.30	0.23	0.07
40504	-0.29	-0.26	0.03	-0.63	-0.98	0.35	-0.05	0.03	0.08	0.31	0.23	0.08
40508	-0.28	-0.31	0.03	-0.74	-1.32	0.58	-0.03	0.11	0.14	0.30	0.25	0.05
40513	-0.28	-0.30	0.02	-0.84	-1.61	0.78	-0.02	0.33	0.35	0.30	0.27	0.03
40004	-0.23	-0.29	0.06	-1.34	-1.35	0.01	0.05	0.15	0.10	0.26	0.25	0.00
40008	-0.25	-0.31	0.06	-1.03	-1.16	0.13	0.00	0.24	0.24	0.28	0.26	0.02
40013	-0.26	-0.26	0.00	-1.46	-2.14	0.68	0.03	0.06	0.03	0.28	0.23	0.06
50045	-0.34	-0.40	0.06	-2.36	-2.50	0.14	0.09	0.17	0.09	0.38	1.11	0.73
50345	-0.45	-0.39	0.06	-5.02	-2.56	2.46	0.06	0.11	0.05	0.49	1.13	0.63
50545	-0.34	-0.73	0.39	-3.06	-2.68	0.38	0.11	0.53	0.42	0.38	1.21	0.83
50040	-0.35	-0.87	0.53	-1.17	-2.49	1.32	0.08	-0.24	0.32	0.37	1.26	0.89
50340	-0.26	-0.90	0.64	-1.46	-2.67	1.21	0.21	-0.35	0.56	0.29	1.30	1.01
50540	-0.29	-0.87	0.58	-1.58	-2.77	1.19	0.23	-0.10	0.33	0.31	1.31	0.99
51040	-0.32	-0.84	0.52	-1.69	-2.54	0.85	0.12	-0.33	0.45	0.35	1.27	0.92
50035	-0.34	-0.75	0.41	-1.22	-3.06	1.84	0.03	-0.05	0.08	0.37	1.22	0.85
50335	-0.29	-0.29	0.01	-1.11	-2.67	1.56	0.13	0.34	0.21	0.31	1.09	0.78
50532	-0.30	-0.75	0.45	-1.51	-3.11	1.60	0.21	-0.06	0.27	0.32	1.25	0.93
51035	-0.34	-0.43	0.09	-1.75	-1.80	0.05	0.36	0.61	0.26	0.37	1.13	0.76
50030	-0.36	-0.52	0.16	-1.68	-2.10	0.42	0.05	0.65	0.60	0.38	1.19	0.81
50330	-0.30	-0.81	0.51	-1.61	-2.59	0.98	0.11	-0.12	0.23	0.33	1.26	0.94
50530	-0.31	-0.32	0.01	-2.20	-2.67	0.47	0.20	0.40	0.20	0.34	1.10	0.76
51030	-0.36	-0.69	0.33	-1.60	-2.20	0.60	0.30	0.38	0.08	0.40	1.25	0.85
50025	-0.28	-0.75	0.47	-1.07	-2.11	1.04	0.16	0.31	0.15	0.30	1.21	0.90
50325	-0.26	-0.81	0.55	-1.33	-2.60	1.27	0.21	-0.21	0.42	0.29	1.27	0.98
50525	-0.30	-0.33	0.03	-1.35	-2.46	1.11	0.21	0.32	0.11	0.33	1.11	0.78
51025	-0.35	-0.84	0.49	-1.60	-2.94	1.34	0.23	0.23	0.00	0.40	1.30	0.91
52845	-1.32	-0.74	0.58	-6.30	-3.52	2.78	-0.02	0.49	0.51	1.45	1.23	0.22
53045	-1.63	-0.33	1.30	-6.30	-1.51	4.79	-0.07	0.49	0.56	1.79	1.10	0.70
51540	-0.43	-0.94	0.51	-2.18	-3.26	1.08	0.27	-0.12	0.39	0.48	1.38	0.90
52040	-0.59	-0.87	0.28	-2.93	-2.73	0.20	0.33	-0.11	0.44	0.67	1.26	0.59
52840	-1.37	-0.57	0.80	-5.13	-1.97	3.16	-0.11	0.27	0.38	1.47	1.16	0.31

53040	-1.32	-0.33	0.99	-5.47	-1.60	3.87	-0.12	0.26	0.38	1.41	1.10	0.32
51535	-0.42	-0.93	0.51	-2.33	-3.55	1.22	0.32	0.30	0.02	0.48	1.41	0.93
51530	-0.49	-0.85	0.36	-3.37	-2.75	0.62	0.36	-0.28	0.64	0.55	1.27	0.72
52030	-0.77	-0.42	0.35	-2.89	-1.78	1.11	0.21	0.25	0.04	0.86	1.12	0.26
52530	-1.19	-0.91	0.28	-4.19	-3.06	1.13	0.10	0.01	0.09	1.28	1.38	0.10
52830	-1.26	-0.82	0.44	-4.29	-2.94	1.35	-0.15	-0.29	0.14	1.36	1.25	0.10
53030	-1.22	-1.00	0.22	-6.30	-4.40	1.90	-0.27	-0.11	0.16	1.31	1.69	0.38
51525	-0.51	-0.39	0.12	-2.50	-2.00	0.50	0.22	0.40	0.18	0.57	1.11	0.55
52025	-0.79	-0.78	0.01	-3.24	-2.28	0.96	0.15	-0.27	0.42	0.87	1.25	0.37
52525	-1.21	-0.58	0.63	-4.44	-2.44	2.00	0.55	0.68	0.14	1.31	1.17	0.15
52825	-1.29	-1.17	0.12	-4.80	-3.99	0.81	-0.23	-0.37	0.15	1.39	1.52	0.13
53025	-1.24	-1.21	0.03	-5.47	-3.71	1.76	-0.39	-0.12	0.27	1.33	1.47	0.13
51520	-0.49	-1.31	0.82	-2.74	-6.92	4.18	0.31	-0.11	0.42	0.55	2.03	1.48
52020	-0.78	-0.95	0.17	-3.96	-3.06	0.90	0.28	0.37	0.09	0.86	1.37	0.51
52520	-1.16	-0.58	0.58	-4.39	-2.02	2.37	-0.05	0.12	0.17	1.26	1.16	0.10
52820	-1.24	-0.40	0.84	-5.21	-1.74	3.47	-0.19	0.26	0.45	1.35	1.11	0.23
53028	-1.19	-0.27	0.92	-5.13	-1.99	3.14	-0.29	0.45	0.74	1.29	1.08	0.22
51515	-0.50	-0.24	0.26	-2.64	-1.66	0.98	0.31	0.27	0.04	0.56	1.06	0.50
52015	-0.74	-0.25	0.49	-3.24	-1.84	1.40	0.19	0.21	0.02	0.81	1.06	0.25
52515	-1.18	-0.28	0.90	-4.30	-1.76	2.54	0.04	0.57	0.53	1.28	1.08	0.20
52815	-1.28	-0.92	0.36	-4.66	-2.58	2.08	-0.19	-0.28	0.09	1.37	1.30	0.08
53015	-1.25	-0.29	0.96	-4.58	-1.54	3.04	-0.35	0.40	0.75	1.35	1.09	0.26
51510	-0.47	-0.97	0.50	-2.03	-2.83	0.80	0.29	-0.36	0.65	0.52	1.35	0.83
52010	-0.72	-0.68	0.04	-3.79	-2.44	1.35	0.27	0.36	0.09	0.80	1.22	0.43
52510	-1.21	-0.35	0.86	-4.89	-1.56	3.33	-0.04	0.29	0.33	1.33	1.10	0.23
52810	-1.31	-0.75	0.56	-4.52	-2.32	2.20	-0.09	-0.24	0.15	1.41	1.22	0.19
53010	-1.25	-0.51	0.74	-6.20	-3.38	2.82	-0.33	0.42	0.75	1.35	1.17	0.17
51505	-0.47	-0.68	0.22	-2.00	-1.94	0.06	0.10	-0.08	0.18	0.51	1.17	0.66
52005	-0.65	-0.53	0.12	-2.51	-1.96	0.55	0.23	0.34	0.11	0.72	1.14	0.43
52505	-1.10	-0.75	0.35	-3.97	-2.27	1.70	0.06	-0.17	0.23	1.20	1.21	0.01
52805	-1.32	-0.34	0.98	-5.03	-1.99	3.04	0.04	0.48	0.44	1.42	1.12	0.30
53005	-1.32	-0.72	0.60	-6.16	-2.16	4.00	-0.33	0.22	0.55	1.42	1.21	0.21
52500	-0.98	-0.79	0.19	-4.44	-2.27	2.17	0.11	-0.28	0.39	1.08	1.23	0.15
52800	-1.18	-0.25	0.93	-4.36	-2.00	2.36	-0.03	0.64	0.67	1.29	1.09	0.20
53000	-1.48	-0.48	1.00	-5.91	-1.72	4.19	-0.19	0.30	0.49	1.62	1.13	0.50
50020	-0.28	-0.83	0.55	-1.05	-2.40	1.35	0.15	0.03	0.12	0.30	1.25	0.95
50320	-0.30	-0.83	0.53	-2.20	-2.71	0.51	0.29	-0.17	0.46	0.33	1.25	0.92
50520	-0.31	-0.23	0.08	-2.98	-1.95	1.03	0.17	0.10	0.07	0.35	1.08	0.73
51020	-0.38	-0.31	0.07	-2.43	-1.52	0.91	0.23	0.42	0.19	0.42	1.08	0.66
50015	-0.32	-0.80	0.48	-1.48	-2.70	1.22	0.01	-0.21	0.22	0.34	1.25	0.91
50315	-0.28	-0.27	0.01	-1.55	-1.61	0.06	0.13	0.51	0.38	0.31	1.09	0.78
50515	-0.33	-0.27	0.06	-2.25	-1.34	0.91	0.18	0.92	0.74	0.36	1.07	0.71
51015	-0.41	-0.27	0.14	-1.97	-1.81	0.16	0.26	0.36	0.10	0.45	1.07	0.63
50005	-0.34	-0.85	0.51	-1.32	-3.00	1.68	0.10	-0.21	0.31	0.36	1.27	0.91
50305	-0.26	-0.27	0.01	-1.32	-1.56	0.24	0.17	0.65	0.48	0.29	1.07	0.78
51055	-0.33	-0.83	0.50	-1.56	-2.54	0.98	0.26	-0.14	0.40	0.36	1.24	0.88
50000	-0.36	-0.29	0.07	-2.55	-2.14	0.41	0.00	0.20	0.20	0.40	1.08	0.68
50300	-0.38	-0.30	0.08	-2.05	-3.18	1.13	0.07	0.28	0.21	0.41	1.09	0.67

APPENDIX B
NOMENCLATURE

Atmospheric Boundary Layer: is the lowest part of the atmosphere and is behavior is directly influence by the Earth's Surface. The depth of the boundary layer ranges from a few hundred meters to several kilometers depending upon wind turbulence, terrain roughness and angle of latitude (Simiu and Scanlan, 1996)

Boundary Layer Flow: a layer of fluid flow that is in the immediate vicinity of a bounding surface where effect of viscosity are considered

Drag Coefficient: a dimensionless quantity that is used to quantify the drag or resistance of an object in a fluid environment such as air or water

Friction Velocity: also called shear velocity, is a form by which shear stress may be re-written in units of velocity. It is used as a method in fluid mechanics to compare true velocities, such as the velocity of a flow in a stream, to a velocity that relates shear between layers of flow

Integral Length Scales: of the three standard turbulence length scale, the ones that are measures of the largest separation distance over which components of the eddy velocities at two distinct points are correlated

Neutral Atmosphere: a condition in the atmosphere where isolate air parcels do not have a tendency to rise or sink

Reynolds Number: a dimensionless number used in fluid mechanics that represents the ratio of inertial forces to viscous forces and quantifies the relative importance of these two types of force for given flow conditions

Roughness Elements: geometric bodies placed in wind tunnels upwind of a test section to introduce mechanical turbulence typically cubed shaped

Roughness Length: is a parameter of vertical wind profile equations that model the horizontal mean wind speed near the ground, in the log wind profile, it is the equivalent to the height at which speed is zero. It is so named because it is typically related to the height of terrain roughness elements. While it is not a physical length, it can be considered as a length-scale a representation of the roughness of the surface.

Strouhal Number: a dimensionless number used in fluid mechanics that studies the vibrations of a body past which a fluid is flowing, also known as reduced frequency

Turbulence: is a flow regime characterized by chaotic and stochastic property changes, this includes low momentum diffusion, high momentum convection, and rapid variation of pressure and velocity in space and time

Turbulence Intensity: also known as coefficient of variation, is a normalized measure of dispersion of a probability distribution. It is also recognized as unitized risk or the variation coefficient (TI_u, $TI_{v,}TI_w$)

Turbulence Length Scales: Measures of the eddy scale sizes in turbulent flow. The separation between the largest and smallest sizes is determined by the Reynolds number. The largest length scales are usually imposed by the flow geometry, such as the boundary layer depth.

LIST OF REFERENCES

ANSI/ASHRAE 51-07, 2007. Laboratory Methods of Testing Fans for Certified Aerodynamic Performance Rating. American Society of Heating, Refrigerating and Air Conditioning Engineers, Atlanta, GA.

Aponte, L., 2004. Measurement, Validation and Dissemination of Hurricane Wind Data. Masters Thesis, University of Florida, Department of Civil and Coastal Engineering.

Apperley, L., Surry, D., Stathopoulos, T., Davenport, A., 1979. Comparative measurements of wind pressure on a model of the full-scale experimental house at Aylesbury, England. Journal of Industrial Aerodynamics 4, 207-228.

Armitt, J., 1966. The simulation of the atmospherics boundary layer in a wind tunnel. Central Electricity Reasearch Laboratories, Lab Note No. RD/L/N 83/66.

Armitt, J., Counihan, J., 1967. The simulation of the atmospheric boundary layer in a wind tunnel. Atmospheric Environment 2, 49-71.

Baines, W., Peterson, E., 1950. An investigation of flow through screens. Report of Iowa Institute of Hydraulics.

Baines, W., 1963. Effects of velocity distribution on wind loads and flow patterns on buildings. International Conference on Wind Effects on Buildings and Structures, London, England.

Barlow, J., Rae, W., Pope, A., 1999. Low-speed wind tunnel testing. 3rd Ed., John Wiley & Sons, Inc., New York.

Bailey, A., Vincent, N., 1943. Wind pressures on buildings, including effects of adjacent building. Journal for the Institute of Civil Engineering 20, 243-275.

Bendat, J., Piersol, A., 2000. Random data: Analysis and measurement procedures. 3rd Ed., John Wiley & Sons, Inc., New York.

Bienkiewicz, B., Cermak, J., Peterka, J., 1983. Active Modeling of large-scale turbulence. Journal of Wind Engineering and Industrial Aerodynamics 13, 465-475.

Cao, S., Nishi, A., Kikugawa, H., Matusuda, Y., 2002. Reproduction of wind velocity history in a multiple fan wind tunnel. Journal of Wind Engineering and Industrial Aerodynamics 90, 1719–1729.

Cermak, J., 1958. Wind tunnel for the study of turbulence in the atmospheric sureface layer. Final Report Air Force Cambridge Center, Air Research and Development Command, Bedford, MA (Contract AF 19(604)-1706).

Cermak, J., 1970. Determination of wind loading on structural models in wind-tunnel simulated wind. Wind Effect on High-Rise Building; Proceedings of the Chicago Design Symposium, Evanston, Illinois, 61-88.

Cermak, J., 1971. Laboratory simulation of the atmospheric boundary layer. American Institute of Aeronautics and Astronautics Journal 9 (9), 1746-1754.

Cermak, J., 1981. Wind tunnel design for physical modeling of atmospheric boundary layers. American Society of Civil Engineers Journal 107.

Cermak, J., Cochran, L., 1992. Physical modeling on the atmospheric surface layer. Journal of Wind Engineering and Industrial Aerodynamics 41-44, 953-946.

Cochran, L., 2004. Wind Effects on Building. Proceedings of the Second National Conference on Wind Engineering, Indian Society for Wind Engineering 1, 79-99.

Counihan, J., 1969. An improved method of simulating an atmospheric boundary layer in a wind tunnel. Atmospheric Environment 3, 197-214.

Counihan, J., 1975. Adiabatic atmospheric boundary layers: A review and analysis of data from the period 1880-1972. Atmospheric Environment 9, 871-905.

Davenport, A., 1963. The relationship of wind structure to wind loading. Wind Effects on Buildings and Structures; Proceedings of the conference held at the National Physical Laboratory, Middlesex, UK, 53-102.

Davenport, A., Isyumov, N., 1967. The application of the boundary layer wind tunnel to the prediction of wind loading. Wind Effects on Building and Structures: Proceedings from the International Research Seminar, University of Toronto Press 1, 201-230.

Davenport, A., 2002. Past, present and future of wind engineering. Journal of Wind Engineering and Industrial Aerodynamics 90, 1371-1380.

Eaton, K., Mayne, J., 1975. The measurement of wind pressures on two-story houses at Aylesbury. Journal of Industrial Aerodynamics 1, 67-109.

Engineering Science Data Unit (ESDU), 1983. Strong winds in the atmospheric boundary layer part 1: hourly-mean wind speeds.

Engineering Science Data Unit (ESDU), 1983. Strong winds in the atmospheric boundary layer part 2: discrete gust speeds.

Gartshore, I., 1973. The effect of free stream turbulence on the drag of rectangular two-dimensional prisms. Boundary Layer Tunnel Laboratory Report, BLWT-4-73, University of Western Ontario, London, Canada.

Gurley, K., Davis, R., Ferrera, S., Burton, J., Masters, F., Reinhold, T., Abdullah, M., 2006. Post 2004 hurricane field survey- An evaluation of the relative performances of the standard building code and the Florida Building Code. American Society of Civil Engineers Structures Congress.

Irwin, H., 1981. A Simple Omnidirectional Sensor for Wind-Tunnel Studies of Pedestrian-Level Winds. Journal of Wind Engineering and Industrial Aerodynamics 7, 219-239.

Irwin, H., 1981. The design of spires for wind simulation. Journal of Wind Engineering and Industrial Aerodynamics 7, 361-366.

Irwin, P., 2008. Bluff body aerodynamics in wind engineering. Journal of Wind Engineering and Industrial Aerodynamics 96, 701-712.

Jensen, M., 1958. The model law phenomena in natural wind. Ingenioren (international edition) 2 (4), 121-128.

Jensen, M., Franck, N., 1963. Model-scale test in turbulent wind; Part 1: Phenomena dependent on the wind speed. Danish Technical Press, Copenhagen.

Kennedy, C., 1999. Feasibility study for a full-scale wind test facility. Master's Thesis, Clemson University.

Kikitsu, H., Kanda, J., Iwasaki, R., 1999. Flow simulation by wind tunnel with computer-controlled multiple fans. Journal of Wind Engineering and Industrial Aerodynamics 83, 421-429.

Kobyashi, H., Hatanaka, A., 1992. Active generation of wind gust in a two-dimensional wind tunnel. Journal of Wind Engineering and Industrial Aerodynamics 41-44, 959-970.

Kobayashi, H., Hatanaka, A., Ueda, T., 1994. Active simulation of time histories of strong gust in a wind tunnel. Journal of Wind Engineering and Industrial Aerodynamics 53, 315-330.

Kopp, G., Morrison, M., Iizumi, E., Henderson, D., 2008. The 'Three Little Pigs' Project: Integration of wind tunnel model scale tests and full-scale laboratory tests. 3rd International Symposium on Wind Engineering, Tokyo, Japan.

Kristensen, L., Jensen, N.O., 1979. Lateral coherence in isotropic turbulence and in the natural wind. Boundary Layer Meteorology 17, 353-373.

Leatherman, S., 2007. Wall of Wind Full-Scale, Destructive Testing of Coastal Houses and Hurricane Damage Mitigation. Journal of Coastal Research 23 (5), 1211-1217.

Levitan, M., Mehta, K., Chok, C., Millsaps, D., 1990. An overview of Texas Tech's Wind Engineering Field Research Laboratory. Journal of Wind Engineering and Industrial Aerodynamics 36, 1037-1046.

Levitan, M., Mehta, K., 1992. Texas Tech field experiment for wind loads part I: building and pressure measuring system. Journal of Wind Engineering and Industrial Aerodynamics 41-44, 1565-1576.

Levitan, M., Mehta, K., 1992. Texas Tech field experiments for wind load part II: meterological instrumentation and terrain parameters. Journal of Wind Engineering and Industrial Aerodynamics 41-44, 1577-1588.

Lloyd, A., 1967. The generation of shear flow in a wind tunnel. Quarterly Journal of the Royal Meteorological Society 92 (395).

Masters, F., 2004. Measurement, modeling and simulation of ground-level tropical cyclone winds. Doctoral Dissertation, University of Florida, Department of Civil and Coastal Engineering.

Masters, F., Gurley, K., Prevatt, D., 2008. Full-scale simulation of turbulent wind-driven rain effects on fenestration and wall systems. 3rd International Symposium on Wind Effects on Buildings and Urban Environment, Tokyo, Japan.

Mehta, R., Bradshaw, P., 1979. Design rules for small low speed wind tunnels. Aeronautical Journal of the Royal Aeronautical Society, 443-449.

Meroney, R., 1988. Wind-tunnel modeling of the flow about bluff bodies. Journal of Wind Engineering and Industrial Aerodynamics 29, 203-223.

Monroe, J., 1996. Wind tunnel modeling of low rise structures in a validated open country simulation. Master's Thesis, Clemson University, Civil Engineering.

Nagib, N., Morkovin, M., Jung, J., Tan-atichat, J., 1976. On modeling of atmospheric surface layers by the counter-jet technique. American Institute of Aeronautics and Astronautics Journal14 (2), 185-190.

National Research Council, 1999. Review of the need for a large-scale test facility for research on the effects of extreme winds on structures. National Academy of Sciences, National Academy Press, Washington, D.C.

Nise, N., 2004. Control Systems Engineering. 4th ed., John Wiley & Son, Inc., New York.

Nishi, A., Miyagi, H., 1995. Computer-controlled wind tunnel for wind-engineering applications. Journal of Wind Engineering and Industrial Aerodynamics 54, 493-504.

Nishi, A., Kikugawa, H., Matsuda, Y., Tashiro, D., 1999. Active control of turbulence for an atmospheric boundary layer model in a wind tunnel. Journal of Wind Engineering and Industrial Aerodynamics 83, 409-419.

Ho, T., Surry, D., Morrish, D., Kopp, G., 2005. The UWO contribution to the NIST aerodynamic database for wind loads on low building: Part 1: Archiving format and basic aerodynamic data. Journal of Wind Engineering and Industrial Aerodynamics 93, 1-30.

Ho, T., Surry, D., Morrish, D., Kopp, G., 2005. The UWO contribution to the NIST aerodynamic database for wind loads on low building: Part 2: Comparison of data with wind load provisions. Journal of Wind Engineering and Industrial Aerodynamics 93, 31-59.

O'Brien, C., 1996. Full Scale Structural Testing for Severe Wind. Proceedings of the INEL Sever Windstorm Testing Workshop, Idaho National Engineering Laboratory, Idaho Falls, Idaho.

Oh, J., Kopp, G., Inculet, D., 2007. The UWO contribution to the NIST aerodynamic database for wind load on low buildings: Part 3: Internal pressures. Journal of Wind Engineering and Industrial Aerodynamics 95, 755-779.

Okada, H., Ha, Y., 1992 Comparison of wind tunnel and full-scale pressure measurements tests on the Texas Tech Building. Journal of Wind Engineering and Industrial Aerodynamics 41-44, 1601-1612.

Owen, P., Zienkiewics, H., 1957. The production of uniform shear flow in a wind tunnel. Journal of Fluids Mechanics 2.

Piekle, J., Gratz, J., Landsea, C., Collins, D., Sanders, M., Musulin, R., 2008. Normalized hurricane damage in the United States: 1900-2005. Natural Hazard Review 9, 29-42.

Prandtl, L., 1949. Führer durch die Strömunglsehre. 3. Auflage, Friedrich Vieweg & Sohn, Braunschweig, 407

Saffir, H., 1973. Hurricane wind and storm surge, and the hurricane impact scale. The Military Engineer, Alexandria, Virginia 423.

Schon, J., Mary, P., 1971. A preliminary study of the simulation of neutral atmospheric boundary layer using air injection in a wind tunnel. Atmospheric Environment 5, 299-311.

Sill, B., Cook, N., Fang, C., 1992. The Aylesbury comparative experiment: A final report. Journal of Wind Engineering and Industrial Aerodynamics 41-44, 1553-1564.

Simiu, E., Scanlan, R., 1996. Wind effects on structures: Fundamentals and Applications to Design. John Wiley & Sons, Inc., New York.

Simpson R., 1974. The hurricane disaster potential scale. Weatherwise 27, 169-186

Simpson, R., Riehl, H., 1981. The hurricane and its Impact. Louisiana State University Press.

Sluman, T., Van Maanen, H., Ooms, G., 1980. Atmospheric boundary layer simulation in a wind tunnel used air injection, Applied Scientific Research 36, 289-307

Stathopoulos, T., 1984. Design and fabrication of a wind tunnel for building aerodynamics. Journal of Wind Engineering and Industrial Aerodynamics 16, 361-376.

Stathopoulos, T., 1983. Scale effects in wind tunnel testing of low building. Journal of Wind Engineering and Industrial Aerodynamics 13, 313-326.

Surry, D., 1991. Pressure measurement on the Texas Tech Building: Wind tunnel measurements and comparisons with full scale. Journal of Wind Engineering and Industrial Aerodynamics 38, 235-247.

Surry, D., 1992. Wind tunnel simulation of the Texas Tech Building. Journal of Wind Engineering and Industrial Aerodynamics 41-44, 1613-1614.

Talamelli, A., Riparbelli, L., Westin, J., 2004. An active grid for the simulation of atmospheric boundary layers in a wind tunnel. Wind and Structures 7 (2), 131-144.

Tieleman, H., Reinhold, T., Marshall, R., 1978. On the wind-tunnel simulation of the atmospheric surface layer for the study of wind load on low-rise buildings. Journal of Wind Engineering and Industrial Aerodynamics 3, 21-38.

Tieleman, H., 1996. Model/full scale comparison of pressures on the roof of the TTU experimental building. Journal of Wind Engineering and Industrial Aerodynamics 65, 133-142.

Tieleman, H., Hajj, M., Reinhold, T., 1998. Wind tunnel simulation requirements to asses wind loads on low-rise buildings. Journal of Wind Engineering and Industrial Aerodynamics 74-76, 675-685.

Tieleman, H., 2003. Wind tunnel simulation of wind loading on low-rise structures: a review. Journal of Wind Engineering and Industrial Aerodynamics 91, 1627-1649.

Teunissen, H., 1975. Simulation of the planetary boundary layer in a multiple-jet wind tunnel. Atmospheric Environment 9, 145-174.

Weber, R., 1999. Remarks on the definition and estimation of friction velocity. Boundary-Later Meteorology 93, 197-209.

Von Kármán, T., 1948. Progress in the statistical theory of turbulence. Proceedings of the National Academy of Sciences of the United States of America 34(11), 530-539.

Wind Science and Engineering Research Center (WSERC), 2010 Validation of wind and wind-induced pressure data collected at the Institute for Building & Home Safety's state-of-the-art-multi-peril applied research and training facility: task 1. Report submitted to Reinhold T., Lubbock, TX.

BIOGRAPHICAL SKETCH

Jason Thomas Smith was born in Florence, South Carolina to Everette and Sonya Smith; where he was the younger of two children. He lived in Florence, South Carolina until 2003 when he graduated from South Florence High School. Jason then attended The Citadel in Charleston, SC where he earned a bachelor's degree in civil engineering in 2007. He then began his doctoral research in wind engineering during the summer of 2007, at the University of Florida with Dr. Forrest Masters, during which this document was created. Jason Thomas Smith is a student member of the American Association for Wind Engineering.